Royal Norwegian Council
for Scientific and Industrial Research
(NTNF)

NORSAR

NORSAR Scientific Report No. 2-88/89

Semiannual Technical Summary

1 October 1988 – 31 March 1989

L.B. Loughran (ed.)

Kjeller, July 1989

UNCLASSIFIED
SECURITY CLASSIFICATION OF THIS PAGE

REPORT DOCUMENTATION PAGE

Form Approved OMB No. 0704-0188

1a. REPORT SECURITY CLASSIFICATION: UNCLASSIFIED	1b. RESTRICTIVE MARKINGS: NOT APPLICABLE
2a. SECURITY CLASSIFICATION AUTHORITY: NOT APPLICABLE	3. DISTRIBUTION/AVAILABILITY OF REPORT: APPROVED FOR PUBLIC RELEASE DISTRIBUTION UNLIMITED
2b. DECLASSIFICATION/DOWNGRADING SCHEDULE: NOT APPLICABLE	
4. PERFORMING ORGANIZATION REPORT NUMBER(S): Scientific Rep. 2-88/89	5. MONITORING ORGANIZATION REPORT NUMBER(S): Scientific Rep. 2-88/89
6a. NAME OF PERFORMING ORGANIZATION: NTNF/NORSAR; 6b. OFFICE SYMBOL (If applicable):	7a. NAME OF MONITORING ORGANIZATION: HQ/AFTAC/TTS
6c. ADDRESS (City, State, and ZIP Code): Post Box 51, N-2007 Kjeller, Norway	7b. ADDRESS (City, State, and ZIP Code): Patrick AFB, FL 32925-6001
8a. NAME OF FUNDING/SPONSORING ORGANIZATION: Defence Advanced Research Projects Agency; 8b. OFFICE SYMBOL (If applicable): NMRO	9. PROCUREMENT INSTRUMENT IDENTIFICATION NUMBER: Contract No. F08606-89-C-0005
8c. ADDRESS (City, State, and ZIP Code): 1400 Wilson Blvd., Arlington, VA 22209-2308	10. SOURCE OF FUNDING NUMBERS: PROGRAM ELEMENT NO. R&D; PROJECT NO. NORSAR PHASE 3; TASK NO. SOW TASK 5.0; WORK UNIT ACCESSION NO. SEQUENCE No.003A2

11. TITLE (Include Security Classification)

SEMIANNUAL TECHNICAL SUMMARY, 1 OCTOBER 1988 - 31 MARCH 1989 (UNCLASSIFIED)

12. PERSONAL AUTHOR(S)
L.B. Loughran (ed.)

13a. TYPE OF REPORT	13b. TIME COVERED	14. DATE OF REPORT (Year, Month, Day)	15. PAGE COUNT
SCIENTIFIC SUMMARY	FROM 1 Oct 88 TO 31 Mar 89	July 1989	140

16. SUPPLEMENTARY NOTATION

NOT APPLICABLE

17. COSATI CODES			18. SUBJECT TERMS (Continue on reverse if necessary and identify by block number)
FIELD	GROUP	SUB-GROUP	NORSAR, NORWEGIAN SEISMIC ARRAY
8	11		

19. ABSTRACT (Continue on reverse if necessary and identify by block number)

This Semiannual Technical Summary describes the operation, maintenance and research activities at the Norwegian Seismic Array (NORSAR), NORESS and ARCESS for the period 1 October 1988 - 31 March 1989.

(Continued on reverse side)

20. DISTRIBUTION/AVAILABILITY OF ABSTRACT: ☐ UNCLASSIFIED/UNLIMITED ☐ SAME AS RPT ☐ DTIC USERS	21. ABSTRACT SECURITY CLASSIFICATION: UNCLASSIFIED
22a. NAME OF RESPONSIBLE INDIVIDUAL: MR. LEE BRIDGES	22b. TELEPHONE (Include Area Code): (407) 494-7765; 22c. OFFICE SYMBOL: AFTAC/TTS

DD Form 1473, JUN 86 — Previous editions are obsolete — SECURITY CLASSIFICATION OF THIS PAGE

Abstract (cont.)

The NORSAR Dectection Processing System has been operated throughout the reporting period with an average uptime of 98.2 per cent. A total of 1577 seismic events has been reported in the NORSAR monthly seismic bulletin. The performance of the continuous alarm system and the automatic bulletin transfer by telex to AFTAC has been satisfactory. Processing of requests for full NORSAR/NORESS data on magnetic tapes has progressed according to established schedules.

The satellite link for transmitting NORESS data in real time to the U.S. has had an average uptime of 99.9 per cent. On-line NORESS detection processing and data recording at the NORSAR Data Center (NDPC) has been conducted throughout the period, with an average uptime of 98.5 per cent.

The operation of the ARCESS array in Northern Norway has progressed satisfactorily. The average uptime during the period has been 98.5 per cent. No failures of the satellite transmission line or at the array Hub have been registered.

Field maintenance activity has included regular preventive maintenance at all array sites and occasional corrective actions when required. The NORSAR, NORESS and ARCESS field systems performed generally satisfactorily throughout the reporting period.

A considerable effort has been expended in continuing to upgrade the on-line and off-line detection/event processing software which is being developed at NORSAR for general array applications. The program systems have been tested on data from NORSAR, NORESS, ARCESS, FINESA and Gräfenberg, and the implementation will be coordinated with the Intelligent Array System developments.

As a continuation of previous work, a study has been conducted focusing on the problem of determining accurate yields for explosions at the Shagan River test site. We have analyzed all the events reported by the ISC or NEIC to have occurred at this site between 1965 and 1988, a total of 96 events. As a basis for the yield estimation we have used body-wave magnitude (m_b) determined from global network data as well as two additional explosion source size estimators. The first additional method is the long-term level of the reduced displacement potential, Ψ_∞, measured from the initial explosion-generated P pulse recorded at four UK array stations. The second additional method is based on estimating the energy of the Lg wave train recorded at the NORSAR and Gräfenberg arrays for each explosion. The emphasis of the study is on assessing the combined utility of these three methods to obtain

relative yields of explosions. In addition, the estimation of absolute yields from the available seismic information is addressed, using the cratering explosion of 15 January 1965 for calibration purposes. The study reconfirms conclusions from earlier work regarding variations in m_b-m_{Lg} bias across the Shagan area, and shows that this variation can be correlated with surface geological features.

We have developed and tested a method to use seismic network recordings to continuously monitor the seismic noise field. The purpose is to determine to which extent intefering events affect the monitoring of events within a target region. We develop a model that can be used to obtain, at a given confidence level, a continuous assessment of the upper limit of magnitudes of seismic events in the target region that would go undetected by such a network. An example of application is given using data from the network of three regional arrays, NORESS, ARCESS, FINESA in Fennoscandia. We note that this method would be particularly useful to assess the possible magnitudes of non-detected events during the coda of large earthquakes. The approach could further be used to obtain upper confidence limits on M_s when no surface waves are detected, and this would enhance the applicability of the M_s:m_b discriminant at low magnitudes.

A study has been conducted to model Lg wave propagation from Semipalatinsk to NORSAR, allowing for different structures at the source and receiver sites and assuming a smooth, lateral variation in between. It is shown that Lg spectra modelled in this way vary in amplitude when small realistic variations are introduced in the focal depth or in the crustal structure of the source site. Large amplitude variations, equivalent to up to 0.6 magnitude unit difference, can be expected when source focal depth crosses a layer interface with strong velocity contrasts. The equivalent of 0.2 magnitude unit variations may occur when the crustal structure is modified. On the other hand, no significant variation of spectrum slope or spectral content is observed with such source environment modifications.

The surface topography at both NORESS and ARCESS has been digitized and used to calculate the effects of surface topography with regard to slowness and azimuth anomalies for recorded signals at the arrays. These calculations demonstrate that surface topography can explain about half of the observed anomalies. Further they demonstrate that surface topography can produce not only azimuth anomalies, but also deviations in absolute slowness. It is remarkable that the low-frequency group of events at ARCESS produces larger anomalies than the high-frequency group. Clearly, 3-component slowness solutions depend both on surface topography and on the incident signal spectra.

In conducting a study of anelastic attenuation from intraplate earthquake recordings, we have collected and analyzed 87 earthquake

records from 56 earthquakes occurring in predominantly intraplate areas (North America, Europe, China, Australia). The magnitudes of these events are in the range from M_S 3 to 8, the epicentral distances are from less than 10 to more than 1000 km. This work has included the development of a model for amplitude decay by distance, and discusses in particular the dependence of the Q(f) relations on the model used for geometrical spreading.

Developments within data communications and general analysis software have included the establishment of an X.25-based connection between NORSAR and AFTAC, with the purpose to enable effective, on-line retrieval of NORSAR/NORESS/ARCESS data for events of interest. A new version of an Event Processor package has been implemented, and is currently in use to process NORESS and ARCESS data. It also offers flexibility for interactive analysis for research and evaluation purposes.

An initial study of Lg recordings from recent Soviet explosions has been conducted using data from four modern stations recently installed in the Soviet Union by IRIS. While it is too early to state any firm conclusions, some preliminary results can be summarized: a) the IRIS stations provide a much improved signal-to-noise ratio for events near Semipalatinsk as compared to NORSAR, b) the scaling of RMS Lg amplitudes between different sized events recorded at the same IRIS site appears to be consistent with that of NORSAR, c) a possibility of reduced scatter in RMS Lg measurements at single sites may be accomplished by averaging the three-component recordings, and d) RMS Lg amplitudes may be made to about 1.5 magnitude units lower than at NORSAR or Gräfenberg allowing a much lower threshold for yield determination. However, for large explosions, it must still be expected that the array averaging procedure offered by NORSAR and Gräfenberg will produce the most stable estimates.

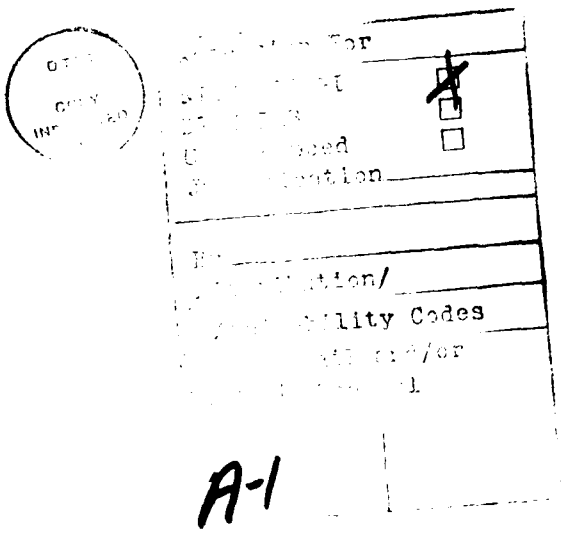

AFTAC Project Authorization	:	T/9141/B/PKP
ARPA Order No.	:	4138 AMD # 16
Program Code No.	:	0F10
Name of Contractor	:	Royal Norwegian Council for Scientific and Industrial Research
Effective Date of Contract	:	1 October 1988
Contract Expiration Date	:	30 September 1989
Project Manager	:	Frode Ringdal (06) 81 71 21
Title of Work	:	The Norwegian Seismic Array (NORSAR) Phase 3
Amount of Contract	:	$ 1,902,447
Contract Period Covered by Report	:	1 Oct 1988 - 31 Mar 1989

This research was supported by the Advanced Research Projects Agency of the Department of Defense and was monitored by AFTAC, Patrick AFB, FL 32925, under contract no. F08606-89-C-0005.

NORSAR Contribution No. 408

TABLE OF CONTENTS

TABLE OF CONTENTS
(cont.)

I. SUMMARY

This Semiannual Technical Summary describes the operation, maintenance and research activities at the Norwegian Seismic Array (NORSAR), Norwegian Regional Seismic Array (NORESS) and the Arctic Regional Seismic Array (ARCESS) for the period 1 October 1988 - 31 March 1989.

The NORSAR Detection Processing System has been operated throughout the reporting period with an average uptime of 98.2 per cent, which is the same as for the previous period. A total of 1577 seismic events have been reported in the NORSAR monthly seismic bulletin. The performance of the continuous alarm system and the automatic bulletin transfer by telex to AFTAC has been satisfactory. Processing of requests for full NORSAR/NORESS data on magnetic tapes has progressed according to established schedules.

The satellite link for transmitting NORESS data in real time to the U.S. has had an average uptime of 99.9 per cent. On-line detection processing and data recording at the NORSAR Data Center (NDPC) of NORESS and ARCESS data have been conducted throughout the period, with an average uptime of 98.5 per cent for both systems.

Field maintenance activity has included regular preventive maintenance at all array sites and occasional corrective actions when required. All the NORSAR communications systems have been checked during the period, including line measurements and cable repair. The performance of the NORESS field equipment has been generally good. During a visit to ARCESS in October 1988, it was found that the modification of the fiber optical system carried out in June 1988 had drifted too much and caused high failure rate, spikes and total loss of data from some of the remote sites. Sandia Laboratories were informed and will report to the manufacturer of the fiber optical transmitter and receiver units about our experience.

New equipment to sample and acquire seismic data is continuously being studied to find suitable solutions for a possible upgrade of NORSAR.

The new event processor package has been tested on NORSAR detections to produce event plots. This has been tested using SUN-UNIX workstations.

NORESS detection processing has been running satisfactorily on the SUN-UNIX system using the RONAPP 20 beam recipe. Parallel to the routine event processing on the IBM equipment, updated event processing on the UNIX systems has been performed. The new event processing is performed in two steps: phase estimation and epicenter determination.

Regular online detection processing for ARCESS has been performed on the SUN system since day 223, 1988. The number of detections on the ARCESS array is significantly higher than for the NORESS array. The phase estimation procedure of the new event processor has been in operation for the ARCESS array since day 365, 1988.

The research activity is summarized in Section VII. Section VII.1 focuses on the problem of determining accurate yields for a set of Soviet underground nuclear explosions at the Shagan River test site. Section VII.2 addresses the problem of using a network to continuously monitor seismic event detection capability. In section VII.3 results from a study on the variability of explosion Lg spectra with near-source structure and focal depth are presented. Section VII.4 is a study of surface topographic effects at NORESS and ARCESS. Section VII.5 discusses anelastic attenuation from intraplate earthquake recordings. An X.25-based communication link between NORSAR and AFTAC is discussed in section VII.6. The new Event Processor program package is presented in section VII.7. Results of an analysis of IRIS data for Soviet nuclear explosions are presented in section VII.8.

II. NORSAR OPERATION

II.1 Detection Processor (DP) Operation

There have been 102 breaks in the otherwise continuous operation of the NORSAR online system within the current 6-month reporting interval. The uptime percentage for the period is 98.2 which is the same as for the previous period.

Fig. II.1.1 and the accompanying Table II.1.1 both show the daily DP downtime for the days between 1 October 1988 and 31 March 1989. The monthly recording times and percentages are given in Table II.1.2.

The breaks can be grouped as follows:

a)	Hardware failure	13
b)	Stops related to program work or error	1
c)	Hardware maintenance stops	5
d)	Power jumps and breaks	5
e)	TOD error correction	25
f)	Communication lines	53

The total downtime for the period was 76 hours and 31 minutes. The mean-time-between-failures (MTBF) was 1.8 days, as compared to 3.3 for the previous period.

J. Torstveit

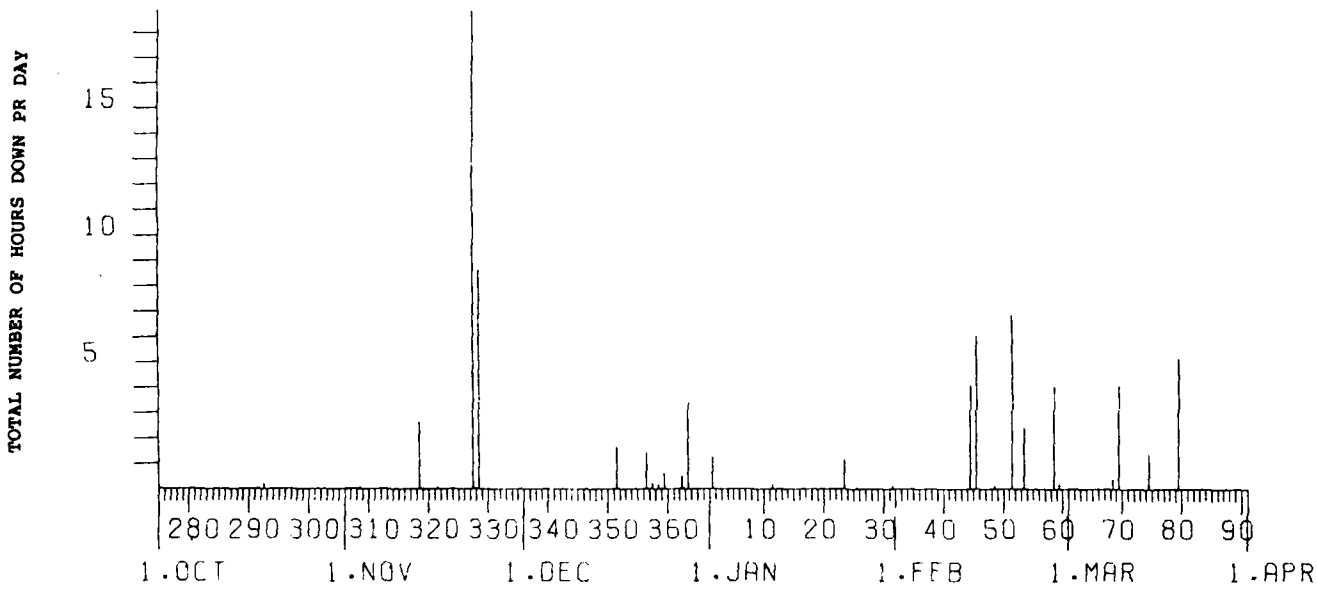

Fig. II.1.1. Detection Processor downtime in the period 1 October 1988 - 31 March 1989.

LIST OF BREAKS IN DP PROCESSING THE LAST HALF-YEAR

DAY	START		STOP		COMMENTS.....	DAY	START		STOP		COMMENTS.....
275	10	40	10	42	LINE FAILURE	25	7	17	7	18	LINE FAILURE
280	7	9	7	10	TOD RETARED 9MS	31	6	13	6	14	TOD RETARED 12MS
284	7	1	7	2	TOD RETARED 10MS	31	6	22	6	23	LINE FAILURE
286	7	5	7	6	LINE FAILURE	31	6	26	6	27	LINE FAILURE
288	7	1	7	2	TOD RETARED 20MS	31	6	32	6	33	LINE FAILURE
291	7	1	7	2	LINE FAILURE	31	6	36	6	37	LINE FAILURE
292	14	34	14	48	POWER BREAK	31	6	40	6	41	LINE FAILURE
300	7	0	7	2	TOD RETARED 20MS	31	6	48	6	49	LINE FAILURE
301	9	19	9	20	LINE FAILURE	31	6	53	6	54	LINE FAILURE
302	8	9	8	10	LINE FAILURE	33	7	2	7	3	TOD RETARED 11MS
306	7	1	7	2	TOD RETARED 12MS	37	6	27	6	29	TOD RETARED 12MS
308	7	19	7	20	LINE FAILURE	44	6	30	6	31	TOD RETARED 10MS
308	7	25	7	26	LINE FAILURE	44	6	44	6	45	LINE FAILURE
308	7	31	7	32	LINE FAILURE	44	6	48	6	49	LINE FAILURE
308	7	37	7	38	LINE FAILURE	44	6	58	6	59	LINE FAILURE
308	7	43	7	44	LINE FAILURE	44	7	5	7	6	LINE FAILURE
313	14	45	14	46	LINE FAILURE	44	20	0	24	0	LINE FAILURE (01A OK)
313	14	49	14	50	LINE FAILURE	45	0	0	6	3	LINE FAILURE (01A OK)
313	14	56	14	57	LINE FAILURE	48	7	3	7	4	TOD RETARED 20MS
314	7	1	7	2	TOD RETARED 23MS	48	7	12	7	13	LINE FAILURE
318	7	26	10	4	POWER BREAK	48	7	19	7	20	LINE FAILURE
321	10	28	10	29	LINE FAILURE	48	7	23	7	24	LINE FAILURE
321	10	32	10	33	LINE FAILURE	48	7	28	7	29	LINE FAILURE
321	10	37	10	38	LINE FAILURE	48	7	36	7	37	LINE FAILURE
321	10	47	10	48	LINE FAILURE	48	7	41	7	42	LINE FAILURE
321	10	53	10	54	LINE FAILURE	51	15	40	21	45	WORK ON NO-BRAKE POWER
327	5	5	24	0	MODCOMP FAILURE	51	21	45	22	30	CPU FAILURE
328	0	0	8	35	MODCOMP FAILURE	53	2	13	2	59	CPU FAILURE
328	9	30	9	31	LINE FAILURE	53	7	5	8	42	CPU FAILURE
335	7	4	7	5	TOD RETARED 13MS	55	7	1	7	3	TOD RETARED 11MS
342	7	2	7	3	TOD RETARED 20MS	58	2	40	6	43	CPU FAILURE
348	7	8	7	9	TOD RETARED 12MS	59	6	12	6	13	LINE FAILURE
351	6	5	7	44	CPU FAILURE	59	6	19	6	20	LINE FAILURE
356	12	47	12	48	TOD RETARED 20MS	59	6	24	6	25	LINE FAILURE
356	14	45	16	8	MODCOMP FAILURE	59	6	28	6	29	LINE FAILURE
357	7	0	7	14	CE MAINTENANCE CPU	59	6	32	6	33	LINE FAILURE
358	15	0	15	11	CPU FAILURE	59	6	36	6	37	LINE FAILURE
359	10	11	10	48	CPU FAILURE	59	6	56	6	57	LINE FAILURE
362	8	19	8	50	CE MAINTENANCE CPU	59	7	1	7	2	TOD RETARED 13MS
363	8	25	10	36	CE MAINTENANCE CPU	59	7	6	7	7	LINE FAILURE
363	11	45	12	58	CPU FAILURE	59	7	11	7	13	LINE FAILURE
364	8	21	8	22	TOD RETARED 14MS	62	7	6	7	7	TOD RETARED 11MS
1	10	39	11	54	DP SOFTWARE	67	7	5	7	6	LINE FAILURE
5	7	0	7	1	TOD RETARED 20MS	68	7	3	7	4	TOD RETARED 20MS
11	9	33	9	43	CE MAINTENANCE	68	14	34	14	35	LINE FAILURE
16	7	1	7	2	TOD RETARED 15MS	68	23	39	24	0	POWER FAILURE
19	7	2	7	3	TOD RETARED 11MS	69	0	0	4	3	POWER FAILURE
19	7	6	7	7	LINE FAILURE	74	10	19	10	55	CPU FAILURE
19	7	20	7	21	LINE FAILURE	74	14	23	14	39	CE MAINTENANCE
23	10	33	11	41	POWER FAILURE	74	14	46	15	17	CPU FAILURE
25	7	1	7	2	TOD RETARED 13MS	79	10	12	10	53	CPU FAILURE
25	7	7	7	8	LINE FAILURE	79	11	16	15	44	CPU FAILURE
25	7	13	7	14	LINE FAILURE	87	7	8	7	9	TOD RETARED 30MS

Table II.1.1. Daily DP downtime in the period 1 October 1988 - 31 March 1989.

Month	DP uptime hours	DP uptime %	No. of DP breaks	No. of days with breaks	DP MTBF* (days)
OCT	743.58	99.9	10	10	2.8
NOV	689.58	95.8	19	9	1.4
DEC	735.93	98.9	12	10	2.4
JAN	741.15	99.6	20	8	1.5
FEB	648.25	96.5	30	10	0.9
MAR	732.98	98.5	11	7	2.5
		98.2	102	54	1.8

*Mean-time-between-failures = total uptime/no. of up intervals.

Table II.1.2. Online system performance, 1 October 1988 - 31 March 1989.

II.2 Array communications

Table II.2.2 reflects the performance of the communications system throughout the reporting period. The performance of the system was most satisfactory in October and November, although 02C and 06C failed weeks 43 and 48, respectively. 02B has been affected over periods between December 1988 and March 1989 due to lack of power to the subarray and a bad cable.

We have in the period also experienced too many system resynchronizations. A test program was initiated by the end of February. This test revealed reduced line quality, including low levels, a bad cable and faulty modem AHS-cards.

Communications systems at 01B, 03C and 06C have been turned off one by one over days, in order to see possible changes in the resynchronization pattern.

October (weeks 40-43), 3 - 30.10.88
02C communications systems failed week 43 due to a faulty line towards the CTV. The downtime was approximately 21.1 hours.

06C was affected by an intermittently operating communications line weeks 40,41. Downtime was 12 / 54.2 hours, respectively.

Otherwise excellent performance that period.

November (weeks 44-48), 31.10 - 4.12.88
The communications machine (Modcomp) was down between 22 and 23 November due to a faulty power supply.

The performance of most subarray communications systems was excellent also this period, an exception was 06C which was affected week 48 (equaled 0.5% degradation).

December (weeks 49-52), 5.12.1988 1.1.89

Bad figures that period with regard to 02B which was down for more than 55% of week 51, and 100% week 52. This time the outage was caused by a broken power line.

02C-06C were affected week 51, resulting in an average error figure of 1.83 %.

Week 52 all communications systems were affected (-02B which was down), and the average error figure was approx. 0.31 %.

January (weeks 1-4), 2 - 29.1.89

Apart from a period between 3 and 9 January (week 1) 02B remained down until 27 January, after trees were removed from the power line.

Average error figures week 1 were 0.13 % (-02B), caused by too many resynchronizations of the systems, which again probably were caused by one or two systems with reduced performance.

Apart from 02B (lack of power) and 06C (week 3), the system performance was satisfactory (weeks 2, 3 and 4).

February (weeks 5-8), 30.1 - 5.2.89

All NORSAR communications systems were frequently affected weeks 5, 6 and 7, apart from 01A / 01B week 5, and 01A week 7.

02B, which resumed operation 27 January, went down again 30 January and remained so until 8 February.

In connection with the start of a test program involving all subarrays, 02B was visited 28 February. The modem "Loop Control Logic" was manually forced to analog and digital loop while transmitting 511 bit (pseudo random pattern) from NDPC through the loop and back. Analog loop indicated reduced performance with a calculated error rate of 6.8×10^{-4}, which for the digital loop was calculated to 5.7×10^{-5}.

In addition, 01B, 03C and 06C had high error figures, mainly in conjunction with NDPC tests to see if any of the three subarrays caused the many resynchronizations, but also due to "real" outages at 06C.

March (weeks 9-17), 27.2 - 5.3.89

During March the remaining subarrays were visited in connection with loop test, but also other subarray-related jobs were carried out.

NTA/Lillestrøm improved the conditions between Kjeller and Lillestrøm, as a bad cable loaded the 02B modem output heavily.

NTA/Hamar made corrections to the 01B, 03C input levels, and the AHS-cards in 01A, 06C modems were replaced. The above-mentioned corrections improved the communications system performance significantly from week 11.

O.A. Hansen

Sub-array	1988 OCT (4) (4.4-1.5)	NOV (5) (2.5-5.6)	DEC (4) (6.6-3.7)	JAN (4) (4-31.7)	1989 FEB (4) (1.8-5.9)	MAR (5) (5.9-2.10)	AVERAGE 1/2 YEAR
01A	0.05	0.02	0.10	0.05	1.39	0.06	0.28
01B	0.18	0.02	0.08	0.04	*4) 1.83	0.05	0.37
02B	0.06	0.03	*3) 0.02	*79.14	*5) 2.72	*8) 1.25	10) 0.82
02C	*1) 0.05	0.02	0.58	0.05	3.17	0.77	0.77
03C	0.06	0.02	0.54	0.06	*6) 2.41	0.75	0.64
04C	0.06	0.02	0.53	0.05	3.16	2.19	1.00
06C	*2) 0.20	0.11	0.51	0.83	*7) 4.59	*9) 0.001	1.04
AVER	0.09	0.03	0.34	0.18	2.75	0.72	0.70
LESS				02B			

* See Section II.2 regarding figures preceded by an asterisk.
Figures representing error rate (in per cent) preceded by a number 1), 2), etc., are related to legend below.

1) Average 3 weeks, week 43 N/A
2) -"- 2 weeks, weeks 41,41 N/A
3) -"- 2 weeks, weeks 51,52 N/A
4) -"- 3 weeks, week 7(89) N/A
5) -"- 2 weeks, weeks 5,6 N/A
6) Average 3 weeks, week 6 N/A
7) -"- 3 weeks, week 7 N/A
8) -"- 3 weeks, weeks 10,11 N/A
9) -"- 3 weeks, weeks 9,10 N/A
10) -"- 5 months, weeks 1,2,3,4 N/A

Table II.2.1 Communications performance. The numbers represent error rates in per cent based on total transmitted frames/week (1 October 1988 - 31 March 1989).

II.3 Event Detection operation

In Table II.3.1 some monthly statistics of the Detection and Event Processor operation are given. The table lists the total number of detections (DPX) triggered by the on-line detector, the total number of detections processed by the automatic event processor (EPX) and the total number of events accepted after analyst review (Teleseismic phases, core phases and total).

	Total DPX	Total EPX	Accepted events P-phases	Core Phases	Sum	Daily
OCT 88	12450	1334	214	59	273	8.8
NOV 88	12900	1248	219	62	281	9.4
DEC 88	12907	1168	200	44	244	7.9
JAN 89	12924	1647	234	35	269	8.7
FEB 89	11050	1505	182	52	234	8.4
MAR 89	13350	1523	223	53	276	8.9
			1272	305	1577	8.7

Table II.3.1 Detection and Event Processor statistics, October 1988 - March 1989.

B.Kr. Hokland

III. OPERATION OF NORESS AND ARCESS

III.1 Satellite transmission of NORESS data to the U.S.

The satellite transmission of data to the U.S. from the NORESS field installation has been very stable. As can be seen from Table III.1.1, there have been only two unplanned outages in the period.

3 Oct	1431 to	1432	power break
9 Oct	0800 to	1200	power break
24 Oct	0010 to	0011	test requested by Intelsat
24 Oct	0950 to	0951	test requested by Intelsat
6 Dec	1151 to	1200	adjusting transmitter
29 Mar	1100 to	1215	working on the UPS in HUB

Table III.1.1. Outage period for NORESS satellite transmission system October 1988 - March 1989.

The total uptime for the NORESS Earth Station for satellite transmission of data to the U.S. was 99.9% as compared to 99.3% for the previous period.

III.2 Recording of NORESS data at NDPC, Kjeller

As can be seen from Table III.2.1, the main reasons for most of the NORESS outages can be placed under the following four groups: Transmission line failure, power failure at HUB, power failure at NDPC and hardware maintenance or failure.

The average recording time was 98.5% as compared to 97.8% for the previous period.

Date	Time	Duration	Cause
1 Oct	2111-2136	25 m	Transmission line failure
3 Oct	1431-	9 h 29 m	Transmission line failure
4 Oct	-0552	5 h 52 m	Transmission line failure
4 Oct	0942-0952	10 m	Hardware failure at NDPC
4 Oct	1051-1128	37 m	Hardware failure at NDPC
4 Oct	1403-1435	32 m	Hardware failure at NDPC
9 Oct	0659-1203	5 h 04 m	Power failure at HUB
12 Oct	2017-2054	37 m	Transmission line failure
13 Oct	1137-1142	5 m	Transmission line failure
13 Oct	1148-1204	16 m	Transmission line failure
16 Oct	2306-2340	34 m	Transmission line failure
17 Oct	0951-0958	7 m	Transmission line failure
18 Oct	1434-1500	26 m	Power failure at NDPC
28 Oct	1959-	4 h 1 m	Transmission line failure
29 Oct	-1134	11 h 34 m	Transmission line failure
31 Oct	2106-2140	34 m	Transmission line failure
31 Oct	2334-	26 m	Transmission line failure
1 Nov	-0006	6 m	Transmission line failure
9 Nov	0346-0548	2 h 2 m	Hardware failure NDPC
13 Nov	0726-0903	1 h 37 m	Power failure at NDPC
13 Nov	1142-1146	4 m	System test at NDPC
13 Nov	1336-1456	1 h 20 m	System test at NDPC
5 Dec	1346-1354	8 m	Hardware maintenance at NDPC
14 Dec	0854-0926	32 m	Transmission line failure
21 Dec	0608-0726	1 h 18 m	Transmission line failure
1 Jan	1055-1100	5 m	System work
5 Jan	1406-1408	2 m	Transmission line failure
10 Jan	1434-1445	11 m	Transmission line failure
11 Jan	0912-0932	20 m	Hardware maintenance at NDPC
17 Jan	1829-1943	1 h 14 m	Transmission line failure
18 Jan	1049-1054	4 m	Hardware maintenance at NDPC

19 Jan	1029-1038	9 m	Transmission line failure
20 Jan	0642-0652	10 m	Transmission line failure
23 Jan	1033-1150	1 h 17 m	Power failure at NDPC
23 Jan	1204-1344	1 h 40 m	Power failure at NDPC
24 Jan	1021-1103	42 m	Transmission line failure
20 Feb	1541-2144	6 h 3 m	Installing UPS at NDPC
28 Feb	1602-1741	1 h 39 m	Transmission line failure
9 Mar	2304-	56 m	Power failure at NDPC
10 Mar	-0410	4 h 10 m	Power failure at NDPC

Table III.2.1. Interruptions in NORESS recordings at NDPC, October 1988 - March 1989.

Monthly uptimes for the NORESS on-line data recording task, taking into account all factors (field installations, transmissions line, data center operation) affecting this task were as follows:

October	:	94.6%
November	:	99.3%
December	:	99.7%
January	:	99.3%
February	:	98.9%
March	:	99.3%

Fig. III.2.1 shows the uptime for the data recording task, or equivalently, the availability of NORESS data in our tape archive, on a day-by-day basis, for the reporting period.

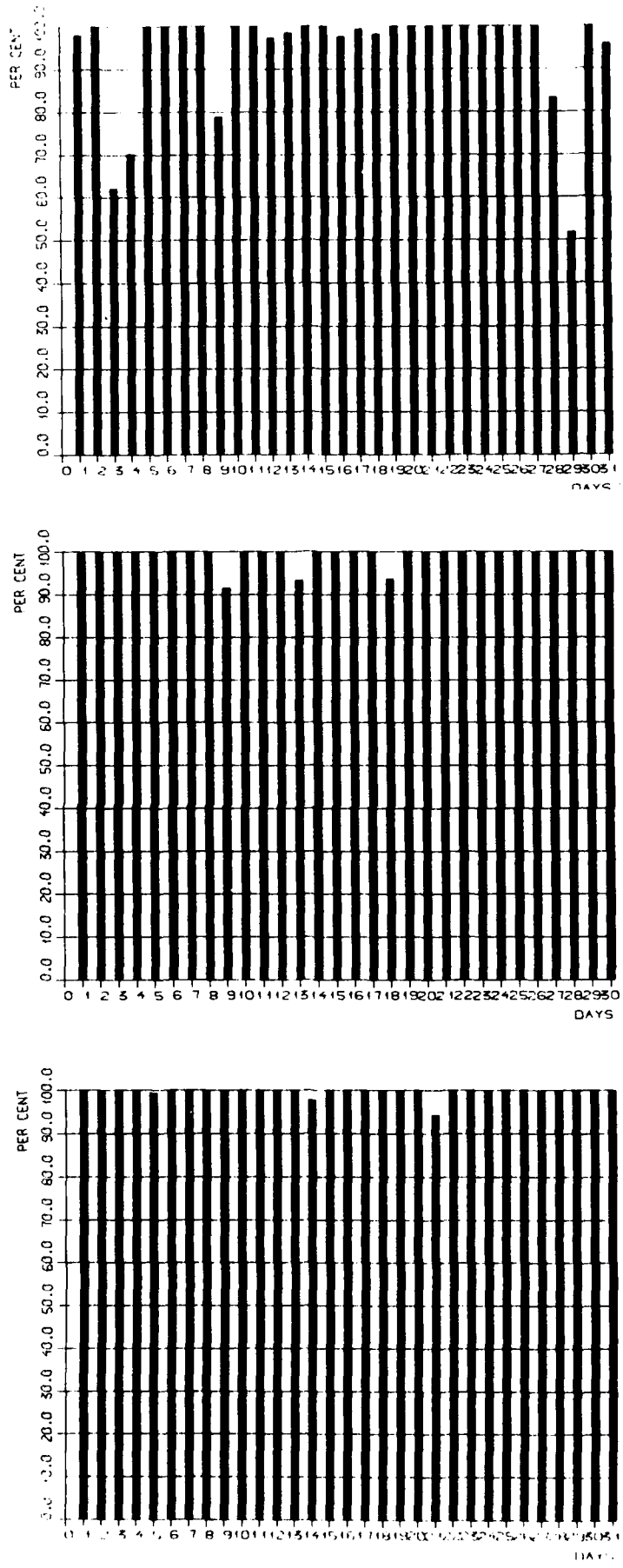

Fig. III.2.1. NORESS data recording uptime for October (top), November (middle) and December 1988 (bottom).

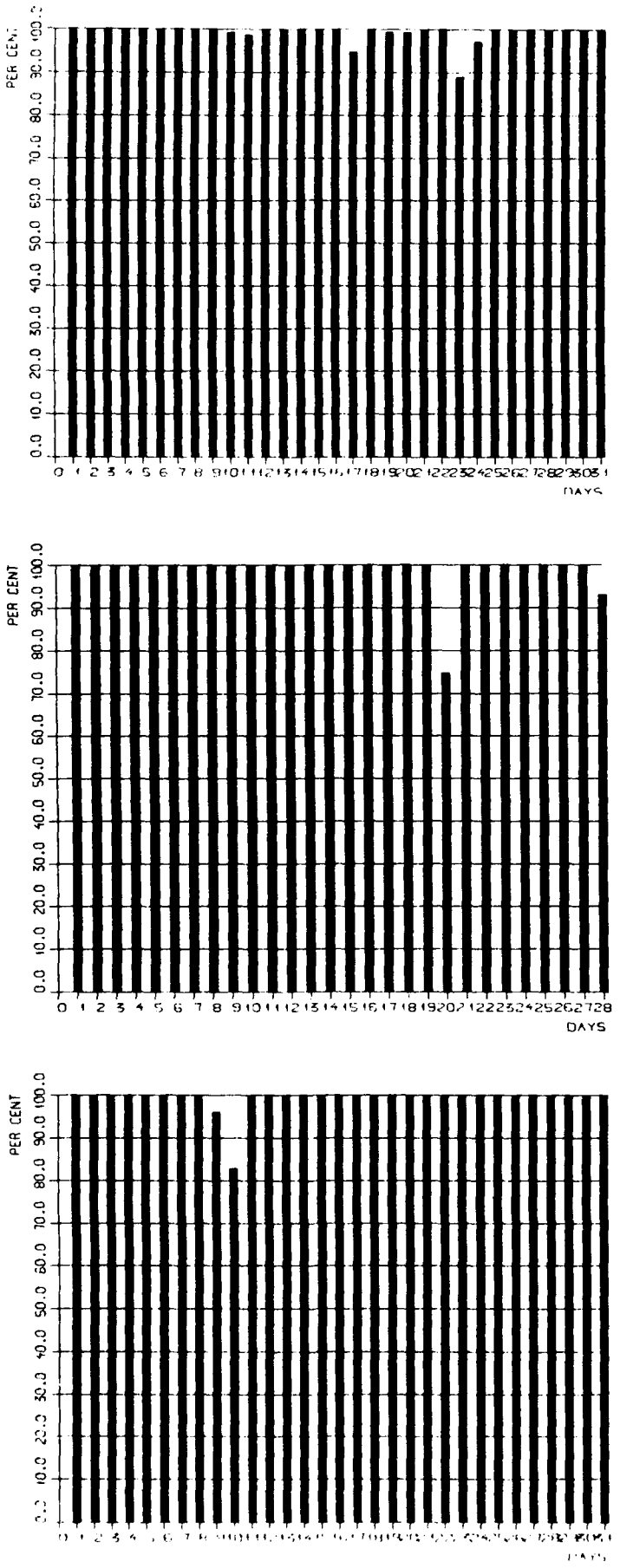

Fig. III.2.1. (cont.) NORESS data recording uptime for January (top), February (middle) and March 1989 (bottom).

III.3 Recording of ARCESS data at NDPC, Kjeller

The main reason causing most of the ARCESS outage in the period are: Power failure at NDPC, Hardware failure at NDPC, Hardware or software work at NDPC. No failures at the HUB or transmission line have been registered.

The average recording time was 98.5% as compared to 77.2% for the previous period.

Monthly uptimes for the ARCESS on-line data recording task, taking into account all factors (field installations, transmissions line, data center operation) affecting this task were as follows:

October	:	99.2%
November	:	98.8%
December	:	97.2%
January	:	97.8%
February	:	99.0%
March	:	98.8%

Fig. III.3.1 shows the uptime for the data recording task, or equivalently, the availability of ARCESS data in our tape archive, on a day-by-day basis, for the reporting period.

J. Torstveit

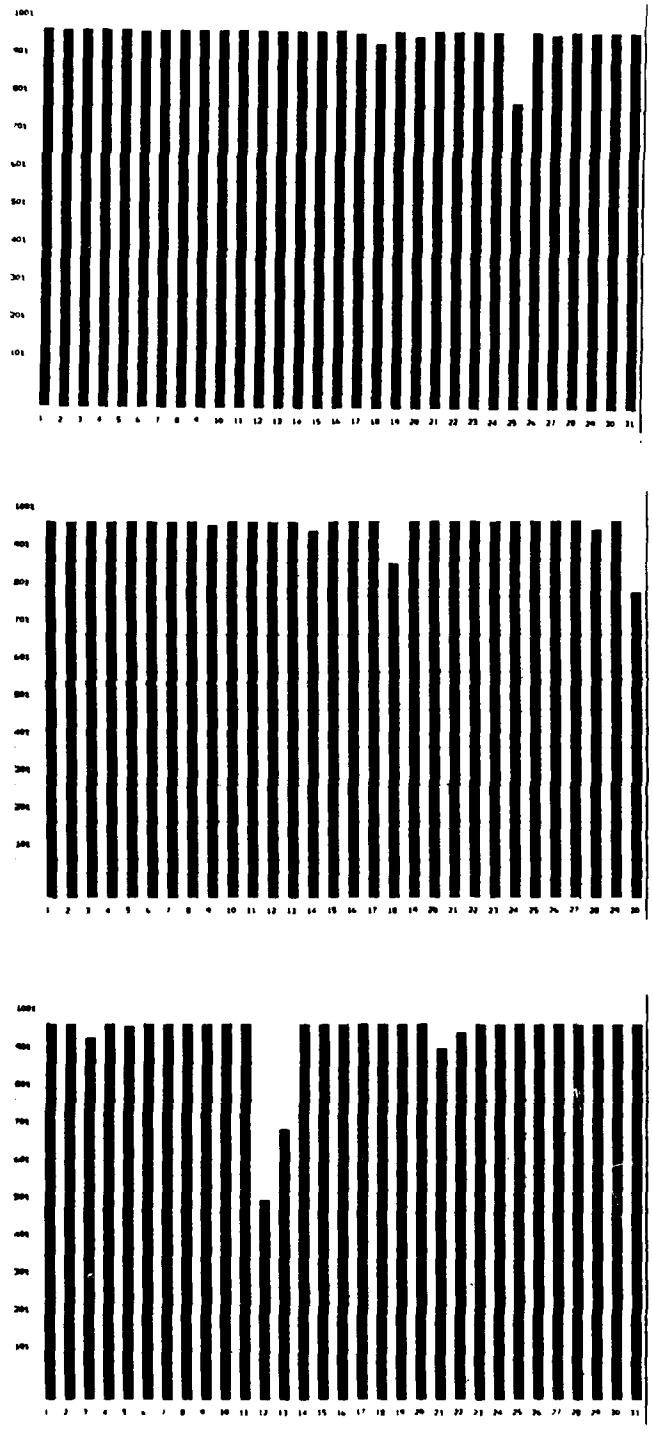

Fig. III.3.1. ARCESS data recording uptime for October (top), November (middle) and December 1988 (bottom).

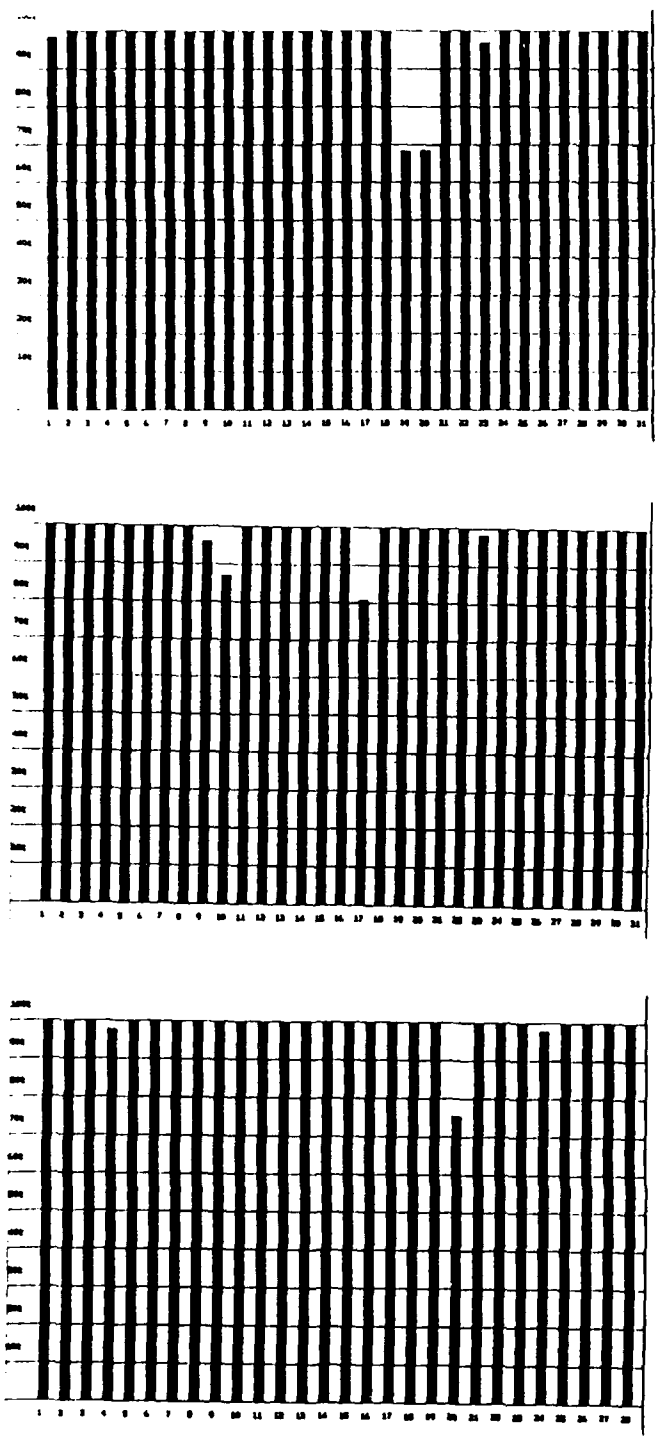

Fig. III.3.1. ARCESS data recording uptime for January (top), February (middle) and March 1989 (bottom).

IV. IMPROVEMENTS AND MODIFICATIONS

IV.1 The NORSAR system

IV.1.1 MODCOMP subarray communication

No modification has been done to the MODCOMP system. The MODCOMP system communicates with the NORSAR subarrays and with the IBM acquisition and processing system.

New equipment to sample and acquire seismic data is continuously being studied. The equipment and architecture of the NORESS/ARCESS, GERESS and FINESA systems has been evaluated with respect to cost and flexibility. NORSAR has developed an SDLC communications interface to SUN systems for direct buffered communication over satellite or land lines. Moreover, analog to digital conversions using PC and VME-based workstation systems have been tested. These studies will be continued to find suitable solutions for a possible upgrade of the NORSAR array to an up-to-date status.

IV.1.2 NORSAR Detection processing

The NORSAR detection processor has been running satisfactorily on the IBM during this reporting period. Detection statistics are given in section II.3.

IV.1.3 NORSAR Event processing

There are no changes in the routine processing of NORSAR events, using the IBM system.

The new event processor package has been tested on NORSAR detections to produce event plots. This has been tested using SUN-UNIX workstations. NORSAR detection lists are accessible through the network, and data

are transferred using ftp. A mail is sent to the IBM system, and data from the NORSAR array are transferred according to the request.

To fully use the NORSAR array for location we need time delay corrections, which have been difficult to convert to the SUN/UNIX system.

IV.2 The NORESS system

IV.2.1 NORESS detection processing

The NORESS detection processing has been running statisfactorily on the SUN/UNIX system using the RONAPP 20 beam recipe. This has been running in parallel with the IBM processing. The number of detections reported from day 027, 1989, through day 090, 1989, was 9711, giving an average of 164 detections per processed day. This was using the RONAPP beam set of 17 coherent beams and 3 incoherent beams. Note that if both coherent and incoherent beams detect the same phase, two detections are reported. This fact does not give an error in the statistics, as such reports are small in numbers. Moreover, experience has shown that a larger beam set would give even more detections.

IV.2.2 NORESS event processing - Phase estimation

There have been no changes in the routine NORESS event processing.

Parallel to the routine processing on the IBM equipment, we have performed updated event processing on the UNIX systems.

The new event processing is performed in two steps. In step 1, all detections are subjected to broadband f-k, polarization, and onset analysis, called phase estimation. Step 1 analysis results in one file per day, e.g., NRS89090.FKX, indicating f-k analysis report (.FKX) for NORESS (NRS), day 090, 1989. The report files give onset time, detection beam, SNR, velocity, preliminary phase name, azimuth,

coherency, quality of f-k, frequency, amplitude, detection STA and polarization results.

This step one processing is performed together with detection processing and data acquisition on the SUN-3/280 for NORESS. This load of processing with 20 beams, is acceptable for the SUN-3. The communication with the NORESS array is through the NORSAR buffered SDLC interface.

FKX files has been produced on a regular basis since day 028, 1989.

IV.2.3 NORESS event processing - Epicenter determination

In step two of the new event processing, all phases from one array are analyzed for association to events. This processing is described in some detail in chapter VII.7. The location analysis results in one file per day, e.g., NRS89090.EPX, indicating event analysis report (.EPX) for NORESS (NRS), day 090, 1989. EPX files have been produced on a regular basis since day 038, 1989. All 'interesting' phases are plotted on an Imagen postscript laser printer, and such plotting has been performed on a regular basis since day 051, 1989.

Where a minimum of two phases (at least one P and one S) have been associated, we have located the event with the TTAZLOC procedure. During days 038 through 090 there were 454 events, giving on the average 12.6 events per processed day. (36 days processed).

IV.3 The ARCESS system

IV.3.1 ARCESS detection processing

Regular 'online' detection processing has been performed on the SUN system since 1988, day 223. See Table IV.3.1 for the RONAPP 20 beam recipe that has been used during this time period. A detailed descrip-

tion of the input command file for the detector program is given in NORSAR Scientific Report No. 2-86/87.

The number of detections on the ARCESS array is significantly higher than for the NORESS array. The number of detections reported during day 275, 1988, through day 090, 1989, was 45113, giving an average of 247 detections per processed day. This was obtained using the same beam set as for NORESS.

IV.3.2 ARCESS event processing - Phase estimation

The phase estimation procedure of the new event processor, has been in operation for the ARCESS array since day 365, 1988.

Phase analysis results in one file per day, e.g., FRS89090.FKX, indicating f-k analysis report (.FKX) for ARCESS (FRS,ARC), day 090, 1989. We note here that the ARCESS array in the future will be identified as ARC, instead of FRS.

This step one processing is performed together with detection processing and data acquisition on the SUN-3/280 for ARCESS. This load of processing with 20 beams, is close to the limit of the system's capacity. Numerous network problems have occurred. The communication with the ARCESS array is through the Science Horizons 'white box' via the DCP interface. This DCP interface is causing problems on the VME bus, and thus the ARCESS system has a lower capacity than the NORESS system. The problem is currently being looked into by Science Horizons.

IV.3.3 ARCESS event processing - Epicenter determination

The location analysis results in one file per day, e.g., FRS89090.EPX, indicating event analysis report (.EPX) for ARCESS (FRS,ARC), day 090, 1989. EPX files has been produced on a regular basis since day 072,

1989. All 'interesting' phases are plotted on an Imagen postscript laser printer, and such plotting has been performed on regular basis since day 074, 1989.

Where a minimum of two phases have been associated, we have located the event with the TTAZLOC procedure. During days 074 through 090 there were 193 located events, giving on an average 11.3 events per processed day. (17 days processed).

IV.3.4 'Funny little events' - FLE in the ARCESS array

Analysis of the data from ARCESS has shown peculiar events of the type shown in Fig. IV.3.1. The signals look like an event close to one of the sensors (D6), but there is no moveout, no delay between the signals as recorded on different sensors. The 'signals' could at times affect almost half of the 33 short period sensors. These 'events' were found to be generated by high frequency noise in the power cables going from the HUB to each remote site. The noise was fed through the ground-wire and down into the concrete pad on which the seismometers are emplaced, thus creating a real ground motion picked up by the seismometers. Seismometers on specially wet sites were affected the most. In order to get rid of these 'events' it was decided to open the ground wire at all remote sites, i.e., the remote sensors now have a common earth ground.

J. Fyen
P.W. Larsen

```
* ARCESS 'RONAPP' 20 beam recipe.
 * This beam-set was started on the UNIX ARCESS system on day 211,
1988.
 * It was running up to day 130, 1989.
 *
 DATA_BUFFER_LENGTH  60.0 SECONDS
 OLD_BUFFER_LENGTH    5.0 SECONDS
 *
 INPUT_THE_FOLLOWING_STATIONS:
  FRS__s
 END_INPUT_STATIONS
 *
 SET_REFERENCE FRS_A0_sz
 SET_REDUCTION      2.000 Seconds
 SET_GROUPING       6.000 Seconds
 SET_INITIAL_LTA   17.000
 SET_THRESHOLD      4.000
 SET_STX_LENGTH     0.250 Seconds
 SET_STA_LENGTH     1.000 Seconds
 SET_LTA_SIGMA      6.000
 SET_LTA_BETA       6.000
 SET_LTA_DELAY      5.000 Seconds
 *
 FILTER_TABLE_FOLLOW:
 FILTER  FILNAM   FILTER FLTTYP BANDLW BANDHG IORD
      1  FB2      BU     BP      1.0    3.0     3
      2  FB3      BU     BP      1.5    3.5     3
      3  FB4      BU     BP      2.0    4.0     3
      4  FB5      BU     BP      2.5    4.5     3
      5  FB6      BU     BP      3.0    5.0     3
      6  BP41     BU     BP      4.0    8.0     3
      7  BP42     BU     BP      8.0   16.0     3
      8  BP60     BU     BP      1.0    2.0     2
      9  BP61     BU     BP      2.0    3.0     2
 END_FILTER_TABLE
 *
 FILTER  FRS_A0_sz  WITH FB4 OUTPUT A0FB4
 FILTER  FRS_D1_sz  WITH FB4 OUTPUT D1FB4
 FILTER  FRS_D2_sz  WITH FB4 OUTPUT D2FB4
 FILTER  FRS_D3_sz  WITH FB4 OUTPUT D3FB4
 FILTER  FRS_D4_sz  WITH FB4 OUTPUT D4FB4
 FILTER  FRS_D5_sz  WITH FB4 OUTPUT D5FB4
 FILTER  FRS_D6_sz  WITH FB4 OUTPUT D6FB4
 FILTER  FRS_D7_sz  WITH FB4 OUTPUT D7FB4
 FILTER  FRS_D8_sz  WITH FB4 OUTPUT D8FB4
 FILTER  FRS_D9_sz  WITH FB4 OUTPUT D9FB4
 *
 *
 FILTER  FRS_A0_sz  WITH BP60 OUTPUT A0BP60
 FILTER  FRS_C1_sz  WITH BP60 OUTPUT C1BP60
 FILTER  FRS_C2_sz  WITH BP60 OUTPUT C2BP60
 FILTER  FRS_C3_sz  WITH BP60 OUTPUT C3BP60
 FILTER  FRS_C4_sz  WITH BP60 OUTPUT C4BP60
 FILTER  FRS_C5_sz  WITH BP60 OUTPUT C5BP60
 FILTER  FRS_C6_sz  WITH BP60 OUTPUT C6BP60
 FILTER  FRS_C7_sz  WITH BP60 OUTPUT C7BP60
 *
```

Table IV.3.1 RONAPP 17 coherent plus 3 incoherent beams.

```
 FILTER  FRS_A0_sz  WITH BP61 OUTPUT A0BP61
 FILTER  FRS_C1_sz  WITH BP61 OUTPUT C1BP61
 FILTER  FRS_C2_sz  WITH BP61 OUTPUT C2BP61
 FILTER  FRS_C3_sz  WITH BP61 OUTPUT C3BP61
 FILTER  FRS_C4_sz  WITH BP61 OUTPUT C4BP61
 FILTER  FRS_C5_sz  WITH BP61 OUTPUT C5BP61
 FILTER  FRS_C6_sz  WITH BP61 OUTPUT C6BP61
 FILTER  FRS_C7_sz  WITH BP61 OUTPUT C7BP61
 *
 DEFINE TELEV  AS FRS_A0_sz
   FRS_C1_sz FRS_C2_sz FRS_C3_sz FRS_C4_sz FRS_C5_sz FRS_C6_sz
FRS_C7_sz
   FRS_D1_sz FRS_D2_sz FRS_D3_sz FRS_D4_sz FRS_D5_sz FRS_D6_sz
FRS_D7_sz
   FRS_D8_sz FRS_D9_sz END
 *
 DEFINE INTER  AS FRS_A0_sz
   FRS_B1_sz FRS_B2_sz FRS_B3_sz FRS_B4_sz FRS_B5_sz
   FRS_C1_sz FRS_C2_sz FRS_C3_sz FRS_C4_sz FRS_C5_sz FRS_C6_sz
FRS_C7_sz
   FRS_D1_sz FRS_D2_sz FRS_D3_sz FRS_D4_sz FRS_D5_sz FRS_D6_sz
FRS_D7_sz
   FRS_D8_sz FRS_D9_sz END
 *
 DEFINE CRING AS FRS_A0_sz
   FRS_B1_sz FRS_B2_sz FRS_B3_sz FRS_B4_sz FRS_B5_sz
   FRS_C1_sz FRS_C2_sz FRS_C3_sz FRS_C4_sz FRS_C5_sz FRS_C6_sz
FRS_C7_sz
   END
 *
 DEFINE BRING AS FRS_A0_sz FRS_A1_sz FRS_A2_sz FRS_A3_sz
   FRS_B1_sz FRS_B2_sz FRS_B3_sz FRS_B4_sz FRS_B5_sz END
 *
 MAKE BEAM FRS01  OUTPUT TELEV1  USING TELEV  VEL 99999.9 AZI 0.0
 MAKE BEAM FRS02  OUTPUT TELEV2  USING TELEV  VEL 99999.9 AZI 0.0
 MAKE BEAM FRS03  OUTPUT INTER3  USING INTER  VEL 99999.9 AZI 0.0
 MAKE BEAM FRS04  OUTPUT CRING4  USING CRING  VEL 99999.9 AZI 0.0
 MAKE BEAM FRS05  OUTPUT CRING5  USING CRING  VEL 99999.9 AZI 0.0
 MAKE BEAM FRS06  OUTPUT BRING6  USING BRING  VEL 99999.9 AZI 0.0
 MAKE BEAM FRS07  OUTPUT BRING7  USING BRING  VEL 99999.9 AZI 0.0
 MAKE BEAM FRS08  OUTPUT INTER8  USING INTER  VEL 14.3    AZI   0.0
 MAKE BEAM FRS09  OUTPUT INTER9  USING INTER  VEL 14.3    AZI  90.0
 MAKE BEAM FRS10 OUTPUT INTER10 USING INTER  VEL 14.3    AZI 180.0
 MAKE BEAM FRS11 OUTPUT INTER11 USING INTER  VEL 14.3    AZI  15.0
 MAKE BEAM FRS12 OUTPUT INTER12 USING INTER  VEL 14.3    AZI  75.0
 MAKE BEAM FRS13 OUTPUT INTER13 USING INTER  VEL 14.3    AZI 135.0
 MAKE BEAM FRS14 OUTPUT INTER14 USING INTER  VEL 14.3    AZI  25.0
 MAKE BEAM FRS15 OUTPUT INTER15 USING INTER  VEL 14.3    AZI  75.0
 MAKE BEAM FRS16 OUTPUT INTER16 USING INTER  VEL 14.3    AZI 125.0
 MAKE BEAM FRS17 OUTPUT CRING17 USING CRING  VEL 99999.9 AZI   0.0
 *
 FILTER TELEV1  WITH FB2    OUTPUT   FR01
 FILTER TELEV2  WITH FB3    OUTPUT   FR02
 FILTER INTER3  WITH FB4    OUTPUT   FR03
 FILTER CRING4  WITH FB5    OUTPUT   FR04
 FILTER CRING5  WITH FB6    OUTPUT   FR05
```

Table IV.3.1 RONAPP 17 coherent plus 3 incoherent beams. (Cont'd).

```
FILTER BRING6  WITH BP41   OUTPUT   FR06
FILTER BRING7  WITH BP42   OUTPUT   FR07
FILTER INTER8  WITH FB4    OUTPUT   FR08
FILTER INTER9  WITH FB4    OUTPUT   FR09
FILTER INTER10 WITH FB4    OUTPUT   FR10
FILTER INTER11 WITH FB5    OUTPUT   FR11
FILTER INTER12 WITH FB5    OUTPUT   FR12
FILTER INTER13 WITH FB5    OUTPUT   FR13
FILTER INTER14 WITH FB6    OUTPUT   FR14
FILTER INTER15 WITH FB6    OUTPUT   FR15
FILTER INTER16 WITH FB6    OUTPUT   FR16
FILTER CRING17 WITH FB4    OUTPUT   FR17
*
SET_THRESHOLD      4.000
DETECT ON  FR01
DETECT ON  FR02
DETECT ON  FR03
DETECT ON  FR08
DETECT ON  FR09
DETECT ON  FR10
DETECT ON  FR11
DETECT ON  FR12
DETECT ON  FR13
DETECT ON  FR14
DETECT ON  FR15
DETECT ON  FR16
DETECT ON  FR04
DETECT ON  FR05
DETECT ON  FR17
SET_THRESHOLD      5.000
DETECT ON  FR06
DETECT ON  FR07
*
MAKE   STX   OF  A0BP60 OUTPUT A0STX60
MAKE   STX   OF  C1BP60 OUTPUT C1STX60
MAKE   STX   OF  C2BP60 OUTPUT C2STX60
MAKE   STX   OF  C3BP60 OUTPUT C3STX60
MAKE   STX   OF  C4BP60 OUTPUT C4STX60
MAKE   STX   OF  C5BP60 OUTPUT C5STX60
MAKE   STX   OF  C6BP60 OUTPUT C6STX60
MAKE   STX   OF  C7BP60 OUTPUT C7STX60
*
DEFINE INCO60 AS A0STX60
                 C1STX60 C2STX60 C3STX60 C4STX60 C5STX60
                 C6STX60 C7STX60   END
*
MAKE   STX   OF  A0BP61 OUTPUT A0STX61
MAKE   STX   OF  C1BP61 OUTPUT C1STX61
MAKE   STX   OF  C2BP61 OUTPUT C2STX61
MAKE   STX   OF  C3BP61 OUTPUT C3STX61
MAKE   STX   OF  C4BP61 OUTPUT C4STX61
MAKE   STX   OF  C5BP61 OUTPUT C5STX61
MAKE   STX   OF  C6BP61 OUTPUT C6STX61
MAKE   STX   OF  C7BP61 OUTPUT C7STX61
*
```

Table IV.3.1 RONAPP 17 coherent plus 3 incoherent beams. (Cont'd).

```
DEFINE INCO61 AS A0STX61
                 C1STX61 C2STX61 C3STX61 C4STX61 C5STX61
                 C6STX61 C7STX61   END
 *
 MAKE   STX   OF  A0FB4 OUTPUT A0STX4
 MAKE   STX   OF  D1FB4 OUTPUT D1STX4
 MAKE   STX   OF  D2FB4 OUTPUT D2STX4
 MAKE   STX   OF  D3FB4 OUTPUT D3STX4
 MAKE   STX   OF  D4FB4 OUTPUT D4STX4
 MAKE   STX   OF  D5FB4 OUTPUT D5STX4
 MAKE   STX   OF  D6FB4 OUTPUT D6STX4
 MAKE   STX   OF  D7FB4 OUTPUT D7STX4
 MAKE   STX   OF  D8FB4 OUTPUT D8STX4
 MAKE   STX   OF  D9FB4 OUTPUT D9STX4
 *
 DEFINE INCO4  AS A0STX4
                 D1STX4 D2STX4 D3STX4 D4STX4 D5STX4
                 D6STX4 D7STX4 D8STX4 D9STX4 END
 SET_THRESHOLD      2.500
 SET_INITIAL_LTA  100.000
 DETECT INCOHERENT ON BEAM FI18 USING INCO60  VEL 99999.9 AZI   0.0
 DETECT INCOHERENT ON BEAM FI19 USING INCO61  VEL 99999.9 AZI   0.0
 SET_THRESHOLD      2.100
 SET_INITIAL_LTA   60.000
 DETECT INCOHERENT ON BEAM FI20 USING INCO4   VEL 99999.9 AZI   0.0
```

Table IV.3.1. RONAPP 17 coherent plus 3 incoherent beams.
The detector program will accept this command file as a recipe
for performing STA/LTA detection on the 'RONAPP' beam set.
A detailed description of the input command file for the detector
program is given in NORSAR Scientific Report No. 2-86/87.
The commands INPUT, FILTER, MAKE and DETECT will be executed for
each segment of 60 seconds in a continous processing mode.
Shifting of data to accomodate for recursive filtering and
delaying is done by using an 'old' buffer of 5 seconds.

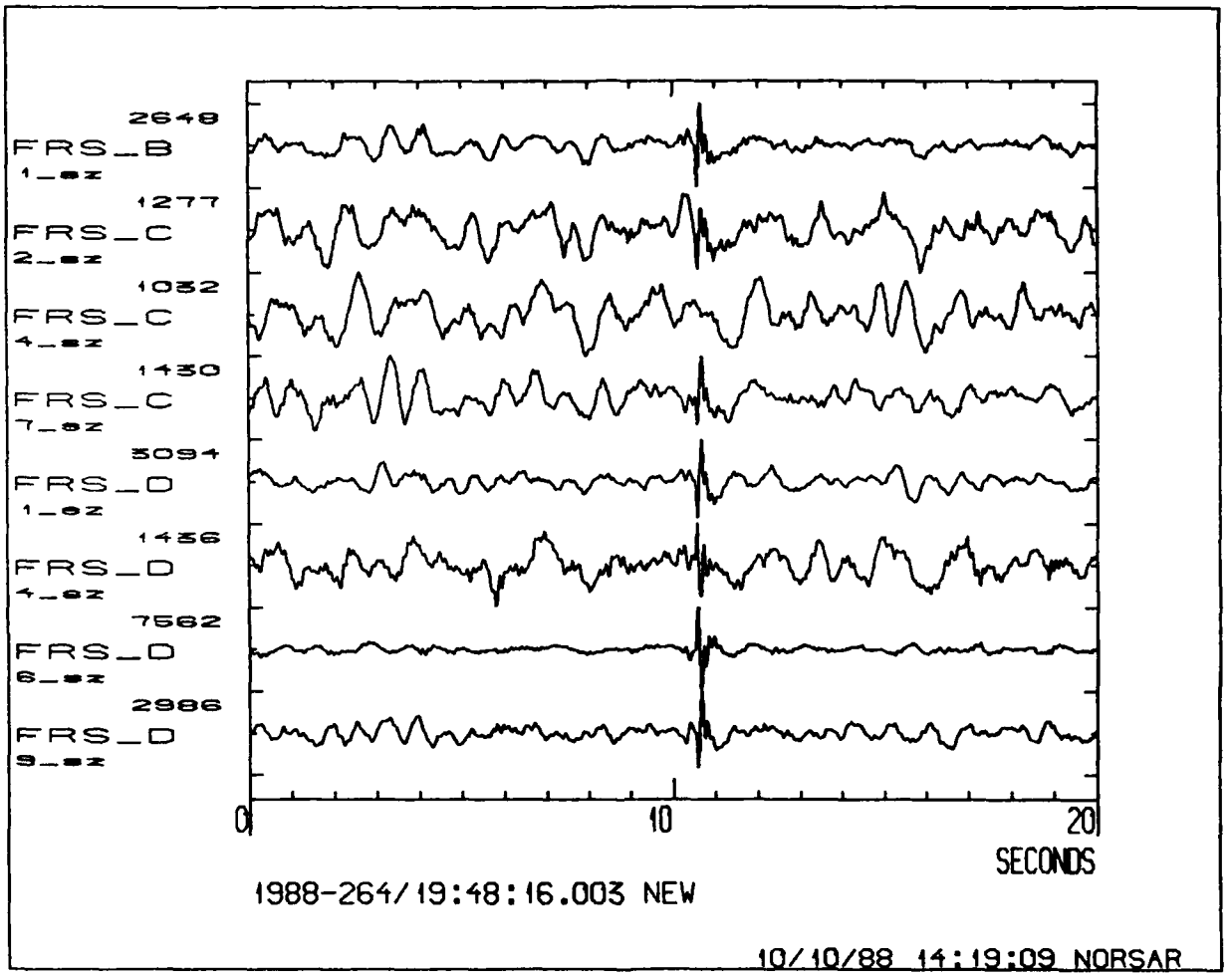

Fig. IV.3.1. Shows seismometers B1, C2, C4, C7, D1, D4, D6 and D9 for large 'event-like' cable noise.

V. MAINTENANCE ACTIVITIES

V.1 Activities in the field and at the Maintenance Center

This section summarizes the maintenance activities in the field, at the Maintenance Center (NMC), Hamar, and NDPC activities related to monitoring and control of the NORSAR, NORESS and ARCESS arrays. Preventive maintenance and other activities are incorporated.

Also during this period activities have been diverse and comprise preventive/corrective maintenance on all the NORSAR subarrays and ARCESS. Other activities have been checking (including line measurements) of all the NORSAR communications systems, location of broken cables (02B, 02C-06C), cable repair (01B), investigation of "false events" at ARCESS (see section IV.3.4), and installation of a new antenna (02B, telemetry). In addition, calibration of NORSAR SP/LP instruments from the NDPC, adjustment of LP instruments when parameters were outside tolerances and monitoring of communications systems were performed.

NORESS

The performance of the field equipment has been generally good during the reporting period. Apart from a defective relay U5 on the DHL70 preamplifier cards at CIDs 0A and 0C, there have been no failures.

ARCESS

During a visit in October 1988, it was found that the modification of the fiber optical system carried out in June 1988 had drifted too much and caused high failure rate, spikes and total loss of data from some of the remote sites. All channels were readjusted, and they all worked properly except for sites B3 and B4. These sites could not be repaired fully due to lack of spare parts. Sandia Laboratories have been informed and they will report to the manufacturer of the fiber optical transmitter and receiver units about our experience.

Details are presented in Table V.1.

Subarray/ area	Task	Date
01B	Located and spliced SP 02 and 05 cables	6,19,26 Oct
02B Telemetry	New antenna poles erected at all stations	17,18,20, 21,24,25, 31 Oct
ARCESS	All 25 remote sites visited. Fiber optic systems cleaned and adjusted. Also found the reason behind the false events. HP-unit returned to Sandia Labs. for repair.	11-14 Oct
NDPC	Daily check of SP/LP data and com. systems. Weekly calibration of SP/LP instruments. Adjustment of MP/FP parameters when outside tolerances.	Oct
02B	Adjusted offset and channel gain all channels Due to a bad cable to SP02, SP seismometer in 60 m borehole connected to channel 02. On LP instruments NS/EW the mass pos. Remote Centering Devices (RCDs) were replaced. On LP seismometers VE, replaced Free Period RCD LP vertical seismometer tank was opened and vertical seismometer readjusted.	2 Nov 7 Nov 16 Nov 25 Nov
02C	Located broken cable SP05 On LP vertical seismometer replaced FP Remote Centering Device (RCD)	10 Nov
03C	All channels adjusted with respect to channel gain and offset. Adjusted FP and MP Remote Centering Devices all LP channels	23 Nov
04C	All channels adjusted, gain and offset. Otherwise mass position on all LP seismometers adjusted. Work in connection with NS seismometer carried out. Finally the data coil was replaced	8 Nov 17,18,22 Nov
02B	SP gain channel 3 and 6 and LP system adjusted	2 Dec
01B	The following adjustments were made: Gain all SP channels Mass pos. all LP seismometers Free period NS LP seismometer Gain NS LP channel Replacements: Remote Centering Devices (RCDs) FP and MP for the NS LP seismometers.	12 Dec

Subarray/ area	Task	Date
02B Telemetry	Line measurements	
NORESS	Satellite Tx carrier frequency adjusted up to 600 Hz.	12 Dec
ARCESS	Ralph Alewine and NORSAR representatives visited the ARCESS array.	5 Dec
NDPC	Daily check of SP/LP data and communications system. Weekly calibration of SP/LP instruments. Free period and mass position measurements. Adjustments when outside tolerances.	Dec
02B Telemetry	Battery replacement carried out.	4,5,27 Jan
02B	Visits to the subarray in connection with power outages	9,20 Jan
06C	Data coil replaced on EW seismometer	30,31 Jan
NORESS	At sites A1, C2 the preamplifier DHL70 cards were replaced. At sites A3, B3 and B5 otpical fiber connectors cleaned.	5 Jan 30 Jan
NDPC	Daily check of SP/LP data and communications system. Weekly calibration of SP/LP instruments. Adjustment of LP seismometer when outside specifications.	Jan
06C	Data coil on EW seismometer replaced. Offset SP channel 1 and 2, VE and NS LP seismometer adjusted.	1,27 Feb
02B	Replaced data coil on vertical LP seismometer Mass position and Free Period adjusted on all LP seismometers	27,28 Feb
NDPC	Daily check of NORSAR, NORESS and ARCESS data carried out. Calibration of SP and LP instruments weekly (NORSAR array) Measurements and adjustments of LP seismometer parameters when outside tolerances.	Feb

Subarray/ area	Task	Date
01A	Battery charger timer replaced. Batteries refilled. Adjusted Mass Position and Free Period on all LP seismometers Line (incl. modems) measured in B/C loop (analog/digital). Modem AHS-card replaced.	9,10 Mar
01B	Mass Position and Free Period all LP seismometers adjusted. Line check in B/C loop. Hamar telestation raised level toward the subarray by 2 dBm.	1 Mar
02B	Adjusted MP/FP on LP seismometers (- MP VE seismometer). Remote Centering Device (RCD) on Vert. seismometer replaced, adjustment afterwards. SLEM Digital Unit replaced and power supply adjusted. Besides + BB and 4X gain (Digital Unit Converter) and RSA offset adjusted. DC offset channel 2, 3, 5 and 6 also adjusted.	2,3,6 Mar
02C	Adjusted gain channel 2, 3 and 6. Adjusted DC offset ch. 6. Adjusted MP/FP all LP seismometers. Line check B/C loop.	13 Mar
03C	Adjusted gain ch. 3. Adjusted MP/FP on all LP seismometers.	6 Mar
04C	Adjusted gain ch. 1 and 6 Adjusted DC offset ch. 2 and 5 Adjusted MP/FP all LP seismometers Line check B/C loop NTA/Lillestrøm raised level towards Hamar by 3 dBm	14 Mar
06C	Adjusted EW LP seismometer MP and FP Line check in B/C loop. AHS-card in modem replaced.	7 Mar
02B Telemetry	Installed new batteries on receiving station and ch. 23,24. Repaired power supplies remote sites	17,30 Mar 30 Mar

Subarray/ area	Task	Date
NDPC	Daily routines carried out, incl.: Check of NORSAR, NORESS and ARCESS data Weekly calibration of SP and LP instruments Measurements/adjustments of LP seismometer parameters outside tolerances.	Mar

Table V.1. Activities in the field and the NORSAR Maintenance Center including NDPC activities related to the NORSAR array, 1 October 1988 - 31 March 1989.

V.2 Array status

No changes or modifications have been implemented since the last report.

As of 31 March 1989, the following NORSAR channels deviated from tolerances:

01A	01	8 Hz filter
	02	8 Hz filter
	04	30 dB attenuation
01B	02	Bad cable
02B	02	Bad cable
02C	05	Bad cable
04C	04	Bad cable
06C	05	Broadband filter installed

Oddmund A. Hansen

VI. DOCUMENTATION DEVELOPED

Bungum, H., A. Alsaker, L.B. Kvamme & R.A. Hansen: Seismicity and seismotectonics of Norway and the surrounding continental shelf. Submitted for publication.

Loughran, L.B. (ed.): Semiannual Tech. Sum., 1 Apr - 30 Sep 88, NORSAR Sci. Rep. 1-88/89, NORSAR, Kjeller, Norway.

Ringdal, F. & T. Kværna: A multichannel processing approach to real time network detection, phase association and threshold monitoring. In press, Bull. Seism. Soc. Am.

VII. SUMMARY OF TECHNICAL REPORTS / PAPERS PUBLISHED

VII.1 Yield determination of Soviet underground nuclear explosions at the Shagan River Test Site

Introduction

The signing of the Threshold Test Ban Treaty (TTBT) by the United States and the Soviet Union in 1974, which limits the size of underground nuclear explosions, focused attention on methods for estimating the size of explosions. Since 1974, considerable research efforts have been devoted to developing various methods of yield estimation, and much progress has been achieved. Reviews of some of these developments may be found in the report OTA-ISC-361 (1988) published by the U.S. Congress, Office of Technology Assessment, and by Bache (1982), Heusinkveld (1982), Lamb (1988) and Storey et al (1982).

In this paper, we focus on the problem of determining yields by teleseismic methods for a set of explosions conducted at the Shagan River test site near Semipalatinsk, USSR. We have analyzed all the events reported by the ISC or NEIC to have occurred at this site between 1965 and 1988, a total of 96 events. As a basis for the yield estimation we have used body-wave magnitude (m_b) determined from global network data as well as two additional explosion source size estimators. The first additional method is the long-term level of the reduced displacement potential, Ψ_∞, which in this paper is measured from the initial explosion-generated P pulse recorded at four UK array stations. The second additional method is based on estimating the energy of the Lg wave train recorded at the NORSAR and Gräfenberg arrays for each explosion. The emphasis of the paper is on assessing the combined utility of these three methods to obtain relative yields of explosions, but we will also briefly address the estimation of absolute yields from the available seismic information.

The Shagan River test site

The principal Soviet testing area for nuclear explosions is located near the city of Semipalatinsk in Eastern Kazakhstan. Marshall, Bache and Lilwall (1985) identify three distinct test sites within this area: Shagan River, Degelen Mountains and Konystan. After 1976, all of the largest Soviet nuclear tests have been conducted at the Shagan River site, and our discussions in this paper will focus on this area.

A review of available information on the tectonics and geology of the Eastern Kazakhstan area can be found in Leith (1987). Geologically, he describes the test area as located within the Kazakh fold system, which is a complex of deformed Paeozoic rocks along the eastern edge of the so-called "Kazakh shield". Seismically, the region is characterized by relatively modest earthquake activity, but it is noteworthy that some of the explosions at the Shagan River test site have been accompanied by a significant amount of tectonic release (Helle and Rygg, 1984; Given and Mellman, 1986).

A map summarizing the surface geology of the Shagan River area is shown in Fig. VII.1.1. This map is based on imagery from the SPOT satellite as well as information available from the literature (Sukhonikov, Akhmetov and Orlov, 1973; Izrael, 1972; Peyre and Mossakovsky, 1982). A particularly noteworthy feature is the presence of two approximately parallel faults extending across parts of the test site. One of these, the Chinrau fault, appears to show evidence of recent offset on SPOT imagery to the region northwest of Shagan River (Leith, 1987).

Also identified from the satellite observations, and indicated on Fig. VII.1.1, is a crater formed by the explosion of 15 January 1965. This location has been used as a reference point in the relocation of explosions in the test area (Marshall et al, 1985), using the Joint Epicenter Determination method described by Douglas (1967). In the further analysis presented in this paper, we will refer to epicenters calculated from this procedure to the extent such data area available.

Data base

The data base for this study consists of seismic recordings for 96 presumed nuclear explosions at the Shagan River test area, occurring from 1965 through 1988 and located by the ISC or NEIC.

Data sources are the four UK array stations: (Eskdalemuir (ESK), Scotland, Yellowknife (YKA), Canada, Gauribidanur (GBA), India, and Warramunga (WRA), Australia, in addition to the two large arrays NORSAR in Norway and Gräfenberg (GRF) in the Federal Republic of Germany.

The four UK arrays have been in operation since the mid-1960s and are described in detail by Mowat and Burch (1977). Briefly, these are medium-aperture arrays (10-30 km diameter), with 19 or 20 vertical-component Willmore SP seismometers deployed in two roughly perpendicular lines. Their outputs are recorded on analog or digital magnetic tape. The sampling rate, for both digitally recorded data and digitized analog data, is 20 samples per second.

The NORSAR array (Bungum, Husebye and Ringdal, 1971) was established in 1970, and originally comprised 22 subarrays, deployed over an area of 100 km diameter. Since 1976 the number of operational subarrays has been 7, comprising altogether 42 vertical-component SP sensors (type HS-10). In this paper, analysis has been restricted to data from these 7 subarrays. Sampling rate for the NORSAR SP data is 20 samples per second, and all data are recorded on digital magnetic tape.

The Gräfenberg array (Harjes and Seidl, 1978) was established in 1976, and today comprises 13 broadband seismometer sites, three of which are 3-component systems. The instrument response is flat to velocity from about 20 seond period to 5 Hz. Sampling rate is 20 samples per second, and the data are recorded on digital magnetic tape.

Source size estimators

Network m_b magnitude

Body-wave magnitudes averaged over a well-distributed global network have traditionally been the most commonly used measure for yield estimation purposes. In recent years the maximum-likelihood technique (Ringdal, 1976; Christoffersson, 1980) has become widely accepted as a means to obtain m_b estimates that avoid bias due to detection threshold characteristics at individual network stations.

Maximum-likelihood m_b for the explosions in the present data base have been computed at Blacknest applying the method of Lilwall, Marshall and Rivers (1988). Note that this method uses a standardized set of stations and includes individual station corrections for the Shagan River area. The station observations given in the Bulletin of the ISC have been used in these computations, except for events after 1986, where the data have been obtained from the NEIC monthly earthquake data report.

Reduced displacement potential, Ψ_∞

The reduced displacement potential $\Psi(t)$ is a convenient mathematical description of the source function of an explosion, assuming a spherical wave in an ideal, infinite homogeneous, isotropic elastic solid. It is directly related to the moment function $M_0(t)$ of the explosion as follows (Mueller, 1973):

$$M_0(t) = 4\Pi \rho v_p^2 \Psi(t) \qquad (1)$$

where ρ is the density of the medium and v_p is the compressional wave velocity.

The long-term (static) level of $M_0(t)$ is often denoted the seismic moment of the explosion, and is a measure of the seismic source size.

Thus, the long-term level of $\Psi(t)$, Ψ_∞, can be used to estimate source size, assuming that the source material properties are known.

The method used in this paper for estimating Ψ_∞ is based on UK array data and has been described in detail by Stewart (1988).

Lg magnitude

The seismic Lg wave propagates in the continental lithosphere and can be observed from large explosions as far away as 5000 km in shield and stable platform areas (Nuttli, 1973; Baumgardt, 1985). Lg is generally considered to consist of a superposition of many higher-mode surface waves of group velocities near 3.5 km/s, and its radiation is therefore expected to be more isotropic than that of P waves. Thus, full azimuthal coverage is not essential for reliable determination of Lg magnitude. Furthermore, Lg is not affected by lateral heterogeneities in the upper mantle, which can produce strong focussing/defocussing effects on P-waves, and therefore contribute to a significant uncertainty in P-based m_b estimates.

Nuttli (1986a) showed that the amplitudes of Lg near 1 second period provide a stable estimate of magnitude, m_b(Lg) and explosion yield for Nevada Test Site explosions. He also applied his measurement methods to Semipalatinsk explosions (Nuttli, 1986b), using available WWSSN records to estimate m_b(Lg) and yields of these events.

Ringdal (1983) first suggested a method to determine Lg magnitudes based on digitally recorded array data. The main idea was to improve the precision of such estimates by averaging over time (computing RMS values over an extended Lg window), frequency (using a bandpass filter covering all frequencies with significant Lg energy) and space (by averaging individual array elements). The method, which can also be

used for P coda magnitude estimation, has been described by Ringdal and Hokland (1987) and Ringdal and Fyen (1988).

Data analysis

Results from applying the analysis methods described in the preceding section are summarized in Table VII.1.1. The following comments apply:

Origin times and epicentral information of each event are those calculated at Blacknest using ISC and NEIC data for events up to and including 1985, and are taken from NEIC listings for later events. The magnitude (m_b) values have been computed as earlier described.

For each event an indicator is given corresponding to a subdivision of the Shagan River area into three main areas. These are defined by the two faults marked on Fig. VII.1.1 and an assumed prolongation of the stippled lines indicated on that figure. The three areas are denoted "NE" (Northeast), "TZ" (transition zone between the faults) and "SW" (Southwest), respectively.

Estimates of log Ψ_∞ in Table VII.1.1 are network averages using UK array data. The number of stations available and standard deviations of the estimates are listed for each event. Individual array measurements for most of the events may be found in Stewart (1988).

NORSAR and Gräfenberg (GRF) Lg magnitude estimates are noise-corrected array averages, obtained by applying individual bias corrections for each array element. The number of operative array channels are given for each event. Standard deviations of the array averages have been computed taking into account both the number of sensors and the signal-to-noise ratios (for details, see Ringdal and Fyen, 1988). Estimates have been made for all events for which array recordings were available, except those with too low Lg signal-to-noise ratio to allow reliable measurement. Table VII.1.1 also contains weighted averages (discussed later in this section) of the NORSAR and GRF Lg magnitudes.

The Lg magnitude estimates in Table VII.1.1 are, except for a few minor revisions, consistent with those presented in earlier Semiannual Reports. We have not included corrections for epicentral distance differences in this paper, since these are small to begin with, and also difficult to estimate accurately given the limited knowledge of local attenuation in the Shagan River area.

As noted by Ringdal and Fyen (1988), the Lg array estimates at NORSAR and Gräfenberg may be made with very high precision, due to the large number of channels (up to 42 and 13, respectively). Thus, the standard deviation across NORSAR of individual measurements is typically 0.07 magnitude units for uncorrected data, and 0.035 units when individual channel corrections are applied. The precision of NORSAR averages are thus better than 0.01 units for high SNR events, but somewhat poorer at lower SNR. At Gräfenberg, the standard deviation of the mean values is typically 2-3 times that of NORSAR, depending on the number of available channels. It should be noted that this high precision does not necessarily imply a correspondingly high degree of accuracy in estimating Lg source energy since the effects of near-source geology remain unknown.

In the comparison which follows of the various source size estimators, we will in particular focus on the subdivision of the Shagan River site into apparently geophysically distinct subregions. Marshall et al (1985) discuss this feature in detail, showing that explosions in the northeast and southwest portions of the test site produce distinctly different P waveforms when recorded at the UK arrays. We note that their northeast region also includes the area denoted by us as a transition zone (TZ). We will pursue this subdivision further by analyzing the differences between P-based and Lg-based magnitude measurements, and later discuss the implications for yield estimation.

Figs. VII.1. 5 through VII.1.8 are scatter plots comparing pairs of source size estimators. In all these figures, we use the following

symbols for the three subareas: open squares (SW), filled squares (NE) and crosses (TZ).

We first compare the two P-based estimators, m_b and $\log\Psi_\infty$. Fig. VII.1.2 shows that they are quite consistent, with no systematic difference between the SW, TZ and NE events. In assessing the scatter in this plot, we must take into account that many of the Ψ_∞ estimates are based on data from only one or two arrays (Table VII.1.1).
The least-squares fit to this data set, assuming no errors in m_b, is:

$$\log \Psi_\infty = 1.1\ m_b - 2.57 \qquad (\pm\ 0.11) \qquad (2)$$

where the standard deviation of 0.11 refers to the set of residuals in $\log \Psi_\infty$ relative to the straight line fit.

We next compare the two Lg-based measurements. Fig. VII.1.3 shows a scatter plot of NORSAR versus GRF Lg magnitudes for all events (54) measured at both arrays. The straight line represents a least squares fit to the data, assuming no errors in NORSAR magnitudes, and is given by

$$m_{Lg}(\mathrm{GRF}) = 1.15 \cdot m_{Lg}(\mathrm{NORSAR}) - 0.90 \qquad (\pm\ 0.042) \qquad (3)$$

We note that the two arrays show excellent consistency, although there is some increase in the scattering at low magnitudes. There is no significant separation between events from NE, TZ and SW areas with regard to the relative Lg magnitudes observed at the two arrays.

Fig. VII.1.4 shows a subset of these data (35 events), using only events for which we have the most reliable Lg estimates (at least 6 stations for each array, and estimated standard deviation of m_{Lg} less than 0.04). We note that the scatter is significantly reduced (the standard deviation in the vertical direction is now only 0.031 units, compared to 0.042 units for the entire data set), thus emphasizing the excellent consistency between NORSAR and Gräfenberg.

The slope (1.15) of the straight-line fit in Figs. VII.1.3 and VII.1.4 is slightly greater than 1.00, a tendency also noted by Ringdal and Fyen (1988). The interpretation of this observation is somewhat uncertain; a possible explanation is scaling differences in the Lg source spectrum (Kværna and Ringdal, 1988), in combination with the response differences of the NORSAR and GRF instruments. It is interesting in this connection to note that Patton (1988) observed significant differences between stations in slopes for M(Lg) versus yield, when studying a network of stations recording Nevada Test Site explosions.

In the comparison which follows of P and Lg-based magnitudes, we find it convenient to use as reference a weighted average of the NORSAR and GRF Lg magnitudes. This average is obtained by first using equation (3) to adjust the GRF values to "equivalent" NORSAR magnitudes, and then use the inverse variance obtained from Table VII.1.1 as weighting factors in the averaging procedure. The resulting values, which we denote m_{Lg}, are listed as the rightmost column in Table VII.1.1.

In Fig. VII.1.5, m_b is plotted versus m_{Lg} defined above for all events with both measurements available. Three lines, with slopes restricted to 1.0, have been drawn, representing the three subregions. To obtain improved reliability in calculating the intercepts, we have in that calculation used only events of $m_{Lg} \geq 5.5$, and required that NORSAR Lg measurements are available. The resulting relationships are:

SW region: $m_b = m_{Lg} + 0.05 \quad (\pm 0.041)$ (4a)

TZ region: $m_b = m_{Lg} - 0.02 \quad (\pm 0.031)$ (4b)

NE region: $m_b = m_{Lg} - 0.10 \quad (\pm 0.047)$ (4c)

Taking into account the number of observations in each group, the average bias estimates ($m_b - m_{Lg}$) and their precisions are: 0.05 ± 0.007 (SW region), -0.02 ± 0.009 (TZ region) and -0.10 ± 0.012 (NE region). In light of the low standard deviations, the differences in bias values are highly significant, and we note that the NE and SW regions differ by as much as 0.15 magnitude units in this regard.

Fig. VII.1.6 shows a plot of m_{Lg} versus "adjusted" m_b, using the regional correction factors given above. We note that the consistency is excellent, although there are two outliers in the plot (Events 25 and 28 of Table VII.1.1). Event 25 is small, and both the m_b and m_{Lg} measurements for this event are uncertain. Event 28 has an m_{Lg} measurement based on only 3 GRF channels, with no NORSAR data available, and is therefore less precisely determined than the majority of data points. The standard deviation of the m_b-m_{Lg} differences in Fig. VII.1.6 is 0.050 magnitude units, which is reduced to 0.039 units if the two outliers are disregarded.

Fig. VII.1.7 shows a comparison of m_{Lg} to log Ψ_∞ observations. We note a tendency for the SW events to exhibit relatively larger values of log Ψ_∞ than events from the other two regions. However, this bias is less pronounced than that previously observed for m_b versus m_{Lg}. Partly, this is due to increased scatter in the data, since the log Ψ_∞ measurements are based only on a few observations. Nevertheless, it would appear that log Ψ_∞ is less sensitive than m_b to regional bias effects. This can be explained by the longer wavelengths used in log Ψ_∞ measurements in combination with the fact that log Ψ_∞ to a large extent avoids the pP contamination that may adversely influence m_b measurements.

Requiring at least 3 individual array measurements for log Ψ_∞, and using a slope of 0.9 suggested from Fig. VII.1.2 and the general consistency between m_b and m_{Lg}, we obtain the following two relations (marked on the figure)

$$\text{SW} : m_{Lg} = 0.9 \cdot \log \Psi_\infty + 2.35 \quad (\pm 0.05) \qquad (5a)$$

$$\text{NE and TZ} : m_{Lg} = 0.9 \cdot \log \Psi_\infty + 2.43 \quad (\pm 0.075) \qquad (5b)$$

Note that the NE and TZ regions have been grouped together in this case, as we in our analysis have not been able to identify any systematic differences for this data set.

Fig. VII.1.8 shows magnitude differences m_b-m_{Lg} plotted as a function of event location, using only events of $m_b \geq 5.5$ and requiring NORSAR Lg data to be available. The subdivision of the test site as earlier discussed is marked on the figure. The systematic differences, in particular between the NE and SW parts of the test site, are clearly seen. If we attempt to explain this anomaly as resulting from the systematic differences in P recordings only, we obtain a relative m_b(P) bias of about 0.15 m_b units between these two areas. We consider this a realistic interpretation, since it is well known that P-waves are subject to strong focusing effects in the upper mantle, both underneath the source and the receiver. However, the possibility of an m_b(Lg) bias contributing to the mentioned difference cannot be entirely ruled out.

Yield estimation

Yield of the 15 January 1965 explosion

Determination of the appropriate absolute magnitude-yield relationship for explosions at a specific test site requires knowledge of the true yields and testing conditions of some number of representative explosions at that particular site. In the case of the Shagan River nuclear test site, thus far, there has been a discussion in the literature of the yield of only one explosion. This explosion was conducted on 15 January 1965 within the Soviet Peaceful Nuclear Explosion program for the purpose of constructing a reservoir.

We have reviewed available data on this explosion, and obtained a yield estimate which we will use in calibrating the various magnitude-yield relationships. Clearly, in the absence of more detailed calibration data, the relationships will have a significant uncertainty. This applies especially in the absolute yield levels, whereas the relative yield estimates between explosions will be somewhat better constrained.

In IAEA proceedings, the yield of the 1965 explosion is quoted as "above 100 kt". Myasnikov et al (1970) indicates that the scaled

apparent radius is 51 m/kt$^{1/3.4}$, which for a crater radius of 204 m gives a yield of 111 kt. Myasnikov et al (1970) uses a scaled depth of burst for this explosion equal to 50 m/kt$^{1/3.4}$. The depth of emplacement is reported to be 200 m (Kedrovskiy, 1970; Izrael, 1972; Myasnikov et al, 1970), which corresponds to the same yield estimate. For the purposes of the work presented here, the yield of the 15 January 1965 explosion is taken to be 111 kt.

Available seismic data

Turning now to the question of relating this yield to the observed data, we first note that the 1965 explosion differs from all the other explosions in our data base by not being fully contained. This means that the interference effects between P and pP will be different for this event and the others.

Our Ψ_∞ measurements rely on the characteristics of the initial positive P-pulse of the explosion, and are therefore less affected by the free surface reflection. However, our m_b estimate of the 15 January 1965 explosion is likely biased low. The actual bias may, from theoretical considerations, typically approach 0.1-0.2 m_b units (Marshall et al, 1979; McLaughlin et al, 1988).

We have reviewed available data for 46 Shagan River explosions recorded at EKA, comparing the maximum peak-to-peak amplitude (c) (the phase which is normally used for magnitude estimation) and the initial zero-to-peak amplitude (a). The average values of r = log (c/a) for contained explosions were 0.78 (SW), 0.77 (TZ) and 0.72 (NE), with an overall mean of r = 0.75. The corresponding value for the 15 January 1965 explosion was r = 0.62.

Assuming that the initial pulse is unaffected by pP, this would suggest that a correction factor of about 0.13 m_b units would be appropriate. Since the uncorrected m_b value for the 1965 explosion was 5.87, we consequently obtain an estimated m_b value of 6.00 for a contained

explosion of the same size as the 15 January 1965 event. We note that McLaughlin et al (1988) obtained a similar correction factor (0.13) based on theoretical considerations, whereas their observational data indicate a slightly higher value of 0.16 (McLaughlin, personal communcation).

No Lg measurements are available for NORSAR or GRF for the 1965 event. Nuttli (1986b) estimates m_{Lg} = 5.87 for this explosion, but we note that his estimates for events before 1979 tend to be lower (by 0.08 magnitude units on the average) than NORSAR m_{Lg} observations, and his value would therefore correspond to a NORSAR m_{Lg} of about 5.95.

Magnitude-yield relationship

Our basic assumption will be that m_{Lg}, as a yield estimator, is largely independent of the geological variations within the Shagan River test site. This suggests that a single yield-magnitude relationship would be appropriate, and we ill in the following assume a relation of the form

$$m_{Lg} = 0.9 \log Y + k \qquad (6)$$

where k will be estimated using data from the 15 January 1965 explosion. The slope of 0.9 in (6) is consistent with our previous relations between log Ψ_∞, m_b and m_{Lg}, taking into account that log Ψ_∞ has previously been found to scale to logY with a slope of 1 (Stimpson, 1988; Gillbanks et al, 1989).

Since the NORSAR or GRF m_{Lg} for the 15 January 1965 explosion is not known, we need to estimate it indirectly, and then insert the value in (6) for Y = 111 kt in order to obtain an estimate of k. For this purpose, we use the previously discussed estimates of m_b, log Ψ_∞ and m_{Lg} (Nuttli), with the proper adjustments for regional and other bias factors.

(i) For m_b, the value of 6.00 for an explosion in the TZ region corresponds (by 4b) to $m_{Lg} = 6.02$.

(ii) For log Ψ_∞, the value of 3.87 in the TZ region corresponds (by 5b) to $m_{Lg} = 5.91$.

(iii) For Nuttli's m_{Lg}, the value of 5.87 corresponds, as earlier mentioned, to NORSAR $m_{Lg} = 5.95$.

The average (5.96) of these three values is then taken as our best estimate of m_{Lg} for a fully contained explosion of Y = 111 kt. Inserted in (6), this gives k = 4.12, i.e.:

$$m_{Lg} = 0.9 \log Y + 4.12 \qquad (7)$$

In line with our previous considerations, the formula (7) will then be applicable to the entire test site and this enables us to estimate yields for all explosions for which m_{Lg} has been determined.

Supplementary yield estimates from m_b and log Ψ_∞ can now be calculated by using (7) in conjunction with the regionally based formulas (4a-c) and (5a-b).

We obtain, by direct substitution for m_b:

$$\text{SW region}: \quad m_b = 0.9 \cdot \log Y + 4.17 \qquad (8a)$$

$$\text{TZ region}: \quad m_b = 0.9 \cdot \log Y + 4.10 \qquad (8b)$$

$$\text{NE region}: \quad m_b = 0.9 \cdot \log Y + 4.02 \qquad (8c)$$

and for log Ψ_∞:

$$\text{SW region}: \quad \log \Psi_\infty = \log Y + 1.97 \qquad (9a)$$

$$\text{NE and TZ regions}: \quad \log \Psi_\infty = \log Y + 1.88 \qquad (9b)$$

We note that the constant terms in equations (9a-b) are between the values earlier determined for water-saturated rock at the Nevada Test Site (Gillbanks et al, 1989) and granite at the French test site in S. Algeria (Stimpson, 1988), which were 1.8 and 2.0, respectively.

Table VII.1.2 summarizes yield estimates of individual Shagan River explosions, using the formulas developed earlier. Both P and Lg-based estimates are listed, together with their (logarithmic) average value for each event. The P-based yields represent a weighted average between m_b and log Ψ_∞ estimates, using the inverse variances as weighting factors. Here, we use for log Ψ_∞, the standard deviations listed in Table VII.1.1, and for m_b a standard deviation of 0.04, which is the average of the deviations relative to NORSAR m_b(Lg) within each of the three regions.

Discussion

A method, combining several measurements of the radiated seismic energy of underground nuclear explosions, has been developed which offers the possibility for precise yield estimates in a relative sense. A reliable assessment of the results presented here would require access to independently measured yields, which, with the exception of the data on the 1965 explosion given here, currently is not available. We note, however, that the yield estimate quoted by Sykes and Ekström (1989) of 115-122 kt for the explosion of 9/14/88 compares closely with the values of 113-117 kt derived independently in this study.

It has been noted in this paper that the estimation of the absolute values of the yields by the method presented here relies on knowledge of the yield and geophysical conditions of a single explosion. The estimation of absolute yields by this method relies on a number of critical assumptions, including the assumption that the yield value taken in this study is the appropriate yield, the assumption of correcting the bodywaves for depth of burial effects, the assumption of the equivalent Lg value of the 1965 explosion, and the assumption that

the corrected magnitude values for the 1965 explosion are representative of explosions in that area. Incorrect assumptions in these areas would lead to different yield estimates than those given in Table VII.1.1. For instance, a 10% increase in the assumed yield of the 1965 explosion would result in a 10% increase in the predicted yields in Table VII.1.1.

Our measurements on Ψ_∞ show general consistency with maximum likelihood m_b estimates from a global network, and have the advantage of requiring only a few stations for reliable measurement. Furthermore, the associated estimates of P-pulse rise time and duration provide important information related to source corner frequency and near-source geology. These parameters, as discussed by Stewart (1988), are useful for identifying systematic differences between the NE and SW Shagan areas, although determining the source of these differences would require more information on site geology than is currently available.

The m_{Lg} measurements presented in this paper, based on NORSAR and Gräfenberg array recordings, show excellent promise to provide very precise relative yields of individual explosions, but would again require calibration data to determine more reliably the absolute yields. Part of the reasons for this high precision lies in the fact that our Lg magnitudes, as discussed before, are based on averaging the observed Lg signals both in time, frequency and space. The basic assumption is that Lg generation at the source is largely azimuth independent and also independent of local variations in geology.

Because of the large distances (more than 4000 km) from Semipalatinsk to NORSAR and Gräfenberg, reliable measurements of Lg magnitudes can only be made at these arrays for explosions of approximately $m_b = 5.5$ or greater. This corresponds to about 30-40 kilotons for fully coupled explosions, depending on the location within the test site. In order to apply the method to smaller events, seismograph stations at shorter epicentral distances, with good Lg propagation paths, must be avail-

able. Again, each station must be individually calibrated in order to obtain reliable estimates.

This paper has demonstrated that observations from three distinct subregions of the Shagan site show systematic differences, supporting and extending earlier studies (e.g., Marshall et al, 1985), suggesting that the NE and SW areas are characterized by different geophysical properties. In particular, the P-Lg magnitude bias shows systematically different behavior for these regions.

This variation, as illustrated in Fig. VII.1.8, is in fact quite smooth, and indicates a knowledge of precise epicenter location would make possible, through interpolation, to obtain an estimate of P-Lg bias also for events for which Lg magnitudes are not available. Such events could be low-magnitude explosions, "double" explosions (for which Lg magnitude would represent the combined yields), explosions followed by large earthquakes causing interference with the Lg wavetrain or events occurring during outage times for the stations reporting Lg measurements.

It is noted that the current bilateral negotiations on nuclear testing offer the possibility for validated yields of future explosions at the Shagan River nuclear test site. Such additional yield information is invaluable in testing, and modifying if necessary, the teleseismic yield estimation method developed in this report.

F. Ringdal
P.D. Marshall, MOD PE, UK

References

Bache, T.C. (1982): Estimating the yield of underground nuclear explosions, Bull. Seism. Soc. Am., 72, S131-S168.

Baumgardt, D.R. (1985): Comparative analysis of teleseismic P coda and Lg waves from underground explosions in Eurasia, Bull. Seism. Soc. Am., 75, 1413-1433.

Bungum, H., E.S. Husebye and F. Ringdal (1971): The NORSAR array and preliminary results of data analysis, Geophys. J., 25, 115-126.

Christoffersson, A. (1980): Statistical models for seismic magnitude, Phys. Earth Planet. Inter., 21, 237-260.

Douglas, A. (1967): Joint epicentre determination, Nature, 215, 47-48.

Gillbanks, T.G.A., P.D. Marshall and R.C. Stewart (1989): P-wave seismograms recorded at Yellowknife, Canada from underground nuclear explosions in Nevada, USA, AWE Report No. O 26/88, HMSO, London.

Given, J.W. and G.R. Mellman (1986): Estimating explosion and tectonic release source parameters of underground nuclear explosions from Rayleigh and Love wave observations. Final Report, Part 1, SGI-R-86-126 (Sierra Geophysics, Kirkland, WA), 1-70.

Harjes, H.-P. and D. Seidl (1978): Digital recording and analysis of broadband seismic data at the Gräfenberg (GRF) array, J. Geophys. Res., 44, 511-523.

Helle, H.B. and E. Rygg (1984): Determination of tectonic release from surface waves generated by nuclear explosions in eastern Kazakhstan, Bull. Seism. Soc. Am., 74, 1883-1898.

Heusinkveld, M. (1982): Analysis of shock wave arrival time from underground explosions, J. Geophys. Res., 87, 1891-1898.

Izrael, Yui.A. (1972): Phenomenology of the containment of the atmosphere and ground by the radioactive products of underground nuclear explosions, IAEA-388-3/23, Vienna.

Kedrovski, O.L. (1970): The application of contained nuclear explosions in industry. (In Russian with English abstract). In: Peaceful Nuclear Explosions Phenomenology and Status Report, 1970, IAEA, Vienna, 163-185.

Kværna, T. and F. Ringdal (1988): Spectral analysis of Shagan River explosions recorded at NORSAR and NORESS, In: Semiann. Tech. Summ. 1 Apr - 30 Sep 88, NORSAR Sci. Rep. 1-88/89, Kjeller, Norway.

Lamb, F.K. (1988): Monitoring yields of underground nuclear tests using hydrodynamic methods, Nuclear Arms Technology in the 1990s, American Institute of Physics Publications, D. Schroeer and D. Hafmeister (eds.)

Leith, W. (1987): Tectonics of eastern Kazakhstan and implications for seismic source studies in the Shagan River area, In: Papers presented at the 9th Annual DARPA/AFGL Seismic Research Symposium, 15-18 June 1987, 34-37.

Lilwall, R.C., P.D. Marshall and D.W. Rivers (1988): Body wave magnitudes of some underground nuclear explosions at the Nevada (USA) and Shagan River (USSR) test sites, AWE Report No. 0 15/88, HMSO, London.

Marshall, P.D., T.C. Bache and R.C. Lilwall (1985): Body wave magnitudes and locations of Soviet underground explosions at the Semipalatinsk test site, AWRE Report No. 0 16/84 (re-issue), HMSO, London.

Marshall, P.D., D.L. Springer and H.C. Rodean (1979): Magnitude corrections for attenuation in the upper mantle, Geophys. J.R. astr. Soc., 5, 609-638.

McLaughlin, K.L., T.G. Barker, S.M. Day, B. Shkoller and J.L. Stevens (1988): Effects of depth of burial and tectonic strain release on regional and teleseismic explosion waveforms, Report No. AFGL-TR-88-0314, S-CUBED, La Jolla, California.

Mowat, M.W.H. and R.F. Burch (1977): Handbook for the stations which provide seismograms to the Blacknest Seismological Centre, United Kingdom, AWRE Blacknest Tech. Rep. 44/47/29 Blacknest, Brimpton, RG7 4RS, UK.

Mueller, G. (1973): Seismic moment and long period radiation of underground nuclear explosions, Bull. Seism. Soc. Am., 63, 847-858.

Myasnikov, K.V., L.B. Prozorov and I.E. Sitnikov (1970): Mechanical effects of single and multiple underground nuclear cratering explosions and the properties of the excavation dug by them, In: Nuclear Explosions for Peaceful Purposes, Ed. I.D. Morokhov (Atomizdat, Moscow), LLL Report UCRL-Trans-10517, 79-109.

Nuttli, O.W. (1973): Seismic wave attenuation and magnitude relations for eastern North America, J. Geophys. Res., 78, 876-885.

Nuttli, O.W. (1986a): Yield estimates of Nevada test site explosions obtained from seismic Lg waves, J. Geophys. Res., 91, 2137-2151.

Nuttli, O.W. (1986b): Lg magnitudes of selected East Kazakhstan underground explosions, Bull. Seism. Soc. Am., 76, 1241-1251.

Office of Technology Assessment, U.S. Congress (1988): Seismic Verification of Nuclear Testing Treaties, GPO, Washington, D.C., Report OTA-ISC-361, 1-139.

Patton, H.J. (1988): Application of Nuttli's method to estimate yield of Nevada test site explosions recorded on Lawrence Livermore National Laboratory's digital seismic system, Bull. Seism. Soc. Am., 78, 1759-1772.

Peyre, A.V. and A.A. Mossakovsky (1982): Tectonics of Kazakhstan, In: Exploratory Report for Tectonic Map of Kazakhstan, Nauka, Moscow.

Ringdal, F. (1976): Maximum-likelihood estimation of seismic magnitude, Bull. Seism. Soc. Am., 66, 789-802.

Ringdal, F. (1983): Magnitudes from P coda and Lg using NORSAR data, In: NORSAR Semiann. Tech. Summ., 1 Oct 1982 - 31 Mar 1983, NORSAR Sci. Rep. 2-82/83, Kjeller, Norway.

Ringdal, F. and B.Kr. Hokland (1987): Magnitudes of large Semipalatinsk explosions using P coda and Lg measurements at NORSAR, In: Semiann. Tech. Summ., 1 Apr - 30 Sep 1987, NORSAR Sci. Rep. 1-87/88, Kjeller, Norway.

Ringdal, F. and J. Fyen (1988): Comparative analysis of NORSAR and Gräfenberg Lg magnitudes of Shagan River explosions, In: Semiann. Tech. Summ., 1 Apr - 30 Sep 1988, NORSAR Sci. Rep. 1-88/89, Kjeller, Norway.

Stewart, R.C. (1988): P-wave seismograms from underground explosions at the Shagan River test site recorded at four arrays, AWE Report 0 4/88, HMSO, London.

Stimpson, I.G. (1988): Source parameters of explosions in granite at the French test site in Algeria, AWE Report 0 11/88, HMSO, London.

Storey, W.H., D.D. Eilers, T.O. McKown, D.M. Holt and G.C. Conrad (1982): CORRTEX-II, A dual microprocessor-controlled instrument for dynamic shock position measurements, Los Alamos National Laboratory Report LA-UR-82-558.

Sukhorukov, A.A., K.S. Akhmetov and I.V. Orlov (1973): Jubilee deposit, In: Geology of Coal and Oil Shale Deposits of the USSR, 217-230, Nedra, Moscow.

Sykes, L.R. and G. Ekström (1989): Comparison of seismic and hydrodynamic yield determinations for the Soviet Joint Verification Experiment of 1988, Proc. Natl. Acad. of Sci., USA, 86, 3456-3460.

No.	ORIGIN DATE	ORIGIN TIME	LAT	LON	MB	LOG RDP	N	STD	*** NORSAR **** M(LG)	N	STD	***** GRF ***** M(LG)	N	STD	FINAL M(LG)	SUB-REGION
1	01/15/65	5 59 58.4	49.940N	79.010E	5.870	3.87	1	0.14	-	-	-	-	-	-	-	TZ
2	06/19/68	5 05 57.3	49.982N	79.003E	5.280	3.31	4	0.07	-	-	-	-	-	-	-	NE
3	11/30/69	3 32 57.1	49.913N	78.961E	6.020	4.00	2	0.10	-	-	-	-	-	-	-	TZ
4	06/30/71	3 56 57.4	49.949N	78.986E	4.940	2.98	4	0.07	-	-	-	-	-	-	-	TZ
5	02/10/72	5 02 57.5	50.014N	78.878E	5.270	3.22	2	0.10	-	-	-	-	-	-	-	NE
6	11/02/72	1 26 57.6	49.923N	78.815E	6.160	4.38	1	0.14	6.118	42	0.014	-	-	-	6.118	SW
7	12/10/72	4 27 07.3	50.001N	78.973E	5.960	4.36	2	0.10	6.116	42	0.009	-	-	-	6.116	NE
8	07/23/73	1 22 57.6	49.962N	78.812E	6.170	-	-	-	6.199	40	0.006	-	-	-	6.199	TZ
9	12/14/73	7 46 57.2	50.044N	78.987E	5.790	3.84	1	0.14	5.868	42	0.033	-	-	-	5.868	NE
10	04/16/74	5 52 57.4	50.041N	78.943E	4.350	2.25	1	0.14	-	-	-	-	-	-	-	NE
11	05/31/74	3 26 57.5	49.950N	78.852E	5.810	3.88	1	0.14	-	-	-	-	-	-	-	TZ
12	10/16/74	6 32 57.6	49.979N	78.898E	5.410	3.17	3	0.08	5.411	42	0.024	-	-	-	5.411	TZ
13	12/27/74	5 46 56.9	49.943N	79.011E	5.500	3.07	3	0.08	5.708	42	0.056	-	-	-	5.708	NE
14	04/27/75	5 36 57.3	49.949N	78.926E	5.510	3.55	3	0.08	5.547	42	0.057	-	-	-	5.547	TZ
15	06/30/75	3 26 57.6	50.004N	78.957E	4.520	2.40	3	0.08	-	-	-	-	-	-	-	NE
16	10/29/75	4 46 57.3	49.946N	78.878E	5.610	3.42	4	0.07	5.629	42	0.046	-	-	-	5.629	TZ
17	12/25/75	5 16 57.2	50.044N	78.814E	5.690	3.59	4	0.07	5.801	42	0.035	-	-	-	5.801	NE
18	04/21/76	5 02 57.2	49.890N	78.827E	5.120	3.02	3	0.08	-	-	-	-	-	-	-	SW
19	06/09/76	3 02 57.2	49.989N	79.022E	5.070	3.08	3	0.08	5.199	42	0.089	-	-	-	5.199	NE
20	07/04/76	2 56 57.5	49.909N	78.911E	5.850	3.89	1	0.14	5.810	42	0.009	5.783	4	0.024	5.810	SW
21	08/28/76	2 56 57.5	49.969N	78.930E	5.740	3.68	3	0.08	5.735	41	0.013	5.653	3	0.052	5.733	TZ
22	11/23/76	5 02 57.3	50.008N	78.963E	5.790	3.81	3	0.08	-	-	-	5.792	3	0.057	5.819	NE
23	12/07/76	4 56 57.4	49.922N	78.846E	5.800	3.80	2	0.10	-	-	-	5.702	3	0.088	5.741	SW
24	05/29/77	2 56 57.6	49.937N	78.770E	5.750	3.80	1	0.14	5.677	41	0.035	5.573	3	0.038	5.655	SW
25	06/29/77	3 06 58.8	50.006N	78.869E	5.200	3.04	4	0.07	5.077	40	0.091	-	-	-	5.077	NE
26	09/05/77	3 02 57.3	50.035N	78.921E	5.730	3.93	3	0.08	5.897	40	0.017	5.769	3	0.036	5.879	NE
27	10/29/77	3 07 02.5	50.069N	78.975E	5.560	3.75	3	0.08	5.792	41	0.043	5.685	3	0.041	5.757	NE
28	11/30/77	4 06 57.4	49.958N	78.885E	5.890	3.92	2	0.10	-	-	-	5.716	3	0.041	5.753	TZ
29	06/11/78	2 56 57.6	49.898N	78.797E	5.830	3.87	4	0.07	5.752	39	0.029	5.724	4	0.039	5.755	SW
30	07/05/78	2 46 57.5	49.887N	78.871E	5.770	3.82	4	0.07	5.794	39	0.010	-	-	-	5.794	SW
31	08/29/78	2 37 06.3	50.000N	78.978E	5.900	3.98	4	0.07	6.010	39	0.008	6.010	6	0.022	6.010	NE
32	09/15/78	2 36 57.4	49.916N	78.879E	5.890	3.96	3	0.08	5.908	38	0.018	-	-	-	5.908	SW
33	11/04/78	5 05 57.3	50.034N	78.943E	5.560	3.66	4	0.07	5.697	39	0.080	5.636	6	0.080	5.690	NE
34	11/29/78	4 33 02.5	49.949N	78.798E	5.960	4.08	3	0.08	5.973	39	0.013	5.886	2	0.075	5.971	SW
35	02/01/79	4 12 57.6	50.090N	78.870E	5.290	3.30	3	0.08	-	-	-	-	-	-	-	NE
36	06/23/79	2 56 57.5	49.903N	78.855E	6.160	4.08	3	0.08	6.056	21	0.009	6.123	4	0.021	6.064	SW
37	07/07/79	3 46 57.3	50.026N	78.991E	5.840	3.73	3	0.08	5.969	38	0.008	5.938	7	0.021	5.966	NE
38	08/04/79	3 56 57.1	49.894N	78.904E	6.130	4.13	4	0.07	6.099	39	0.008	6.117	9	0.015	6.100	SW
39	08/18/79	2 51 57.1	49.943N	78.938E	6.130	4.13	4	0.07	-	-	-	6.145	7	0.017	6.126	TZ
40	10/28/79	3 16 56.9	49.973N	78.997E	5.980	3.92	2	0.10	6.053	34	0.010	6.046	8	0.023	6.051	NE
41	12/02/79	4 36 57.5	49.891N	78.796E	5.990	3.84	2	0.10	5.917	28	0.021	5.938	11	0.025	5.929	SW
42	12/23/79	4 56 57.4	49.916N	78.755E	6.130	3.92	1	0.14	-	-	-	6.045	9	0.021	6.039	SW
43	04/25/80	3 56 57.5	49.973N	78.755E	5.450	3.46	3	0.08	-	-	-	-	-	-	-	SW
44	06/12/80	3 26 57.6	49.980N	79.001E	5.520	3.55	3	0.08	-	-	-	5.571	11	0.105	5.627	NE
45	06/29/80	2 32 57.7	49.939N	78.815E	5.690	3.71	4	0.07	5.683	16	0.026	5.746	8	0.046	5.706	SW
46	09/14/80	2 42 39.1	49.921N	78.802E	6.210	4.36	1	0.14	-	-	-	-	-	-	-	SW
47	10/12/80	3 34 14.1	49.961N	79.028E	5.880	3.95	4	0.07	5.925	28	0.013	5.933	13	0.034	5.927	NE
48	12/14/80	3 47 06.4	49.899N	78.938E	5.930	3.98	4	0.07	5.929	28	0.018	5.944	10	0.027	5.936	TZ

Table VII.1.1. List of presumed explosions from the Shagan River area used in this study. The table includes, for each event, date, origin time, latitude, longitude, m_b (maximum likelihood), log Ψ_∞ (with number of stations and standard deviation of estimate), NORSAR and Gräfenberg M_{Lg} (including number of available channels and estimated precision of measurement), a weighted average of M_{Lg}, adjusted to NORSAR M_{Lg} scale and a region identifier. (Page 1 of 2)

No.	ORIGIN DATE	ORIGIN TIME	LAT	LON	MB	LOG RDP	N	STD	*** NORSAR **** M(LG)	N	STD	***** GRF ***** M(LG)	N	STD	FINAL M(LG)	SUB-REGION
49	12/27/80	4 9 8.1	50.057N	78.981E	5.870	3.89	3	0.08	5.939	27	0.014	5.885	11	0.034	5.933	NE
50	03/29/81	4 03 50.0	50.007N	78.982E	5.490	3.38	3	0.08	5.556	28	0.085	5.437	11	0.184	5.548	NE
51	04/22/81	1 17 11.3	49.885N	78.810E	5.940	4.07	3	0.08	5.908	28	0.022	5.956	11	0.027	5.929	SW
52	05/27/81	3 58 12.3	49.985N	78.980E	5.300	3.32	4	0.07	5.456	27	0.015	-	-	-	5.456	NE
53	09/13/81	2 17 18.3	49.910N	78.915E	6.060	4.18	4	0.07	6.113	29	0.008	6.106	9	0.015	6.108	TZ
54	10/18/81	3 57 02.6	49.923N	78.859E	6.000	4.05	4	0.07	5.985	34	0.010	5.956	9	0.021	5.981	SW
55	11/29/81	3 35 08.6	49.887N	78.860E	5.620	3.53	4	0.07	5.581	28	0.102	5.511	12	0.192	5.580	SW
56	12/27/81	3 43 14.1	49.923N	78.795E	6.160	4.19	2	0.10	6.074	34	0.009	6.092	10	0.020	6.075	SW
57	04/25/82	3 23 05.4	49.903N	78.913E	6.030	4.16	2	0.10	6.077	35	0.008	6.058	11	0.017	6.072	TZ
58	07/04/82	1 17 14.2	49.960N	78.807E	6.080	4.24	2	0.10	-	-	-	-	-	-	-	SW
59	08/31/82	1 31 00.7	49.924N	78.761E	5.200	3.03	4	0.07	-	-	-	-	-	-	-	SW
60	12/05/82	3 37 12.6	49.919N	78.813E	6.080	4.01	3	0.08	5.990	31	0.019	6.002	13	0.020	5.996	SW
61	12/26/82	3 35 14.2	50.071N	78.988E	5.580	3.60	4	0.07	5.658	39	0.050	5.597	13	0.067	5.655	NE
62	06/12/83	2 36 43.5	49.913N	78.916E	6.020	-	-	-	6.072	25	0.009	-	-	-	6.072	TZ
63	10/06/83	1 47 06.5	49.916N	78.764E	5.950	-	-	-	5.870	19	0.033	5.843	13	0.043	5.868	SW
64	10/26/83	1 55 04.8	49.901N	78.828E	6.040	3.92	3	0.08	6.000	33	0.021	6.036	13	0.021	6.016	SW
65	11/20/83	3 27 04.4	50.047N	78.999E	5.330	3.44	1	0.14	5.409	30	0.170	-	-	-	5.409	NE
66	02/19/84	3 57 03.4	49.885N	78.745E	5.770	3.71	3	0.08	5.725	29	0.038	-	-	-	5.725	SW
67	03/07/84	2 39 06.4	50.049N	78.954E	5.560	3.56	1	0.14	5.698	29	0.065	5.575	12	0.108	5.680	NE
68	03/29/84	5 19 08.2	49.912N	78.955E	5.860	3.73	1	0.14	5.897	29	0.012	5.957	13	0.043	5.902	TZ
69	04/25/84	1 09 03.5	49.929N	78.870E	5.900	-	-	-	5.870	35	0.008	5.803	13	0.031	5.867	SW
70	05/26/84	3 13 12.4	49.969N	79.006E	6.010	4.10	3	0.08	6.072	33	0.007	6.128	13	0.015	6.079	NE
71	07/14/84	1 09 10.5	49.893N	78.884E	6.100	3.97	1	0.14	6.054	32	0.007	6.064	12	0.015	6.054	SW
72	09/15/84	6 15 10.1	49.985N	78.883E	5.040	-	-	-	-	-	-	-	-	-	-	SW
73	10/27/84	1 50 10.6	49.920N	78.777E	6.190	4.13	3	0.08	6.085	33	0.011	6.145	13	0.016	6.098	SW
74	12/02/84	3 19 06.3	49.989N	79.011E	5.770	3.80	2	0.10	5.880	29	0.020	5.860	12	0.036	5.880	NE
75	12/16/84	3 55 02.7	49.926N	78.820E	6.120	4.06	2	0.10	6.048	29	0.010	6.038	13	0.014	6.043	SW
76	12/28/84	3 50 10.7	49.866N	78.703E	6.000	4.00	3	0.08	5.985	35	0.009	5.947	13	0.021	5.980	SW
77	02/10/85	3 27 07.5	49.888N	78.781E	5.830	3.82	4	0.07	5.803	40	0.024	5.801	13	0.058	5.806	SW
78	04/25/85	0 57 06.5	49.914N	78.902E	5.840	3.65	2	0.10	5.858	29	0.045	5.838	9	0.047	5.859	TZ
79	06/15/85	0 57 00.7	49.898N	78.845E	6.050	3.99	1	0.14	5.976	30	0.009	6.031	13	0.017	5.987	SW
80	06/30/85	2 39 02.6	49.848N	78.658E	5.920	3.95	2	0.10	5.931	30	0.009	5.906	13	0.017	5.928	SW
81	07/20/85	0 53 14.4	49.936N	78.785E	5.890	3.86	2	0.10	5.861	37	0.013	5.870	12	0.031	5.865	SW
82	03/12/87	1 57 17.2	49.939N	78.823E	5.310	3.28	4	0.07	5.218	33	0.076	-	-	-	5.218	SW
83	04/03/87	1 17 08.0	49.928N	78.829E	6.120	4.07	4	0.07	6.052	33	0.008	6.127	11	0.017	6.063	SW
84	04/17/87	1 03 04.8	49.886N	78.691E	5.920	4.00	4	0.07	5.901	33	0.020	5.915	12	0.026	5.910	SW
85	06/20/87	0 53 04.8	49.913N	78.735E	6.030	4.00	3	0.08	5.972	36	0.007	5.947	10	0.028	5.971	SW
86	08/02/87	0 58 06.8	49.880N	78.917E	5.830	3.97	3	0.08	5.871	30	0.011	5.853	11	0.022	5.871	SW
87	11/15/87	3 31 06.7	49.871N	78.791E	5.980	4.02	4	0.07	5.974	37	0.008	5.984	13	0.022	5.975	SW
88	12/13/87	3 21 04.8	49.989N	78.844E	6.060	4.17	2	0.10	6.093	31	0.010	6.067	12	0.015	6.082	SW
89	12/27/87	3 05 04.7	49.864N	78.758E	6.000	4.08	2	0.10	6.046	31	0.011	6.033	13	0.019	6.042	SW
90	02/13/88	3 05 05.9	49.954N	78.910E	5.970	4.01	3	0.08	6.042	26	0.009	6.045	13	0.029	6.042	TZ
91	04/03/88	1 33 05.8	49.917N	78.945E	5.990	4.15	2	0.10	6.063	31	0.007	6.071	13	0.014	6.063	TZ
92	05/04/88	0 57 06.8	49.928N	78.769E	6.090	4.06	3	0.08	6.044	31	0.008	6.068	13	0.020	6.046	SW
93	06/14/88	2 27 06.4	50.045N	79.005E	4.800	2.55	2	0.10	-	-	-	-	-	-	-	NE
94	09/14/88	4 00 00.0	49.870N	78.820E	6.030	4.05	2	0.10	5.969	37	0.010	5.970	12	0.043	5.969	SW
95	11/12/88	3 30 03.8	50.056N	78.991E	5.200	-	-	-	-	-	-	-	-	-	-	NE
96	12/17/88	4 18 06.8	49.818N	78.910E	5.800	-	-	-	5.801	37	0.018	-	-	-	5.801	TZ

Table VII.1.1. (Page 2 of 2)

EVENT NO	DATE	REG	ESTIMATED YIELDS LG	P	COMB
1	01/15/65	TZ	-	-	111*)
2	06/19/68	NE	-	26	26
3	11/30/69	TZ	-	135	135
4	06/30/71	TZ	-	9	9
5	02/10/72	NE	-	24	24
6	11/02/72	SW	166	168	167
7	12/10/72	NE	165	159	162
8	07/23/73	TZ	204	200	202
9	12/14/73	NE	88	93	90
10	04/16/74	NE	-	2	2
11	05/31/74	TZ	-	81	81
12	10/16/74	TZ	27	26	27
13	12/27/74	NE	58	36	46
14	04/27/75	TZ	39	39	39
15	06/30/75	NE	-	4	4
16	10/29/75	TZ	47	44	46
17	12/25/75	NE	74	66	70
18	04/21/76	SW	-	11	11
19	06/09/76	NE	16	15	15
20	07/04/76	SW	76	74	75
21	08/28/76	TZ	62	66	64
22	11/23/76	NE	77	91	84
23	12/07/76	SW	63	65	64
24	05/29/77	SW	51	58	54
25	06/29/77	NE	12	19	15
26	09/05/77	NE	90	85	88
27	10/29/77	NE	66	55	60
28	11/30/77	TZ	65	99	80
29	06/11/78	SW	66	72	69
30	07/05/78	SW	72	62	67
31	08/29/78	NE	126	123	125
32	09/15/78	SW	97	85	91
33	11/04/78	NE	56	53	54
34	11/29/78	SW	114	103	108
35	02/01/79	NE	-	26	26
36	06/23/79	SW	145	155	150
37	07/07/79	NE	113	97	105
38	08/04/79	SW	158	149	154
39	08/18/79	TZ	169	180	174
40	10/28/79	NE	140	144	142
41	12/02/79	SW	102	100	101
42	12/23/79	SW	136	145	140
43	04/25/80	SW	-	27	27
44	06/12/80	NE	47	46	47
45	06/29/80	SW	58	50	54
46	09/14/80	SW	-	189	189
47	10/12/80	NE	102	117	109
48	12/14/80	TZ	104	112	108

Table VII.1.2. Estimated yields for the explosions of Table VII.1.1, as discussed in the text. For each event (except for Event 1, see text), we list a) yield estimate based on Lg waves (NORSAR and GRF), b) yield estimate based on P waves (m_b and log Ψ_∞) and c) a combined estimate, obtained by logarithmic averaging of a) and b). (Page 1 of 2)

EVENT NO	DATE	REG	ESTIMATED YIELDS LG	P	COMB
49	12/27/80	NE	103	111	107
50	03/29/81	NE	39	40	40
51	04/22/81	SW	102	98	100
52	05/27/81	NE	31	27	29
53	09/13/81	TZ	162	161	162
54	10/18/81	SW	117	111	114
55	11/29/81	SW	42	40	41
56	12/27/81	SW	149	163	156
57	04/25/82	TZ	148	146	147
58	07/04/82	SW	-	139	139
59	08/31/82	SW	-	13	13
60	12/05/82	SW	121	128	124
61	12/26/82	NE	51	54	52
62	06/12/83	TZ	148	136	142
63	10/06/83	SW	87	95	91
64	10/26/83	SW	128	113	120
65	11/20/83	NE	27	29	28
66	02/19/84	SW	61	59	60
67	03/07/84	NE	54	51	53
68	03/29/84	TZ	95	89	92
69	04/25/84	SW	87	84	85
70	05/26/84	NE	150	163	157
71	07/14/84	SW	141	136	138
72	09/15/84	SW	-	9	9
73	10/27/84	SW	158	169	163
74	12/02/84	NE	90	87	89
75	12/16/84	SW	137	143	140
76	12/28/84	SW	117	108	112
77	02/10/85	SW	75	70	72
78	04/25/85	TZ	85	81	83
79	06/15/85	SW	119	121	120
80	06/30/85	SW	102	89	95
81	07/20/85	SW	87	81	84
82	03/12/87	SW	17	19	18
83	04/03/87	SW	144	141	143
84	04/17/87	SW	98	92	95
85	06/20/87	SW	114	115	114
86	08/02/87	SW	88	75	81
87	11/15/87	SW	115	105	110
88	12/13/87	SW	151	130	140
89	12/27/87	SW	137	111	123
90	02/13/88	TZ	137	123	129
91	04/03/88	TZ	144	133	138
92	05/04/88	SW	138	133	136
93	06/14/88	NE	-	7	7
94	09/14/88	SW	113	117	115
95	11/12/88	NE	-	20	20
96	12/17/88	TZ	74	77	76

Table VII.1.2. (Page 2 of 2)

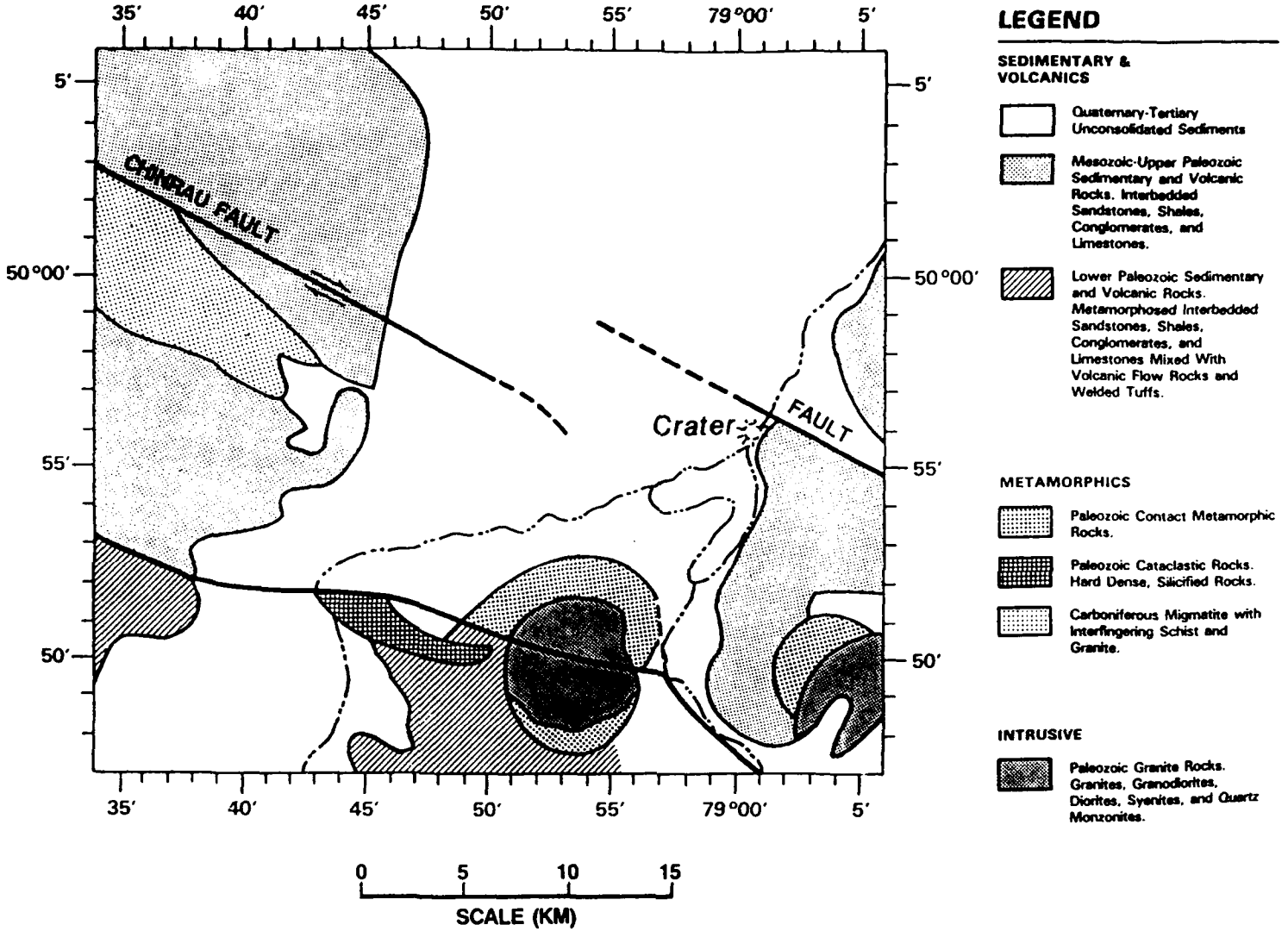

Fig. VII.1.1. Surface geology of the Shagan River area. The crater from the 15 January 1965 explosion is indicated. Note the two faults marked on the figure.

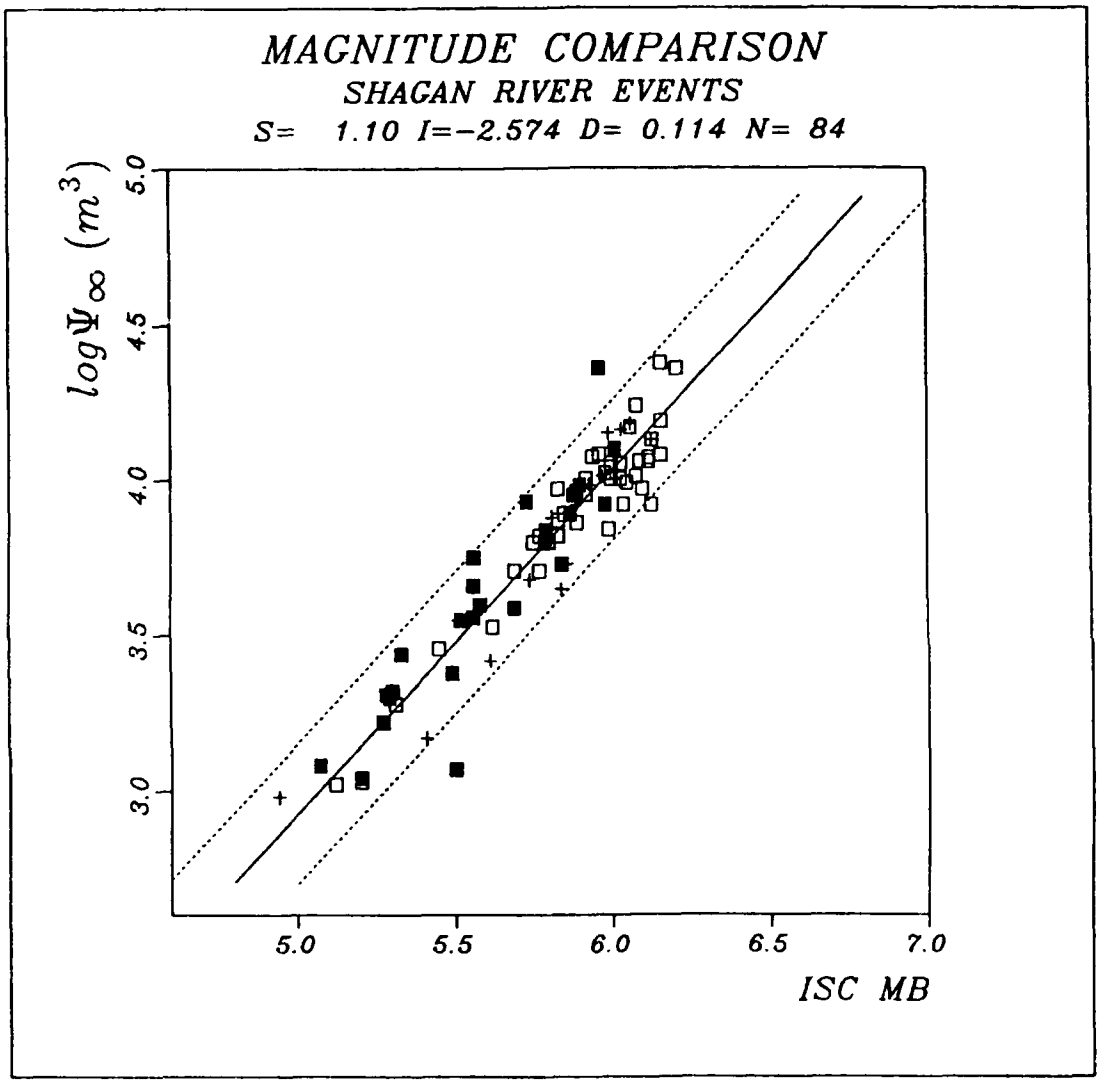

Fig. VII.1.2. Array network log Ψ_∞ plotted against maximum likelihood m_b. Open and filled symbols denote SW and NE events, respectively, whereas crosses denote TZ events. The line drawn through the data is the best least squares straight line, assuming no error in m_b. The dotted lines correspond to plus/minus two standard deviations in the vertical direction.

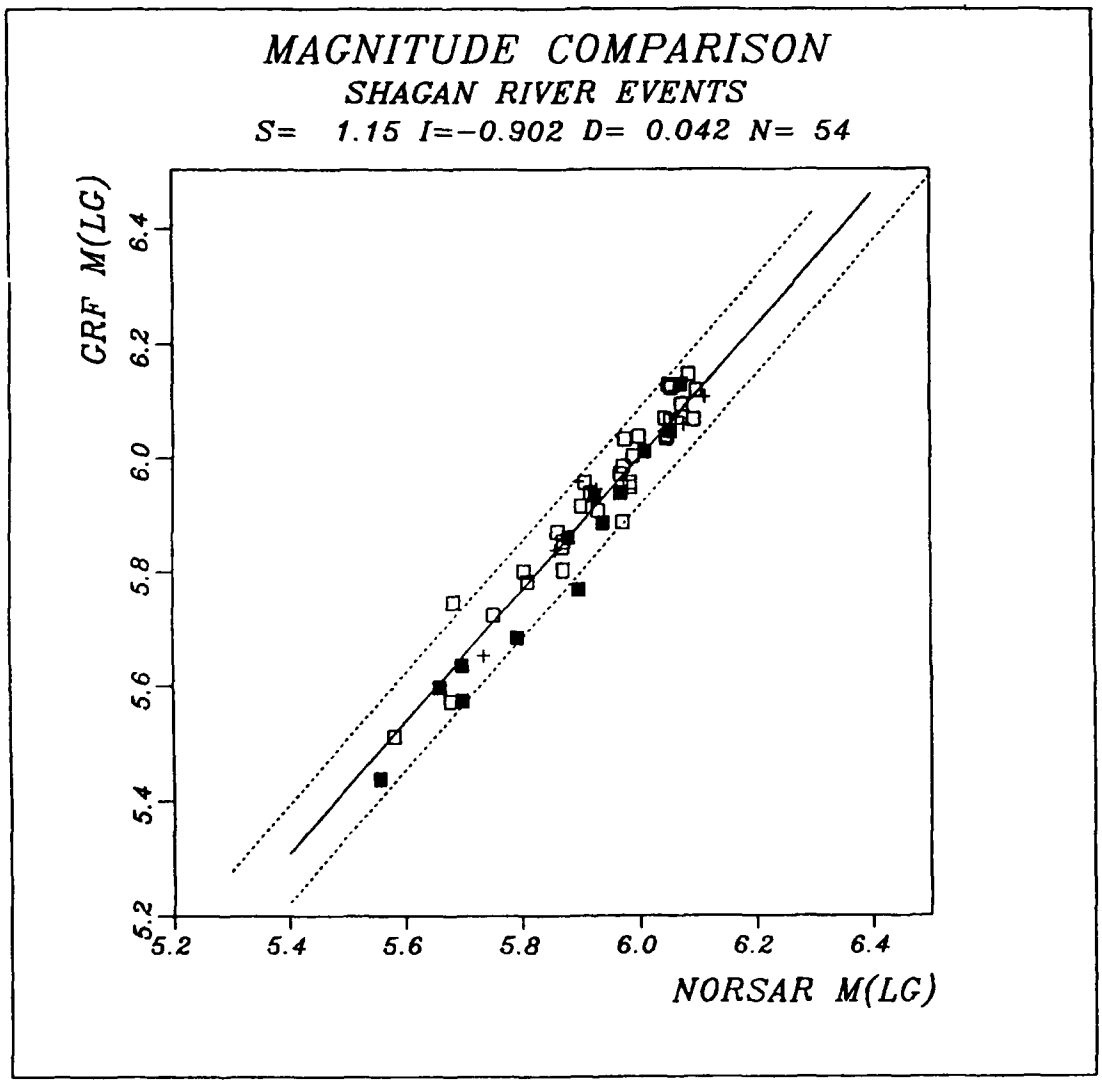

Fig. VII.1.3. Gräfenberg m_{Lg} plotted against NORSAR m_{Lg}. The line drawn through the data is the best least squares fit, assuming no error in NORSAR m_{Lg}. The dotted lines correspond to plus/minus two standard deviations. Note the consistency between SW events (open symbols), NE events (filled symbols) and TZ events (crosses).

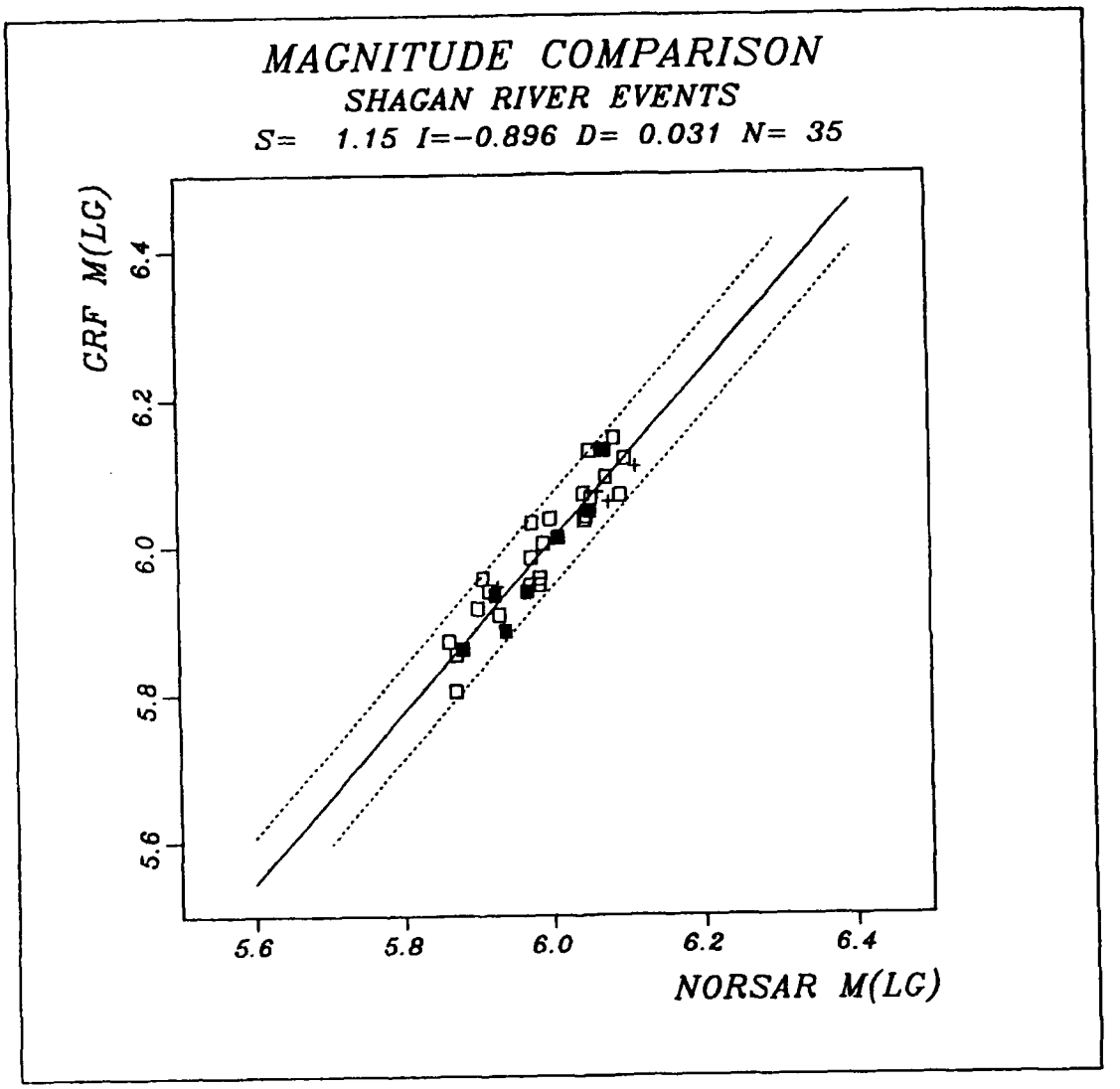

Fig. VII.1.4. Gräfenberg m_{Lg} plotted against NORSAR m_{Lg} for well-recorded events, i.e., requiring at least 6 sensors available, and a precision of measurement better than 0.04 for each array. Note the reduction in scatter compared to Fig. VII.1.3.

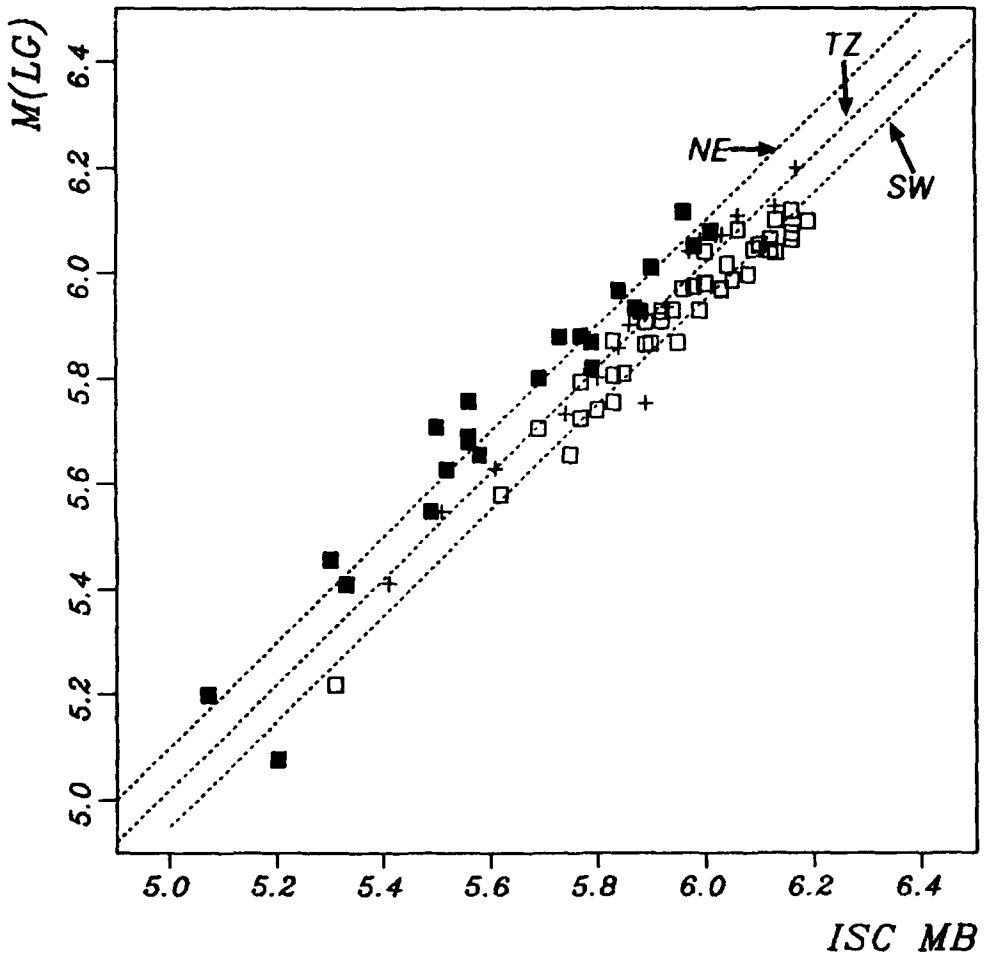

Fig. VII.1.5. NORSAR/GRF m_{Lg} plotted against maximum likelihood m_b. Note the difference between SW events (open symbols), NE events (filled symbols) and TZ events (crosses). A straight line has been fitted to each of these three subsets, with a slope restricted to 1.00.

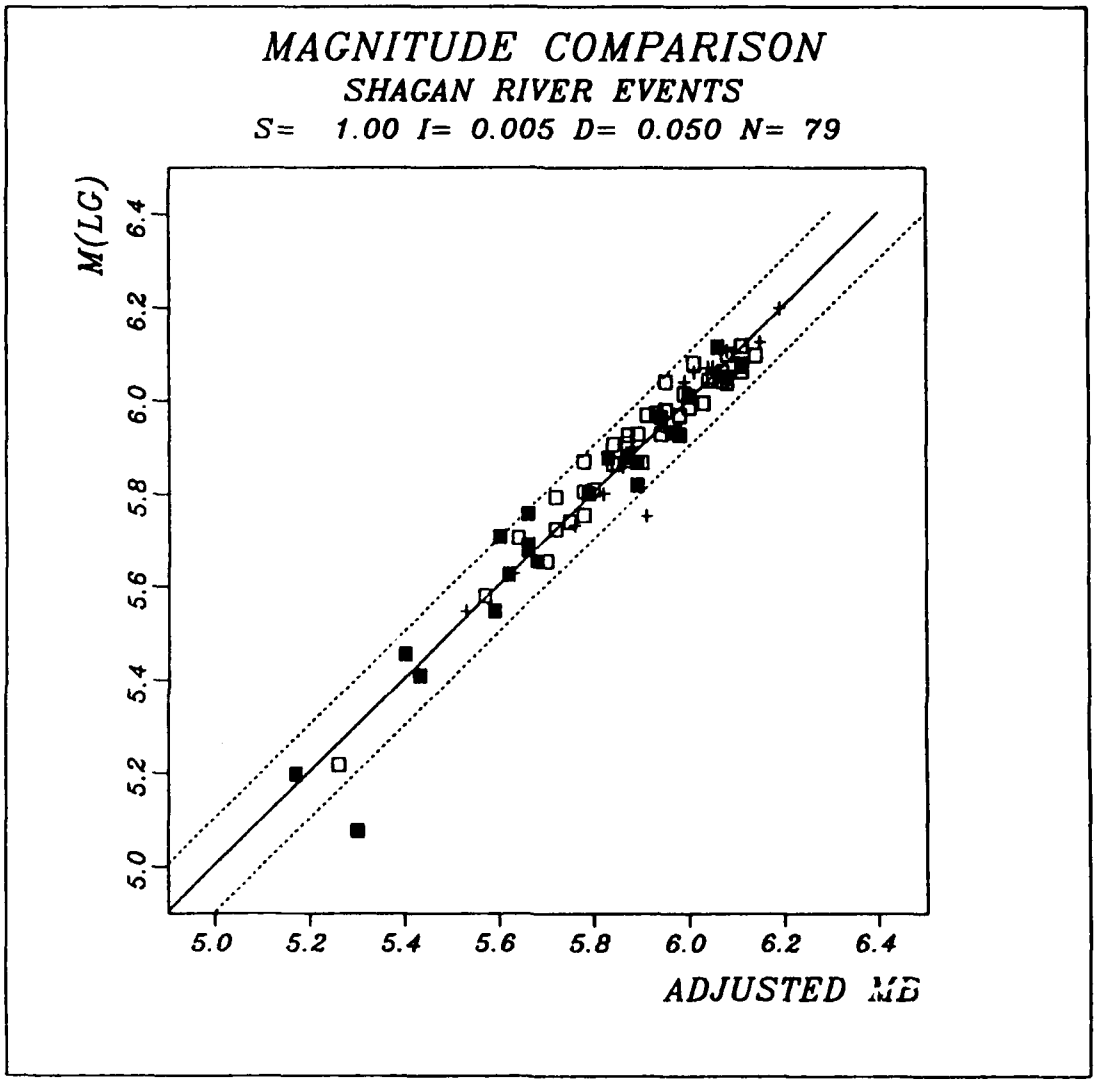

Fig. VII.1. 6. NORSAR/GRF m_{Lg} plotted against "adjusted m_b", i.e., m_b values adjusted for average bias in each of the three subregions. Note the excellent correspondence, with the exception of two outliers as discussed in the text.

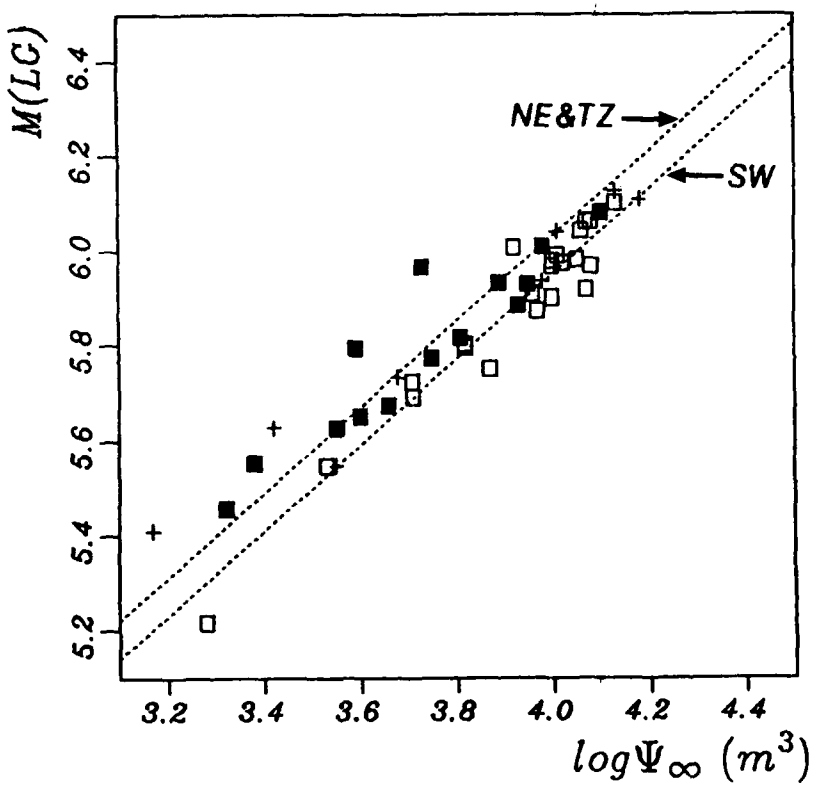

Fig. VII.1.7. NORSAR/GRF m_{Lg} plotted against network averaged log Ψ_∞, requiring at least three station observations for the latter. The two stippled lines (slope of 0.9) represent linear fits to the SW events and the NE/TZ events, respectively. Symbol conventions are as in Fig. VII.1.2.

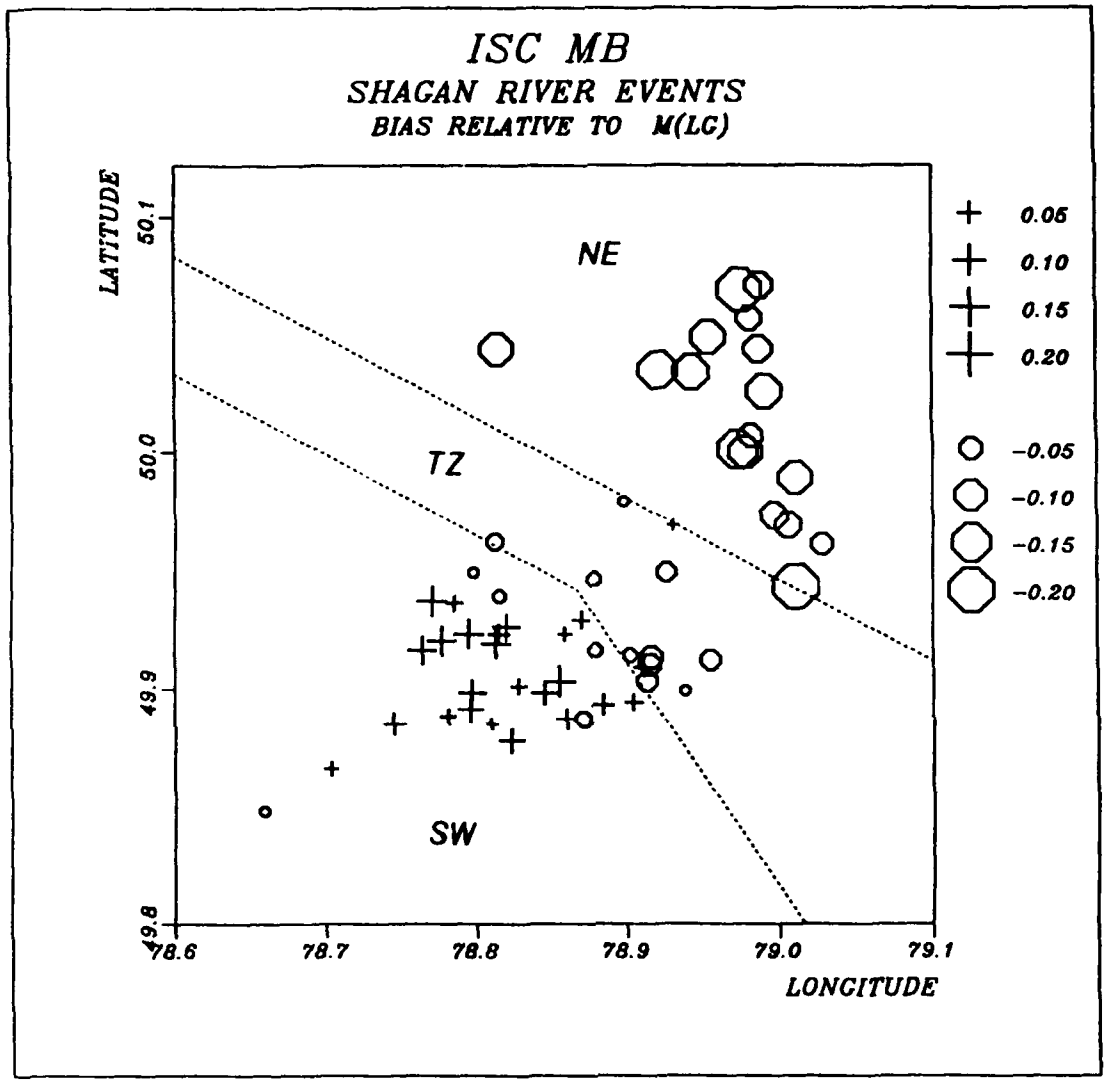

Fig. VII.1.8. Plot of magnitude residuals (maximum likelihood m_b minus m_{Lg}) as a function of event location for events of $m_b \geq 5.50$. Only events with NORSAR data available have been included. Plusses and circles correspond to residuals greater or less than zero, respectively, with symbol size proportional to the deviation. Location estimates are those in Table VII.1.1, and only events prior to 1986 (which have the most precise locations) have been included. Note the systematic variation within the Shagan River areas, with different patterns in the three subregions.

VII.2 Continuous monitoring of seismic event detection capability

Introduction

In this paper we address the problem of using a network to continuously monitor the seismic noise field. The purpose is to determine to which extent interfering events affect the monitoring of events within a target region. We develop a model that can be used to obtain, at a given confidence level, a continuous assessment of the upper limit of magnitudes of seismic events in the target region that would go undetected by such a network. We give an example of application using data from the network of three regional arrays, NORESS, ARCESS, FINESA in Fennoscandia. The application of the model to more general problems in seismic monitoring is also briefly discussed.

Model

In formulating the approach, we consider a given geographical location, and a given "origin time" of a hypothetical event. Assume that this "target area" is to be monitored by a given seismic network, and that we wish to consider N seismic phases (there might be several phases per station).

For each phase, we assume that we have an estimate S_i of the signal (or noise) level at the predicted arrival time. For P-phases, S_i might be the maximum short term average (STA) value (1 second integration window) within $\pm$ 5 seconds of the predicted time. For Lg, a longer STA integration window (e.g., 10 seconds) might be used, and its maximum might be selected allowing a somewhat greater deviation from the predicted arrival time.

We assume that the network has been calibrated (or alternatively that standard attenuation values are available), so that magnitude correction factors (b_i) are available for all phases. Thus, if a detectable signal is present:

$$m_i = \log (S_i) + b_i \qquad (i = 1,2,\ldots N) \tag{1}$$

Here, m_i are estimates of the event magnitude m. Statistically, we can consider each m_i as sampled from a normal distribution (m,σ). Based on NORSAR experience, we consider a standard value of $\sigma = 0.2$ to be reasonable for a small epicentral area, and this value will be used in the following.

Let us now assume a "noise situation", i.e., that there are no phase detections corresponding to events at the given location for the given origin time.

We then have a set of "noise" observations a_i, where (see Fig. VII.2.1):

$$a_i = \log(S_i) + b_i \qquad (i = 1,2,\ldots N) \tag{2}$$

If a hypothetical event of magnitude m were present, it would have phase magnitudes m_i normally distributed around m. We know that for each phase,

$$m_i \leq a_i \qquad (i = 1,2,\ldots N) \tag{3}$$

Following a procedure similar to that of Ringdal (1976), we now consider the function:

$$f(m) = \text{Prob}(\text{all } m_i \leq a_i \;/\; \text{event magnitude m}) \tag{4}$$

For each phase, we obtain probability functions $f_i(m)$ and $g_i(m)$ as follows:

$$f_i(m) = \text{Prob}(m_i \leq a_i/m) = 1 - \Phi\left(\frac{m-a_i}{\sigma}\right) \qquad (i=1,2,\ldots,N) \tag{5}$$

$$g_i(m) = \text{Prob}(m_i > a_i/m) = \Phi\left(\frac{m-a_i}{\sigma}\right) \quad (i=1,2,\ldots,N) \tag{6}$$

where Φ is the standard (0,1) normal distribution.

Thus, assuming independence,

$$f(m) = \prod_{i=1}^{N} f_i(m) \tag{7}$$

The probability g(m) that at least one of the observed noise values would be exceeded by the signals of a hypothetical event of magnitude m, then becomes

$$g(m) = 1 - f(m) \tag{8}$$

As illustrated in Fig. VII.2.2, the 90 per cent upper limit is then defined as the solution of the equation

$$g(m) = 0.90 \tag{9}$$

It is important to interpret the 90 per cent limit defined above in the proper way. Thus, it should not be considered as a 90 per cent network detection threshold since we have made no allowance for a signal-to-noise ratio which would be required in order to detect an event, given the noise levels. Rather, the computed level is tied to the actually observed noise values, and to the fact that any hypothetical signal must lie below these values. Our 90 per cent limit represents the largest magnitude of a possible hidden event, in the sense that above

this limit, there is at least a 90 per cent probability that one or more of the observed noise values would be exceeded by the signals of such an event.

Application to a regional network

As an application of the method, we selected as a target region to be monitored an area as shown in Fig. VII.2.3 situated at similar distance from the three arrays. For each of the three arrays, one Pn beam and one Lg beam were steered to this location. The beam traces were filtered using the frequency bands 3-5 Hz (Pn) and 2-4 Hz (Lg). Magnitude calibration values (b_i) were obtained by processing previously recorded events of known magnitude (M_L) and at similar distance ranges, and then determining b_i values independently for Pn and Lg.

Once these input traces had been formed from the three arrays, a set of time delays was introduced, using a delay for each phase that corresponded to the target location. Arrival time tolerances were set to $\pm$ 5 seconds for Pn and $\pm$ 10 seconds for Lg. This is roughly consistent with a beam radius of 50 km as shown on the figure. STA integration windows were set to 1 second for Pn and 10 seconds for Lg. The values of S_i in eq. (1) were obtained as the maximum STA values within the respective arrival time tolerances, using the mid-point of the integration interval as time reference.

We chose to analyze a 3 1/2 hour interval during which seven regional seismic events were reported in the Helsinki or Bergen bulletin. The highest magnitude (M_L = 2.9) corresponded to a large mining explosion at the USSR-Norway border close to the ARCESS site. These seven events were all located outside the target beam region, and one of our aims was to investigate how interfering signals from these events would influence the monitoring capability for the chosen beam region.

Fig. VII.2.4 shows, for the beam region considered, the computed 90 per cent upper magnitude limits, plotted as a function of time. In this

figure, only the Pn phase has been used, and the three arrays are shown individually and in combination (bottom trace).

It is clear from Fig. VII.2.4 that when considering individual arrays only, there are several possible time intervals when relatively large events (M_L ~ 2.0-3.0) located in the beam area might go undetected because of signals from interfering events. However, when the Pn phases are combined, these instances occur much more seldom.

Fig. VII.2.5 shows a similar plot, but this time including both the Pn and the Lg phase for each array. Even on an individual array basis, this causes substantial reduction in the upper magnitude limits. For the combined plot (bottom trace of Fig. VII.2.5), which takes into account all 6 Pn and Lg phases from the three arrays, we see that the upper limit is well below M_L = 2.0 for the entire time interval. Thus, we may conclude that, at the specified level of confidence, no event of M_L = 2.0 or higher occurred in the beam region during the time period considered.

Discussion

We consider that the method to provide continuous monitoring of upper magnitude limits at specified beam locations provides a useful supplement to standard statistical network capability studies (e.g., Wirth, 1977; Ringdal, 1986). In particular, this application would give a way to assess the possible magnitude of non-detected events during the coda of large earthquakes. In such situations, it would be appropriate to use global network data and include as many relevant phases as possible for each network station. For example, while an expected P phase at a given station may be obscured by the earthquake coda, later phases such as PcP or PP may be less influenced, and the noise level at their respective expected arrival times would therefore provide important information as to the size of possible undetected events.

We also note that the approach presented here to upper limit magnitude calculation could be applied to extend the utility of various discriminants, such as M_S:m_b. For small explosions, surface waves frequently are too weak to be observed at any station of the recording network. Obtaining reliable upper bound on M_S in such cases would expand the range of usefulness of this discriminant. In practice, an "upper bound" for single-station measurements has often been given as the "noise magnitude" at that station, i.e., the M_S value that corresponds to the actually observed noise level at the expected time of Rayleigh wave arrival. The proposed procedure will include this as a special case of a more general network formulation.

F. Ringdal
T. Kværna

References

Ringdal, F. (1976): Maximum-likelihood estimation of seismic magnitude. Bull. Seism. Soc. Am., 66, 789-802.

Ringdal, F. (1986): Study of magnitudes, seismicity and earthquake detectability using a global network. Bull. Seism. Soc. Am., 76, 1641-1659.

Wirth, M.H. (1977): Estimation of network detection and location capability. Teledyne Geotech, Alexandria Virginia.

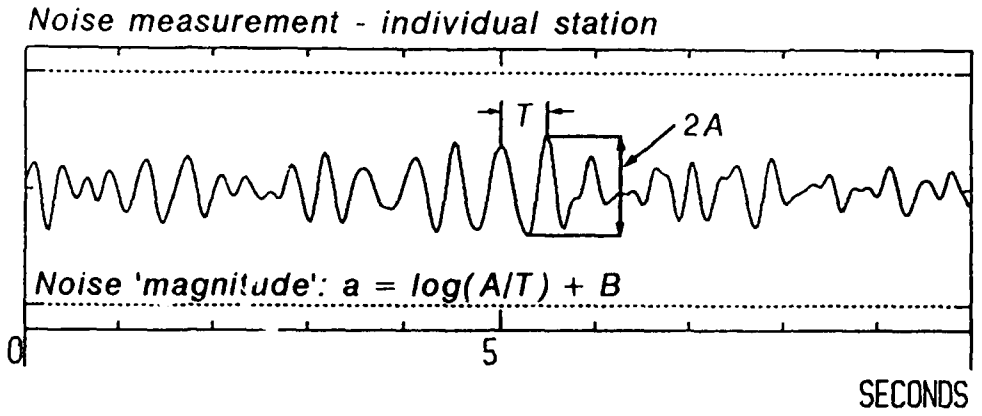

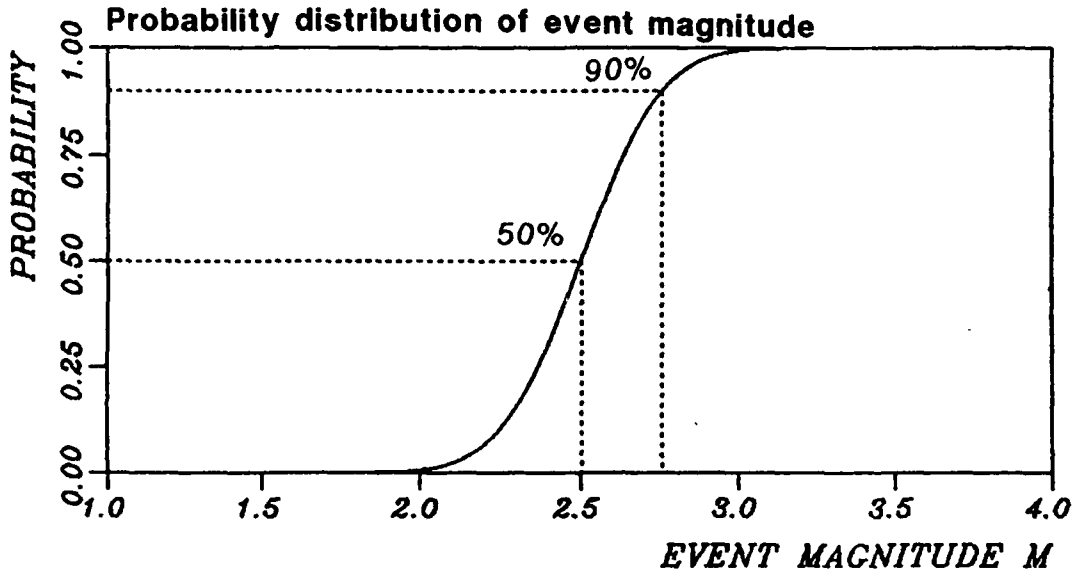

Fig. VII.2.1. Illustration of the method to calculate upper magnitude limits for the single station case. The top part of the figure shows how the noise "magnitude" is computed (given an assumed distance correction term B). The bottom part shows the corresponding probability function $g_i(m)$ defined in the text.

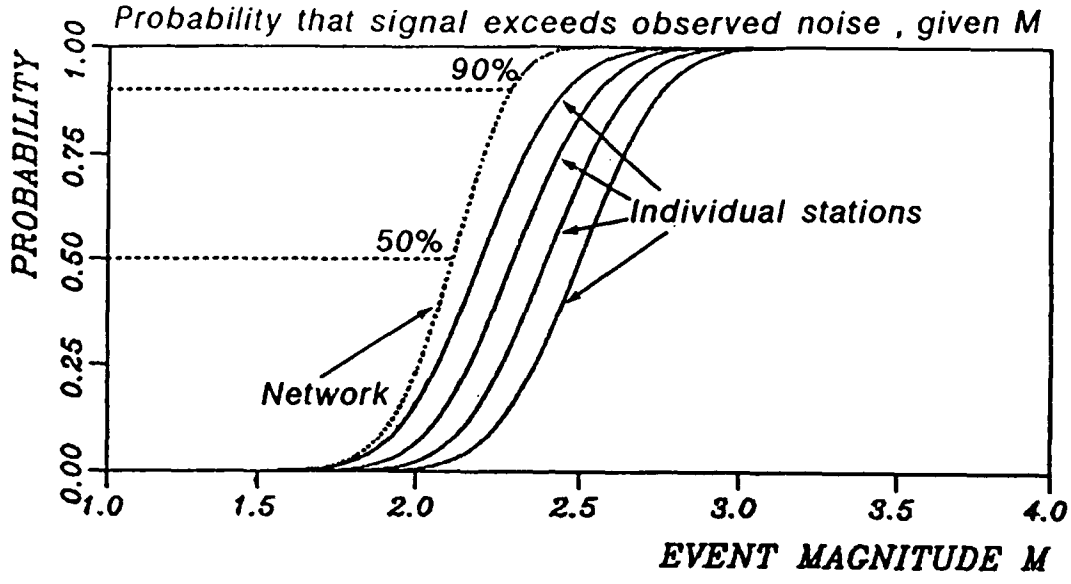

Fig. VII.2.2. Illustration of the procedure for calculating upper magnitude limits given a network of stations. Each network station gives rise to a probability distribution $g_i(M)$ as described in the text and illustrated in Fig. VII.2.1. The dotted curve, g(M), represents the probability, given event magnitude M, that the signal from a hypothetical event would exceed the actually observed noise level at at least one station.

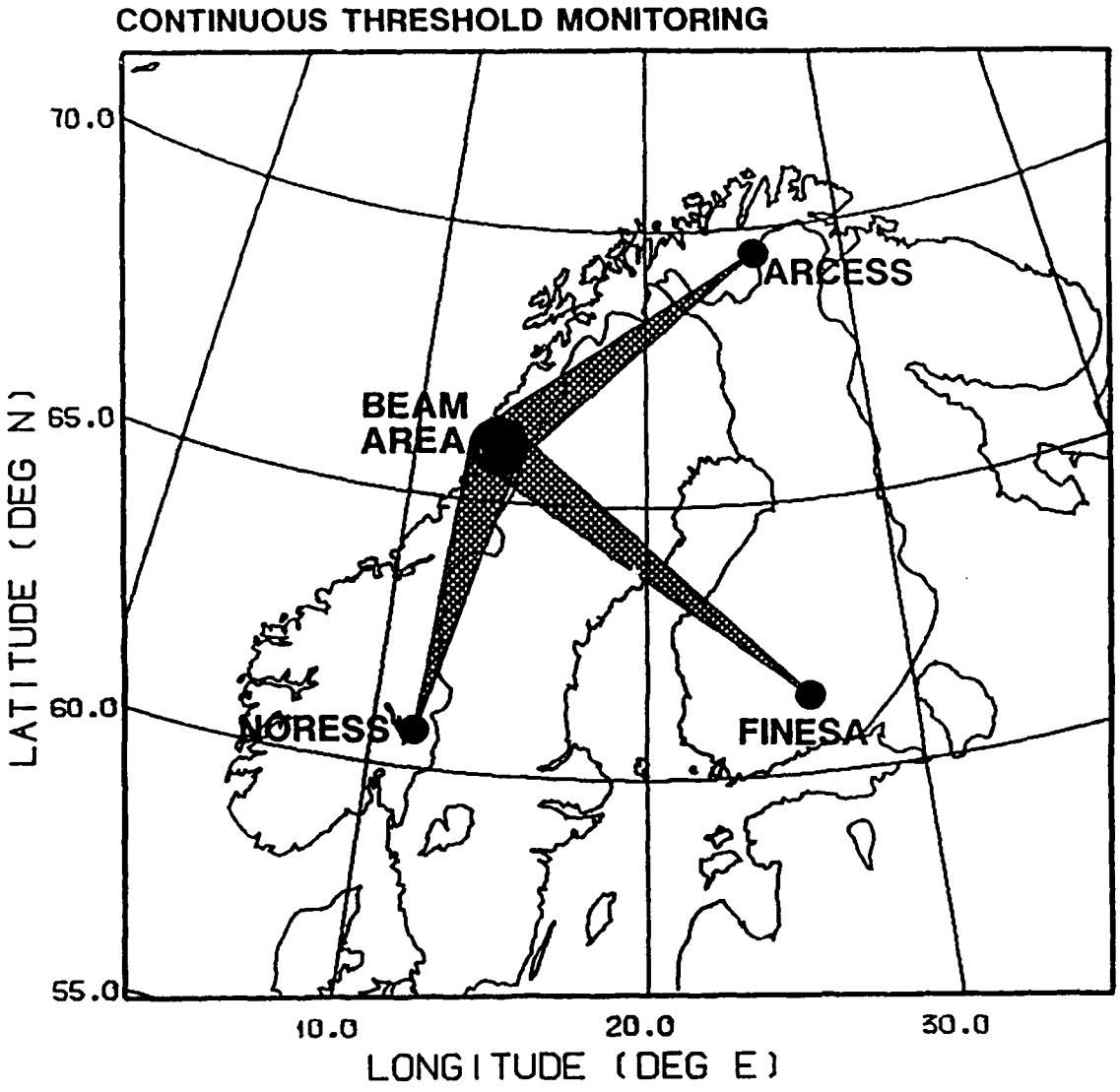

Fig. VII.2.3. Location of the beam area used in the example of continuous monitoring of upper magnitude limits on non-detected events. The area covers a circle of approximately 50 km radius, and is situated at similar distances from the three arrays.

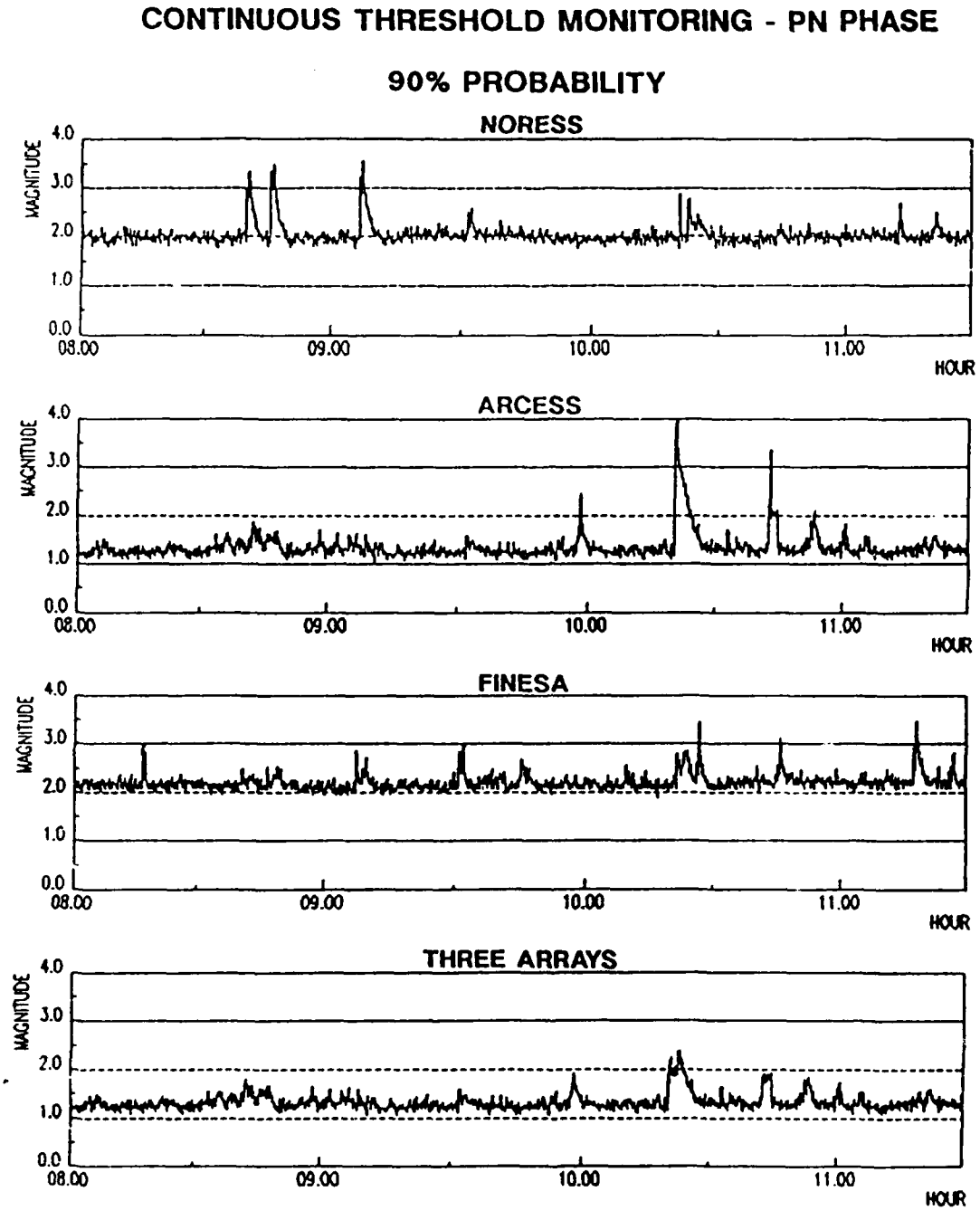

Fig. VII.2.4. Results from the continuous threshold monitoring of the area shown in Fig. VII.2.3 for a 3 1/2 hour period, using Pn phases only. The top three traces show, for each array, the largest magnitude of a possible non-detected event (confidence ^0 per cent) as a function of time. The bottom trace shows the result of combining the observations from all three arrays (Pn phase only) as described in the text.

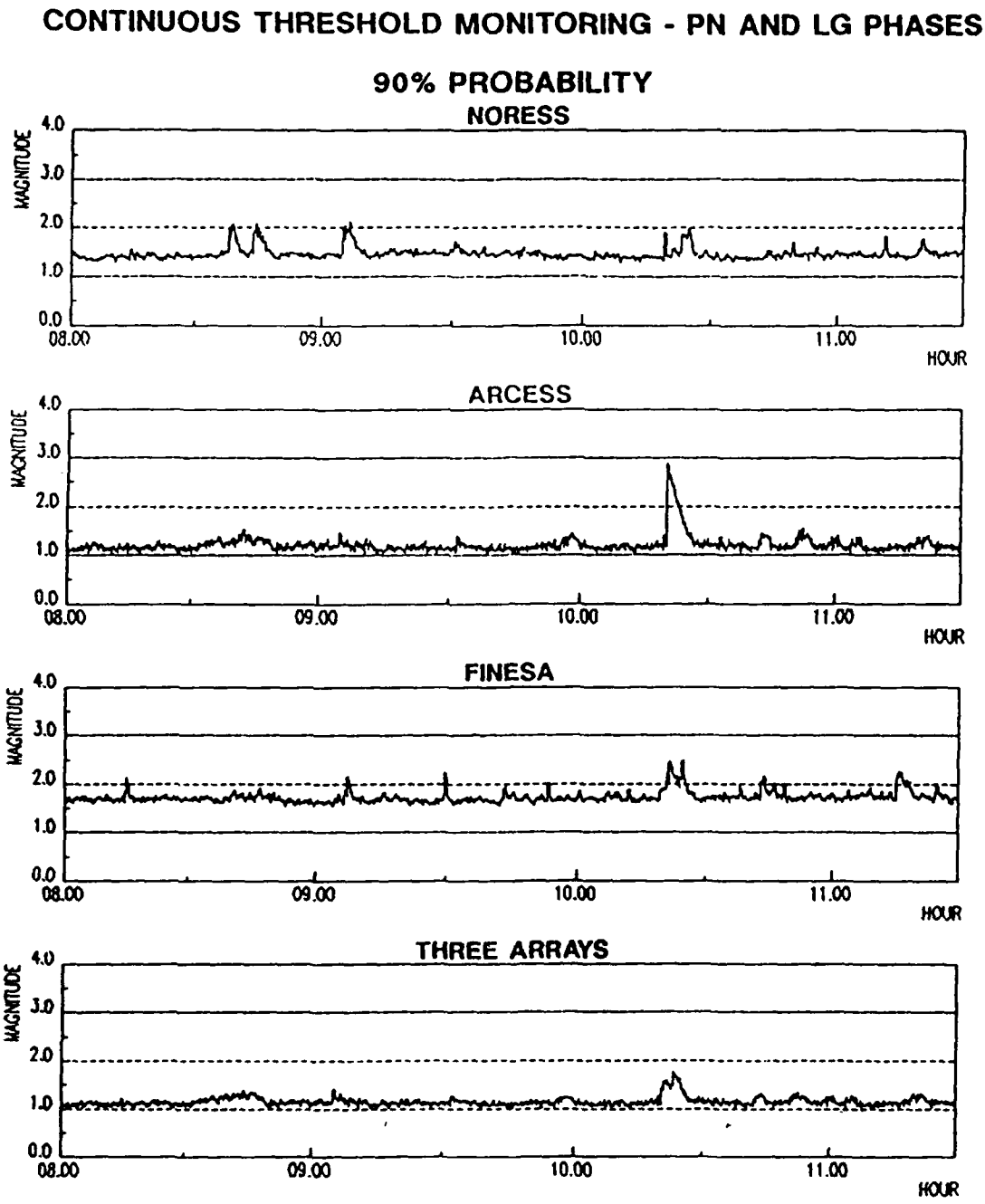

Fig. VII.2.5. Same as Fig. VII.2.4, but using both the Pn and Lg phases for the upper magnitude limit calculations. Comparing with Fig. VII.2.4, we note that this serves to lower the thresholds, both for each individual array (top three traces) and for the combined results (bottom trace).

VII.3 Variability of explosion Lg spectra with near-source structure and focal depth

Introduction

Lg amplitudes are used to estimate magnitudes of seismic events, and in particular of nuclear explosions (see Ringdal and Hokland, 1987). Modelling of Lg waves in the context of seismological verification research has mainly addressed the study of the potential of Lg waves for discrimination between explosions and earthquakes, and has assumed laterally homogeneous structures between the source and recording station (e.g., Nakanishi, 1981; Lilwall, 1988). We study here explosive sources and attempt to assess how small variations in focal depth or in structure around the source region affect recorded Lg-spectra. We use the Eastern Kazakh area as source region and NORSAR as the recording site. Following Levshin (1985), who pointed out the importance in surface wave amplitude modelling of using adequate structures at the source and receiver sites, we allow for different crustal structures in the Eastern Kazakh and the NORSAR region, and assume a smooth, lateral variation in between.

Crustal models

Four different crustal structures of the Eastern Kazakh area are proposed by Priestley et al (1988), one of them originating from the compilation of Russian literature by Leith (1987; written communication to Priestley et al), and the three others by inversion of broad-band teleseismic P-waveforms recorded in the area. We select two of these models: the model compiled by Leith, which presents a regular increase of velocity with depth (hereafter called model 1), and one of the three inverted models (the BAY-Japan model, called model 2) which all differ from model 1 mainly by a low-velocity zone at depths around 5 to 10 km, and higher velocities in the lower crust. In addition to the effect of an overall crustal modification, we study the effect of a local change in the model properties around the focal depth of the explosion. For that purpose, we use models where the interfaces at 1 km depth in

models 1 and 2 are transformed into velocity gradients over depth intervals of 1 km (models 1' and 2'). These gradients may model either a real gradient in velocities, or a splitting of the single interface into a few interfaces with smaller velocity contrasts. At the receiver end, we use a model of the crust under the NORSAR array derived by Gundem (1984). Models 1 and 2 and the crustal model under NORSAR are presented in Fig. VII.3.1.

We assume that the structures vary smoothly around the source and receiver sites. More quantitatively speaking, the models described above should not exhibit variations that are large enough to affect significantly the modal eigenfunctions of the Lg waves in at least 10 wavelengths (40 km here) around the source and station sites. Our own experience is that a 1 km change in Moho depth, and even smaller changes in sediment thicknesses, are large variations in this sense. The lateral variation of the crust is well known around NORSAR, and variations of the Moho depth of a few kilometers have been found in the area (Berteussen, 1977), showing that we are certainly at the limit of our smoothness assumptions at the receiver site. In Eastern Kazakh, the lateral crustal variations are not expected to be strong (Priestley et al, 1988).

The propagation path between Eastern Kazakh and NORSAR lies in an old continental shield and does not cross any significant tectonic feature. In the absence of more detailed information, the more realistic assumption which can be made on the model along the propagation path is that the structure varies smoothly from the source to the receiver region.

Attentuation is introduced in the models with quality factors at 1 Hz increasing from 80 at the top of the crust to 300 at 1 km depth and to 1000 at the Moho depth. The frequency dependence of the quality factors is taken as $\sqrt{f}$, following the observations of Campillo et al (1985) in Central France.

Modelling procedure

Since we have assumed that the model is smooth at the Eastern Kazakh source site, the excited Lg wavefield can be decomposed there on the local Lg modal eigenfunctions, and the modal excitation $e_j(h,\omega)$ at the receiver site. The wavefield produced in Eastern Kazakh and recorded at NORSAR can thus be written, separating excitation, propagation and reception terms (see Levshin (1985) for the details):

$$\underline{u} = \Sigma_{i,j}\ \underline{u}_i(0,\omega)\ a_{ij}\ e_j(h,\omega) \qquad (1)$$

where $\underline{u}_i(0,\omega)$ is the surface site response of mode i, $e_j(h,\omega)$ is the excitation of mode j for a source at depth h, and a_{ij} is the propagation matrix involving velocity, attenuation, geometrical spreading, and possibly mode conversions along the propagation path.

If the structure is smoothly varying along the propagation path, it has been shown that there is no mode conversion (Woodhouse, 1974), and expression (1) reduces to:

$$\underline{u} = \Sigma_i\ \underline{u}_i(0,\omega)\ a_i\ e_i(h,\omega) \qquad (2)$$

Each mode propagates along a ray, and the propagation term a_i depends on the ray pattern for mode i. Since we do not have enough detailed information on the crust between Eastern Kazakh and NORSAR to make ray-tracing worthwhile, we calculate the phase and attenuation of each mode with the assumption that it has followed the great circle between source and receiver, and that its slowness on that path is a symmetric function of distance (all smooth symmetric functions lead to the same result). We use the geometrical spreading factor $1/\sqrt{r}$, where r is the source-station distance.

In order to avoid differences in calculated spectra which would originate from slightly different propagation path characteristics and not from differences in the source area itself, the model along the

propagation path is fixed, whichever model is used for the source area, and is taken as varying from model 1 to the NORSAR model.

Synthetic Lg spectra are calculated for explosions in the four models described previously in this report. We focus our attention on focal depths around 1 km, and we take unit displacement steps as source functions. The spectra are calculated in a period interval between 0.8 and 1.25 s, corresponding to Lg wave periods observed at NORSAR.

The phase and group velocity dispersion curves of the Lg modes are displayed in Figs. VII.3.2 and VII.3.3 for models 1 and 2, and in Fig. VII.3.4 for the NORSAR model. It can be seen that due to the Moho being shallower at NORSAR than in the Eastern Kazakh area, fewer modes are of Lg type at NORSAR than in models 1 and 2. We thus have to define which modes at which frequencies will be considered as part of the Lg wavetrain at NORSAR. We adopt very simple criteria which are similar to the criteria used in data analysis: all arrivals arriving at NORSAR in a time window corresponding to group velocities (which are functions of the local group velocities along the whole path) between 3.1 and 3.62 km/s are considered as Lg waves. With that definition, some of the higher modes which are excited as Lg modes in Eastern Kazkh are excluded from contributing to the seismogram at NORSAR because they convert to Sn modes early during the propagation.

An example of a synthetic displacement spectrum is shown in Fig. VII.3.5. We notice the good agreement of its general characteristics with those of a data spectrum (Fig. VII.3.6). The slopes, which are strongly dependent on the attenuation in the structure, are similar; the peak-and-trough patterns, which originate from the multimodal character of the Lg waves, have similar amplitude and periodicity in both figures.

In order to facilitate the comparison between different spectra, we smooth them by a procedure equivalent to adding spectra from many recording stations distributed in a 60 km distance window around a main

station site. The spectrum of Fig. VII.3.5 is shown after smoothing in Fig. VII.3.7.

Synthetic Lg spectra at NORSAR from Eastern Kazakh explosion sources

The synthetic displacement spectra of Lg waves recorded at NORSAR and originating from explosions at 3 different focal depths in models 1, 1', 2 and 2' are displayed in Figs. VII.3.8 and VII.3.9. We notice in Figs. VII.3.8a and VII.3.9a that the spectra are totally insensitive to a source depth variation from 0.7 to 0.9 km in models with a sharp interface at 1 km depth. Conversely, moving the source from the upper layer to the layer underneath the interface (source at 1.1 km depth) reduces the spectral amplitude by a factor corresponding to about 0.6 magnitude units. When the sources are located in velocity gradient zones (Fig. VII.3.8b and VII.3.9b), the decrease of spectral amplitude with focal depth is more regular but still significant.

Now comparing the spectra for identical source depths but different crustal structures, we notice a general increase in amplitude by a factor of 1.5 to 2, or 0.2 magnitude unit difference, between sources located in models 1 or 1' (Fig. VII.3.8) and sources located in models 2 or 2' (Fig. VII.3.9). There is an overall factor of 10 in the middle frequency range between amplitudes of the lowest and highest spectra of Figs. VII.3.8 and VII.3.9. The detailed crustal model at the source and the source depth appear to be important factors in the Lg spectra amplitude. On the other hand, we do not observe clear and significant differences in the slopes of the different spectra. This modelling does not predict any change in the dominant frequency of the data (the presented spectra multiplied by the instrumental response) for explosions at different depths or in slightly different crustal environments.

Spectra in a laterally homogeneous structure

To appreciate the influence of the NORSAR crustal structure on the spectral shapes, we show in Fig. VII.3.10 spectra calculated with

another structure than NORSAR's at the recording site. We assume lateral homogeneity of the crustal structure along the whole path, which means that we calculate spectra for a station which would be situated at 4200 km distance from the Eastern Kazakh site, but in a crustal structure identical to model 1. The discrepancy between the spectral amplitudes for different source depths and source area models is reduced to a factor of 3 between the extreme cases, in comparison with the factor of 10 computed with the NORSAR model at the receiver end. The difference in structures between the Eastern Kazakh and NORSAR crust enhances the amplitude differences in Lg spectra.

Conclusion

We have shown that Lg spectra modelled in smoothly varying structures from Eastern Kazakh to NORSAR vary in amplitude when small realistic variations are introduced in the focal depth or in the crustal structure of the source site. Large amplitude variations, equivalent to up 0.6 magnitude unit difference, can be expected when the source focal depth crosses a layer interface with strong velocity contrasts. The equivalent of 0.2 magnitude unit variations may occur when the crustal structure is modified. On the other hand, no significant variation of spectrum slope or spectral content is observed with such source environment modifications.

These results can be compared with the characteristics of NORSAR recordings of Lg-waves from Eastern Kazakh explosions. The main difference between spectra from different explosions is an amplitude shift, but no large variation in the dominant frequency is observed (Kværna & Ringdal, 1988). The magnitude histogram presents distinct maxima separated by less than 0.1 magnitude units, and which do not correlate with explosion locations within the test site area (Ringdal and Hokland, 1987).

The stability of the spectral content of the Lg wavetrain is a feature common to our modelling exercise and the observed data. On the other hand, the observed spectral amplitudes are more stable than one would

expect from the modelling results. The distinct character of the observed magnitude peaks, which are uncorrelated with explosion epicenter location, seems to indicate that the 20 x 20 km site area is small and homogenous enough for the epicentral location not to influence the Lg magnitude of the explosions. The different peaks can be interpreted as corresponding to sources of difference sizes fired in similar conditions, but our modelling results show that they could also originate from identical explosions fired in different geological layers or at different depths within a velocity gradient area.

V. Maupin, Postdoctorate Fellow

References

Berteussen, K.-A. (1977): Moho depth determinations based on spectral ratio analysis of NORSAR long period P-waves. Phys. Earth Planet. Inter., 15, 13-27.

Campillo, M., J.-L. Plantet & M. Bouchon (1985): Frequency-dependent attenuation in the crust beneath Central France from Lg waves: data analysis and numerical modeling. Bull. Seism. Soc. Am., 75, 1395-1411.

Gundem, M.B. (1984): 2-D seismic synthesis of the Oslo Graben. M.Sc. Thesis, University of Oslo.

Kværna, T. & F. Ringdal (1988): Spectral analysis of Shagan River explosions recorded at NORSAR and NORESS. Semiann. Tech. Summary, 1 Apr - 30 Sep 1988, NORSAR Sci. Rep. 1-88/89, Kjeller, Norway.

Levshin, A.L. (1985): Effects of lateral inhomogeneities on surface wave amplitude measurements. Ann. Geophys., 3, 511-518.

Lilwall, R.C. (1988): Regional m_b:M_S, Lg/Pg amplitude ratios and Lg spectral ratios as criteria for distinguishing between earthquakes and explosions: a theoretical study. Geophys. J., 93, 137-147.

Nakanishi, K.K. (1981): The effect of focal depth and source type on synthetic seismograms. In: E.S. Husebye & S. Mykkeltveit (eds.), Identification of Seismic Sources -- Earthquake or Underground Explosion, D. Reidel Publ. Co., Dordrecht.

Priestley, K.F., G. Zandt & G.E. Randall (1988): Crustal structure in Eastern Kazakh, USSR, from teleseismic receiver functions. Geophys. Res. Lett., 15, 613-616.

Ringdal, F. & B.Kr. Hokland (1987): Magnitude of large Semipalatinsk explosions using P coda and Lg measurements at NORSAR. In: NORSAR Semiannual Tech. Summ., 1 Apr - 30 Sept 1987, Kjeller, Norway.

Woodhouse, J.H. (1974): Surface waves in a laterally varying structure. Geophys. J.R. astr. Soc., 37, 461-490.

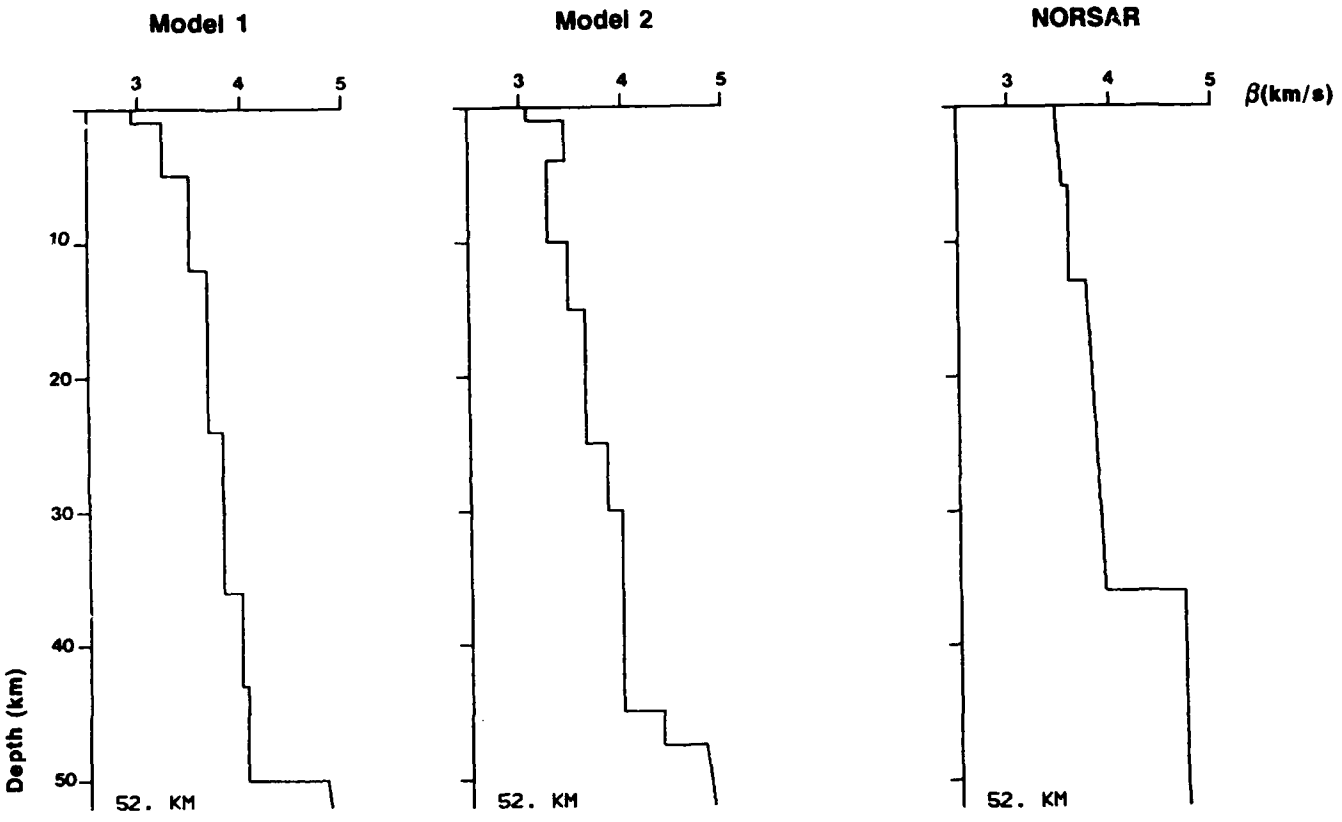

Fig. VII.3.1. S-wave velocity as a function of depth in the Eastern Kazakh models 1 and 2 and in the NORSAR model.

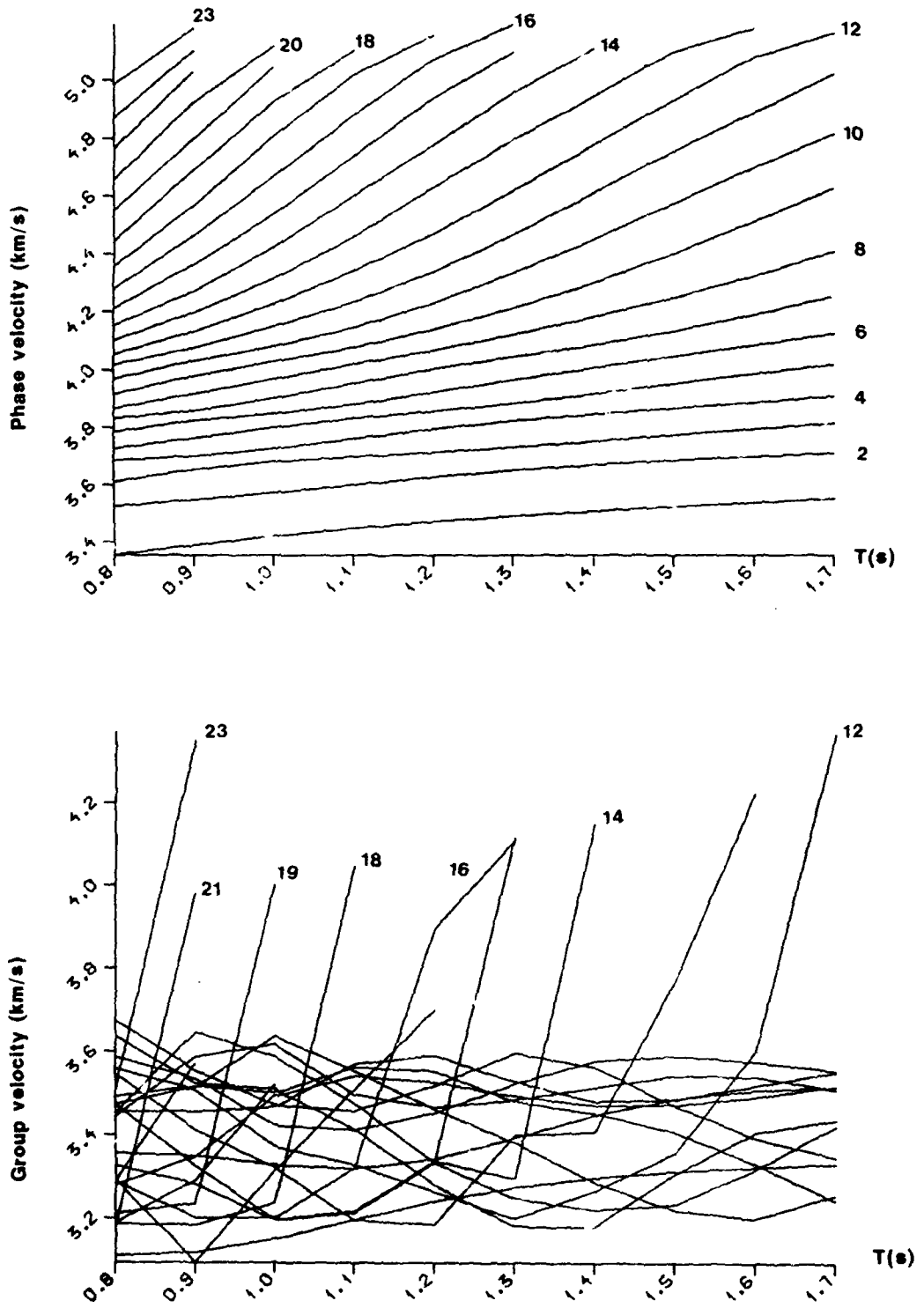

Fig. VII.3.2. Phase and group velocity dispersion curves for the Lg modes in model 1. Some of the curves are labelled with mode number.

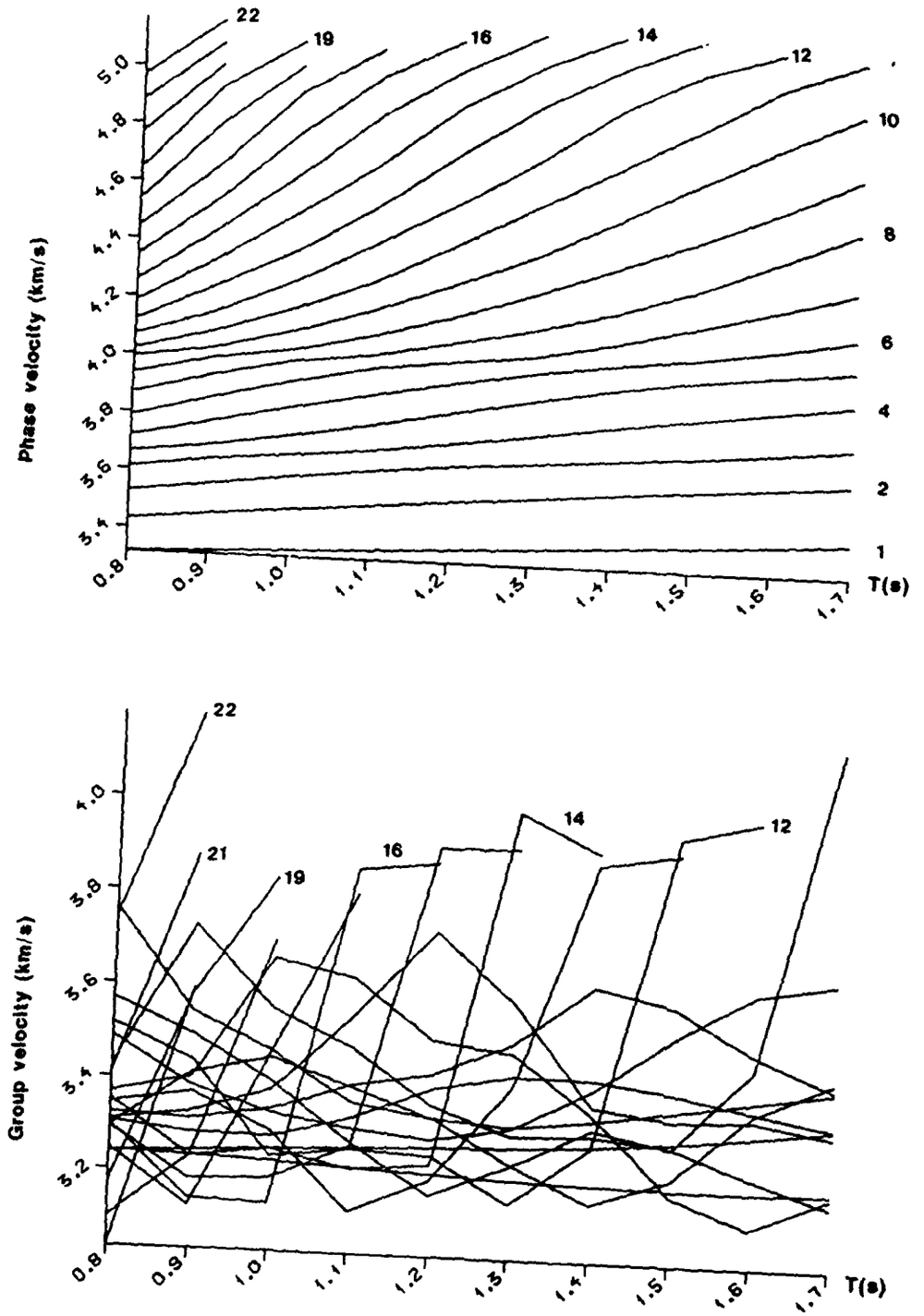

Fig. VII.3.3. The same as Fig. VII.3.2 for model 2.

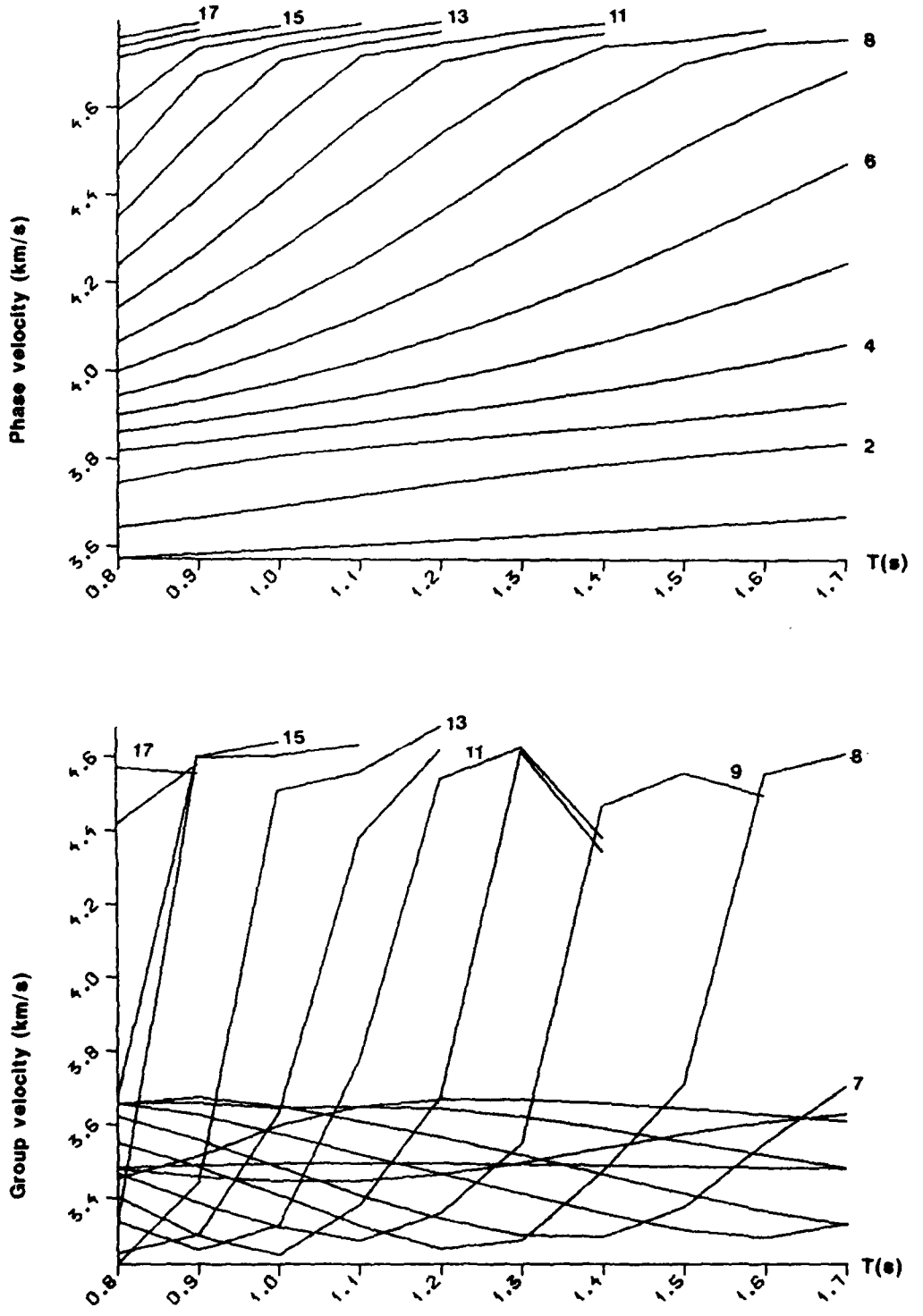

Fig. VII.3.4. The same as Fig. VII.3.2 for the NORSAR model.

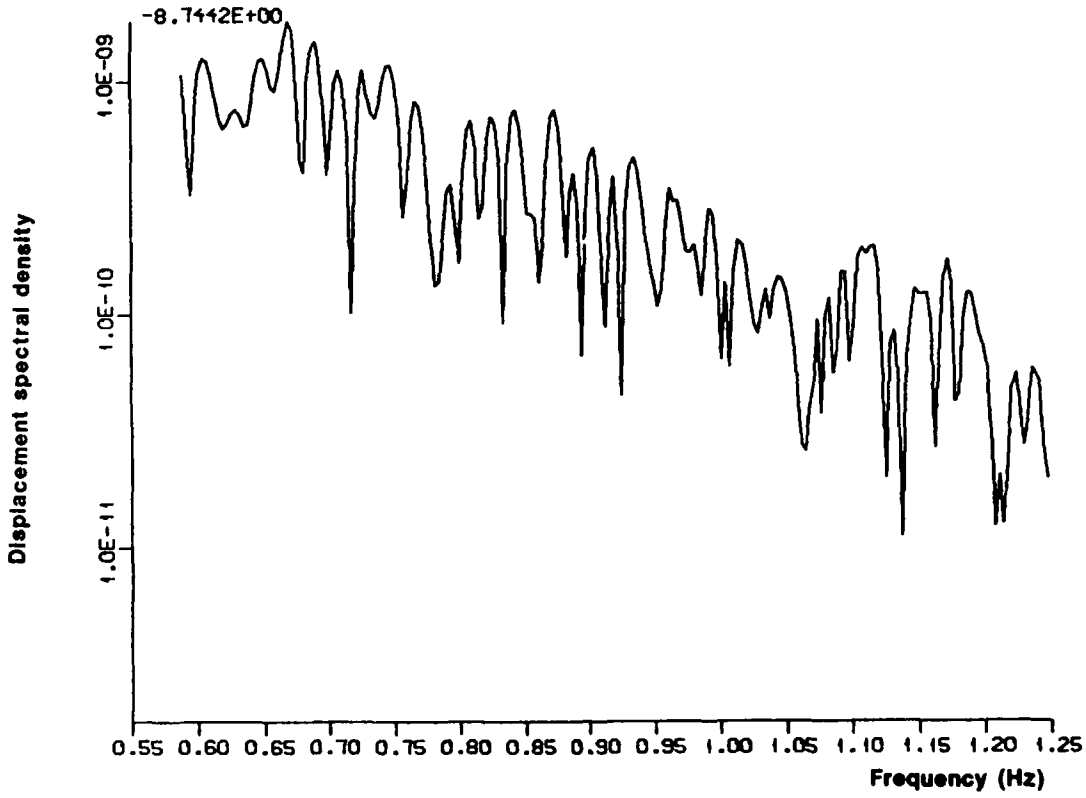

Fig. VII.3.5. Synthetic spectrum for an explosion at 0.9 km focal depth in model 1 and recorded at NORSAR.

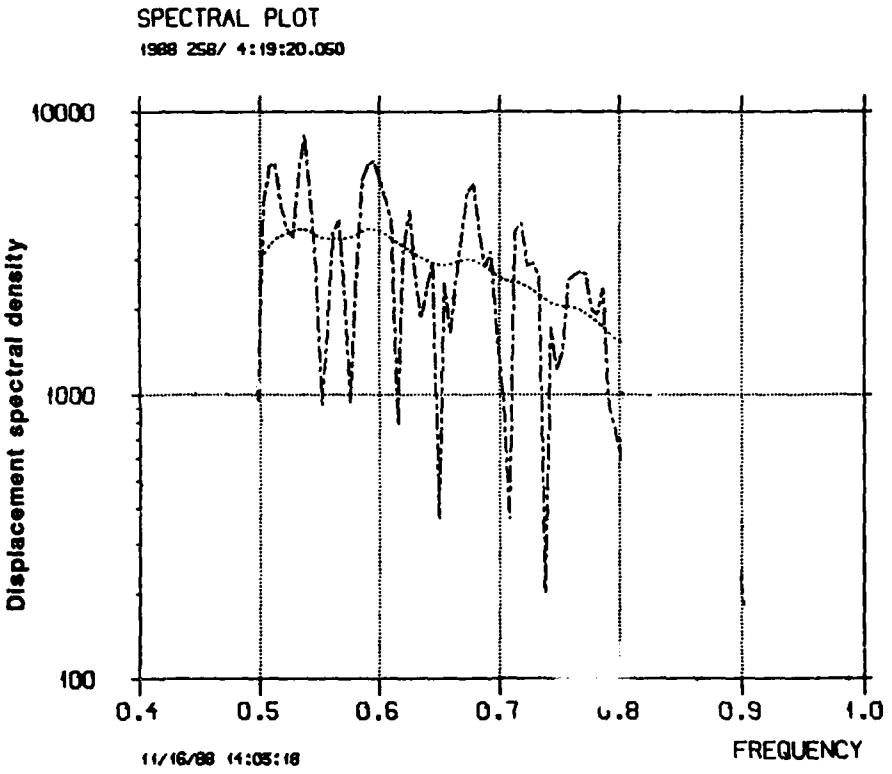

Fig. VII.3.6. Spectrum of the Lg wave recorded at NORESS shown in the frequency interval with best SNR (dashed-dotted line), and associated smoothed spectrum (dotted line).

Fig. VII.3.7. Synthetic spectrum of Fig. VII.3.5 after smoothing by addition of spectra from stations within a 60 km window around the central station.

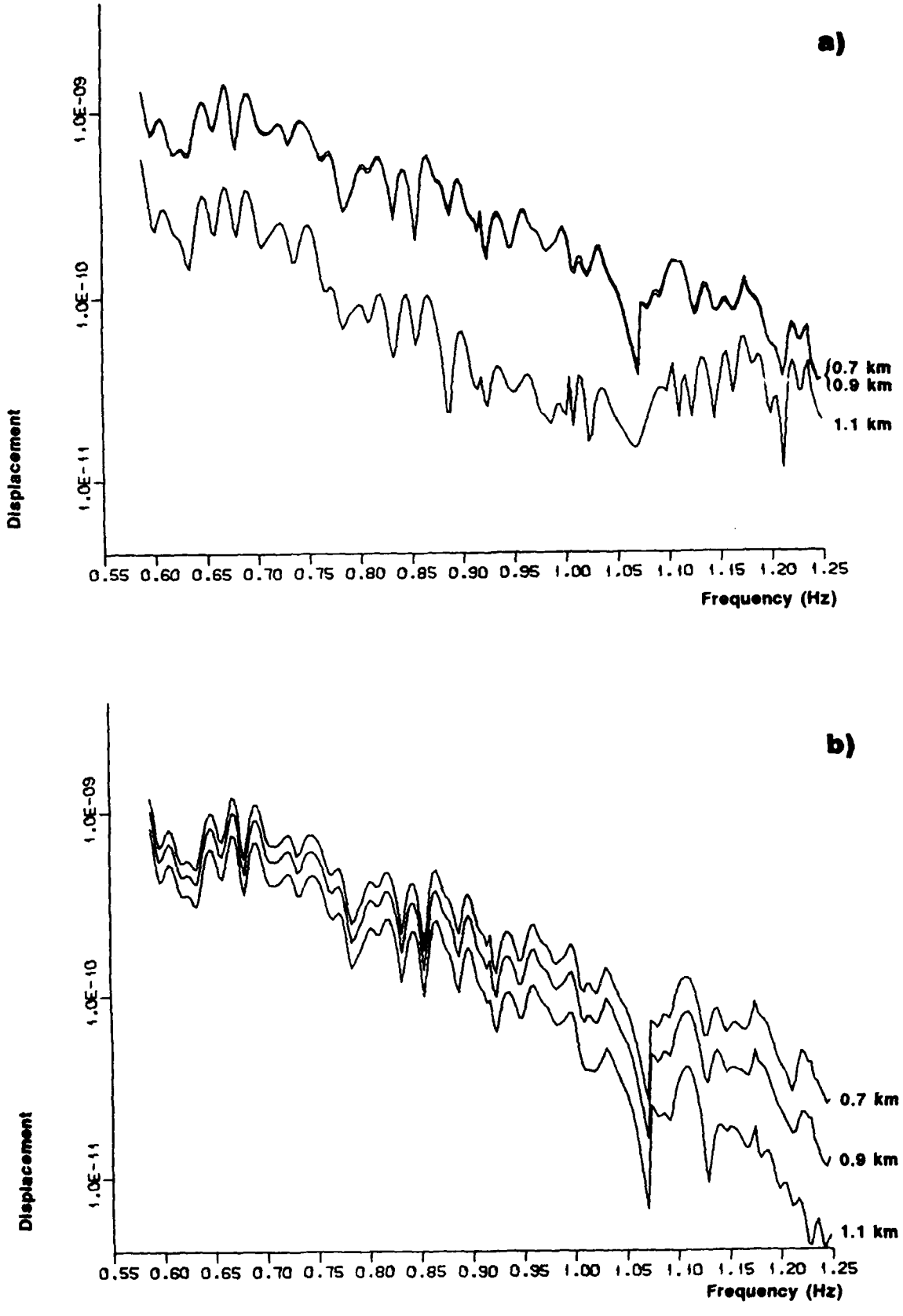

Fig. VII.3.8. Smoothed synthetic Lg spectra at NORSAR from explosions at 0.7, 0.90 and 1.1 km focal depth in model 1 (plot a) and in model 1' (plot b).

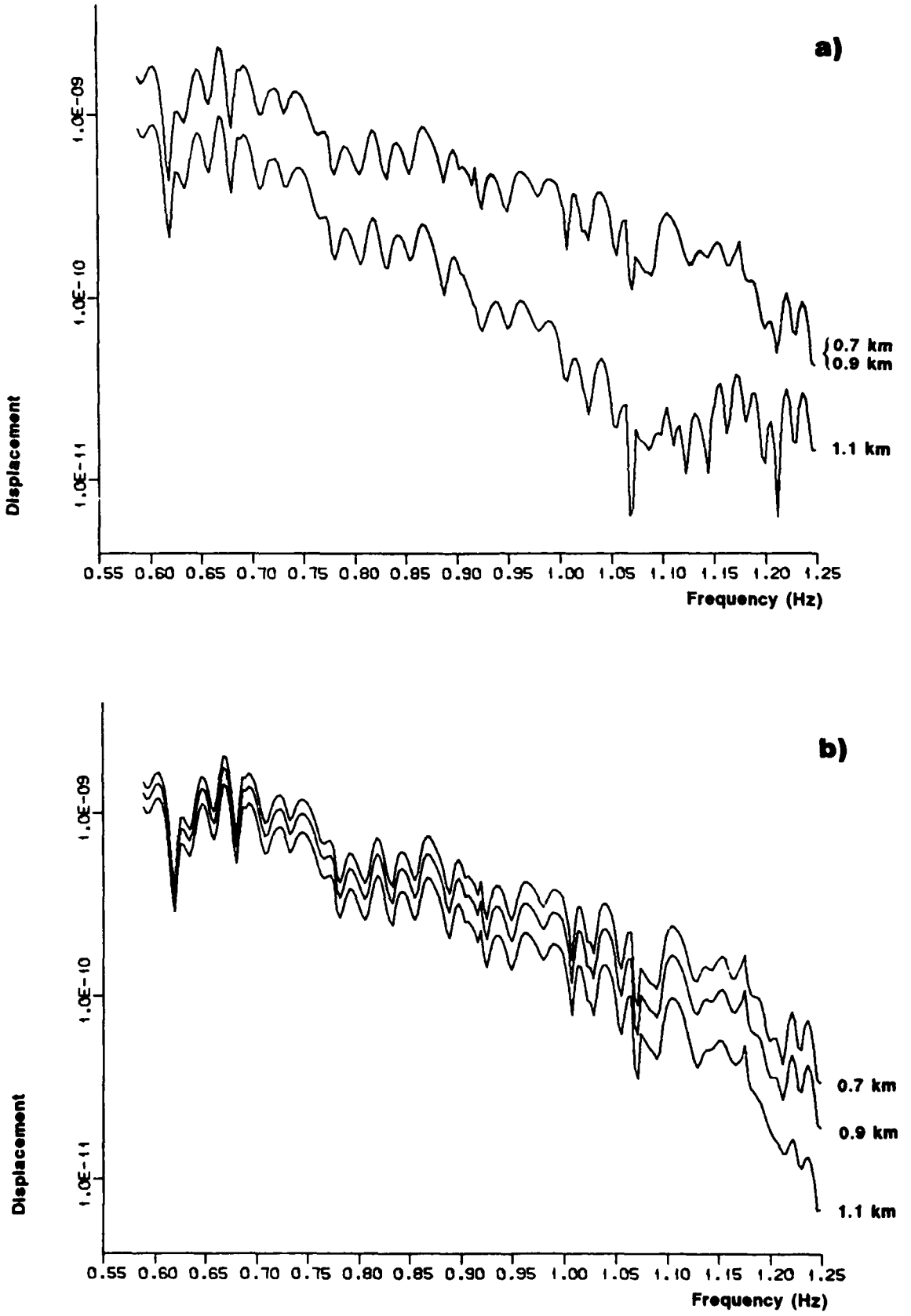

Fig. VII.3.9. The same as Fig. VII.3.8 for model 2 (plot a) and model 2' (plot b).

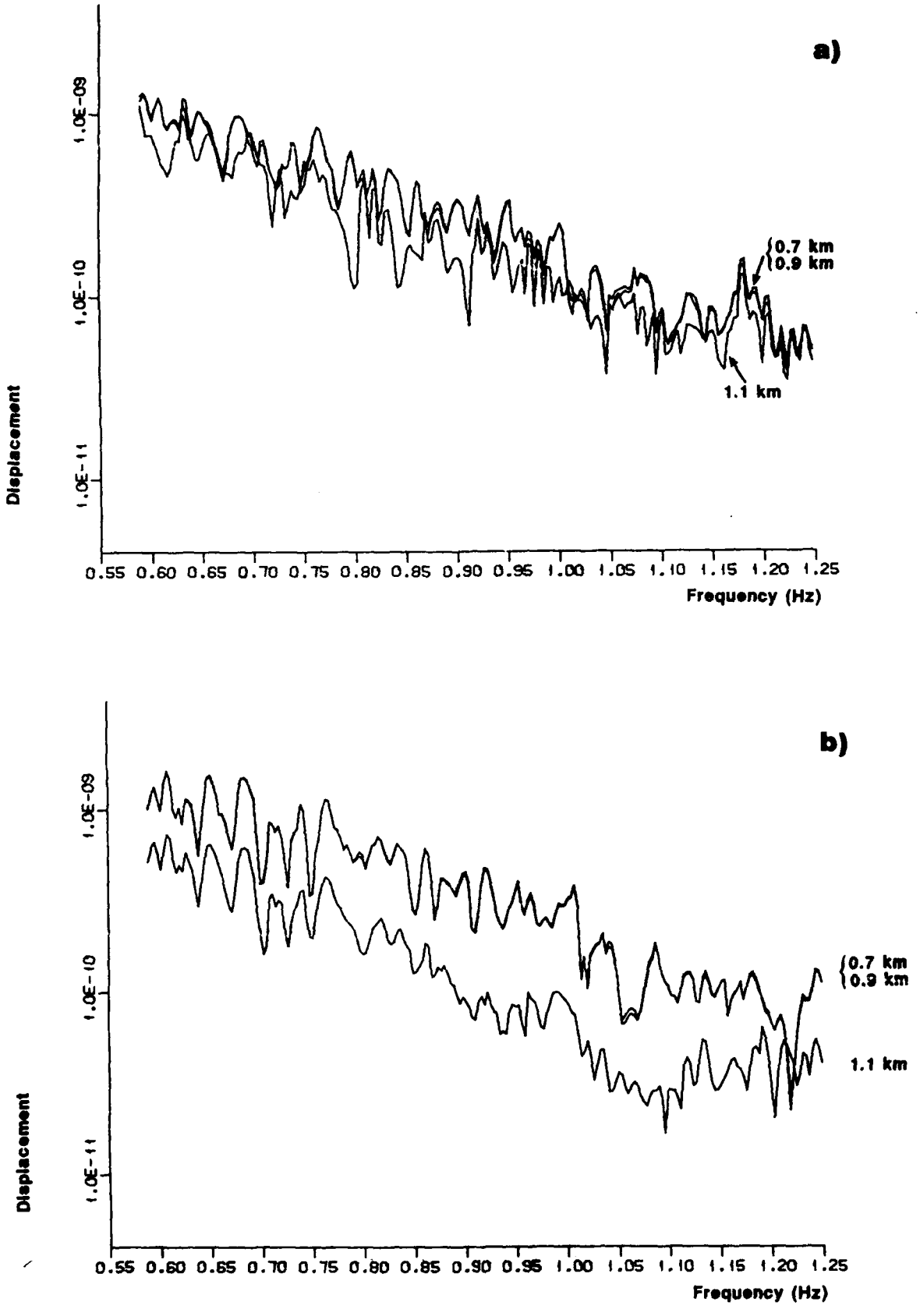

Fig. VII.3.10. Smoothed synthetic Lg spectra from explosions at 0.7, 0.9 and 1.1 km in model 1 (plot a) and model 2 (plot b), assuming complete propagation and recording in model 1.

VII.4 Surface topographic effects at NORESS and ARCESS

In a previous Semiannual Technical Summary Report we analyzed slowness solutions of regional P waves at NORESS from a suite of mining explosions near Leningrad (Ødegaard and Doornbos, 1988). The differences between 3-component slowness solutions at the 3-component sites within the array imply that local structure significantly perturbs the surface particle motion. A synthesis of particle motion based on a multiple scattering method (Doornbos, 1988) explains about half of the observed anomalies by surface scattering, and also explains the observed frequency dependence. Here we report on the results of a similar analysis of teleseismic P waves from Eastern Kazakh nulcear explosions recorded both at NORESS and ARCESS. The P wave spectra from all events are similar at NORESS; a sample of 3 events is shown in Fig. VII.4.1. At ARCESS we can distinguish two groups of events. The spectra within a group are similar, but there are significant differences between the two groups, as illustrated in Fig. VII.4.2 (a and b). The spectral difference requires further investigation, but at this stage we analyze the two groups separately. Average slowness solutions for the events are plotted in Figs. VII.4.3 and VII.4.4. The array slowness solution is based on measured phase differences between all vertical component records within the array and is labeled ALLV; the 3-component slowness solutions are based on relative amplitudes of the 3 components and are labeled by the site identification number. Standard deviations are plotted only for site A0, but the other sites give similar results. There is a slight difference between the array slowness solutions at ARCESS for the two groups, but there is a large difference between the 3-component slowness solutions for the two groups. There are striking differences also between the different sites for each group. A difference between ARCESS and NORESS is that 3-component slowness solutions at ARCESS are relatively high (compared to the array solution), whereas the 3-component solutions at NORESS are relatively low.

We have digitized the surface topography both at NORESS and at ARCESS; elevation maps are shown in Figs. VII.4.5 and VII.4.6. Topography in

the NORESS area is slightly higher, but ARCESS is situated right on top of a hill which is presumably associated with a gabbro intrusion. Topographic effects at ARCESS are therefore not necessarily smaller than at NORESS, but they can be calculated with somewhat higher precision. Calculation of the surface response is done in the frequency domain, and the response is then integrated over frequency in accordance with the observed spectrum. Integration limits were 0.9-2.5 Hz for the events at NORESS and for group A at ARCESS, and 0.9-1.6 Hz for group B at ARCESS. The calculated slowness solutions are plotted (in frames) with the observations in Figs. VII.4.3 and VII.4.4. The figures demonstrate that surface topography explains about half of the observed anomalies. Further they demonstrate that surface topography can produce not only azimuthal anomalies, but also deviations in absolute slowness. Finally, it is remarkable that the low-frequency group of events at ARCESS (group B) produces larger anomalies than the high-frequency group A. Clearly 3-component slowness solutions depend both on surface topography and on the incident signal spectra.

E. Ødegaard, Univ. of Oslo
D.J. Doornbos, Univ. of Oslo

References

Doornbos, D.J. (1988): Multiple scattering by topographic relief with application to the core-mantle boundary. Geophys. J., 92, 465-478.

Ødegaard, E. and D.J. Doornbos (1988): Surface topographic effects on arrays and three-component stations. NORSAR Semiann. Tech. Summ., 1 Apr - 30 Sep 1988, Kjeller, Norway.

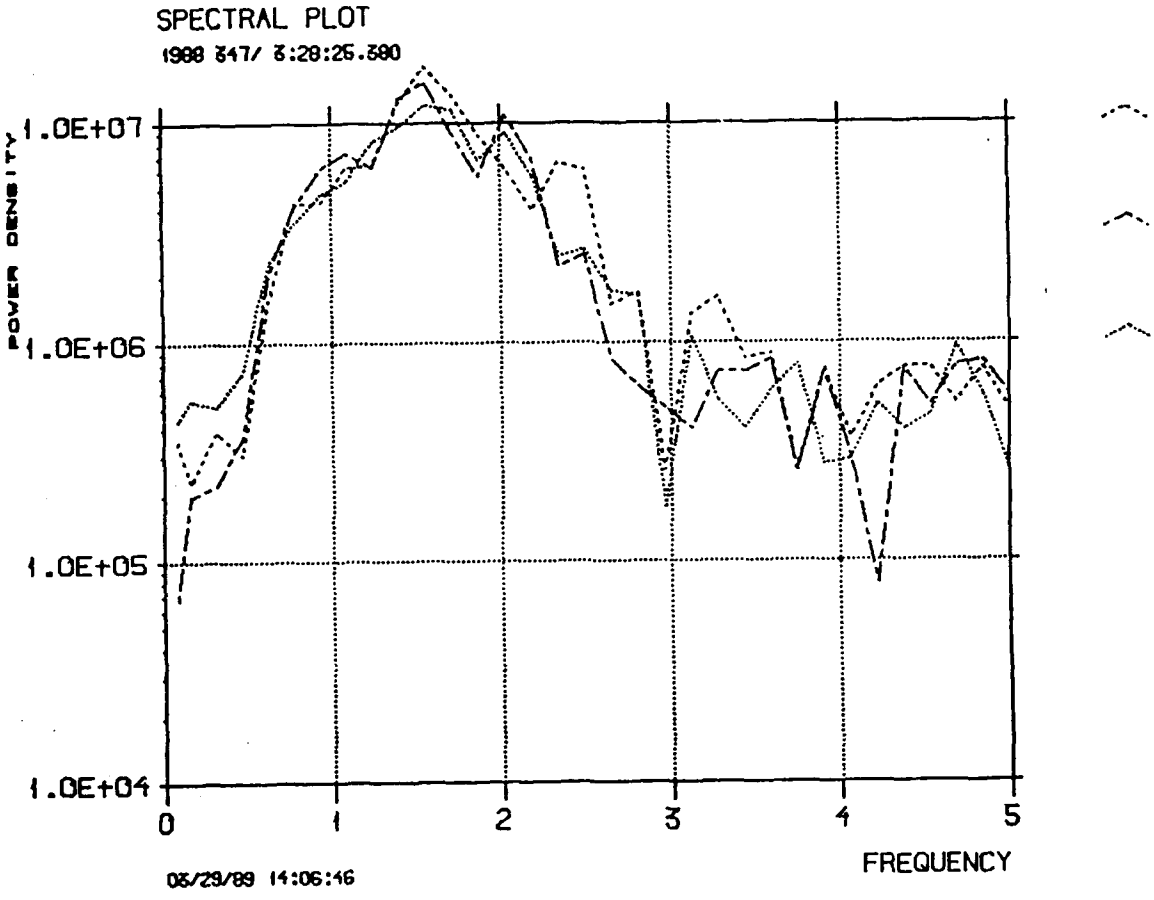

Fig. VII.4.1. P wave signal spectra at NORESS from 3 nuclear explosions in Eastern Kazakh.

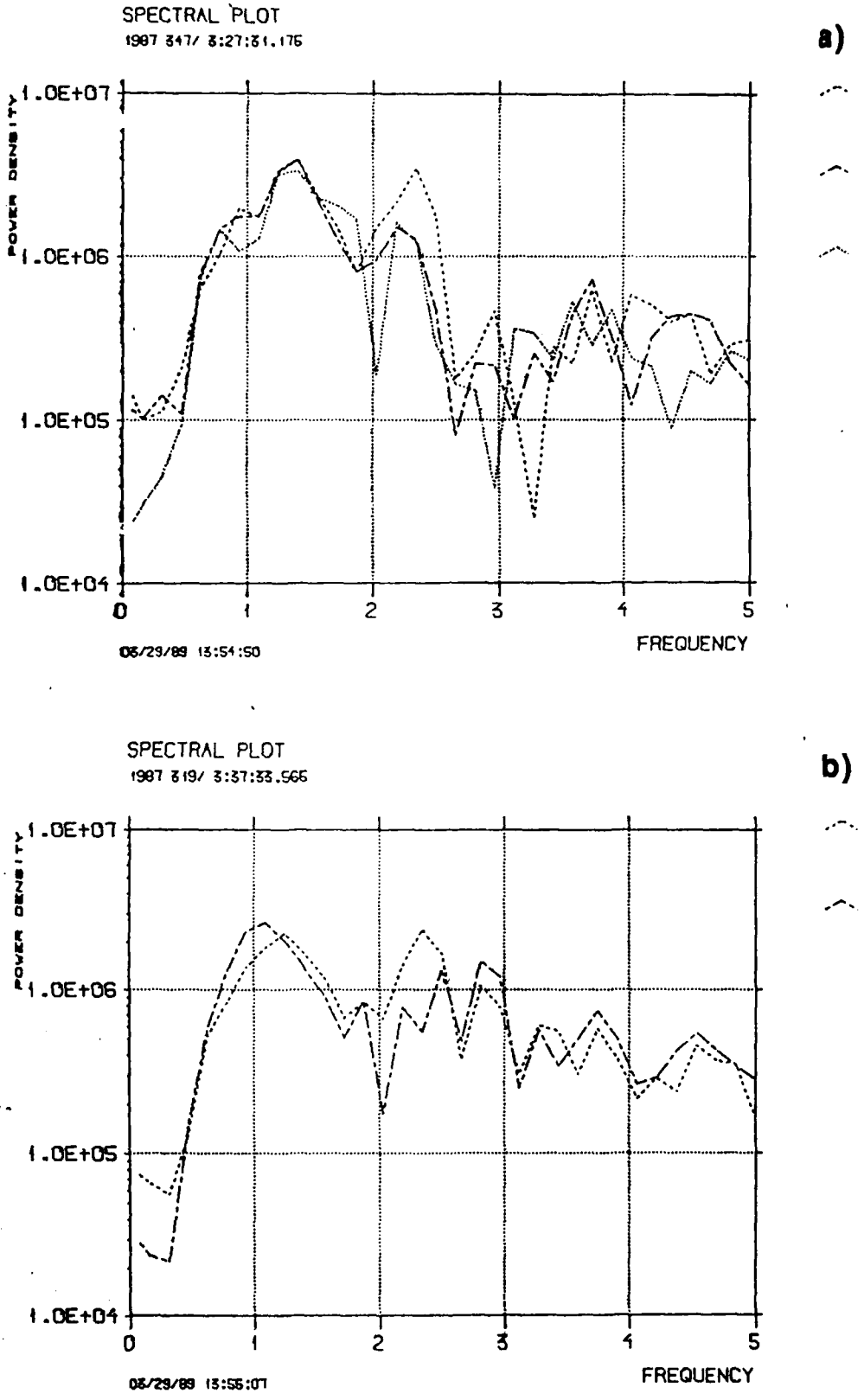

Fig. VII.4.2. P wave signal spectra at ARCESS from nuclear explosions in Eastern Kazakh.
a. 3 events from group A (high-frequency signals)
b. 2 events from group B (low-frequency signals).

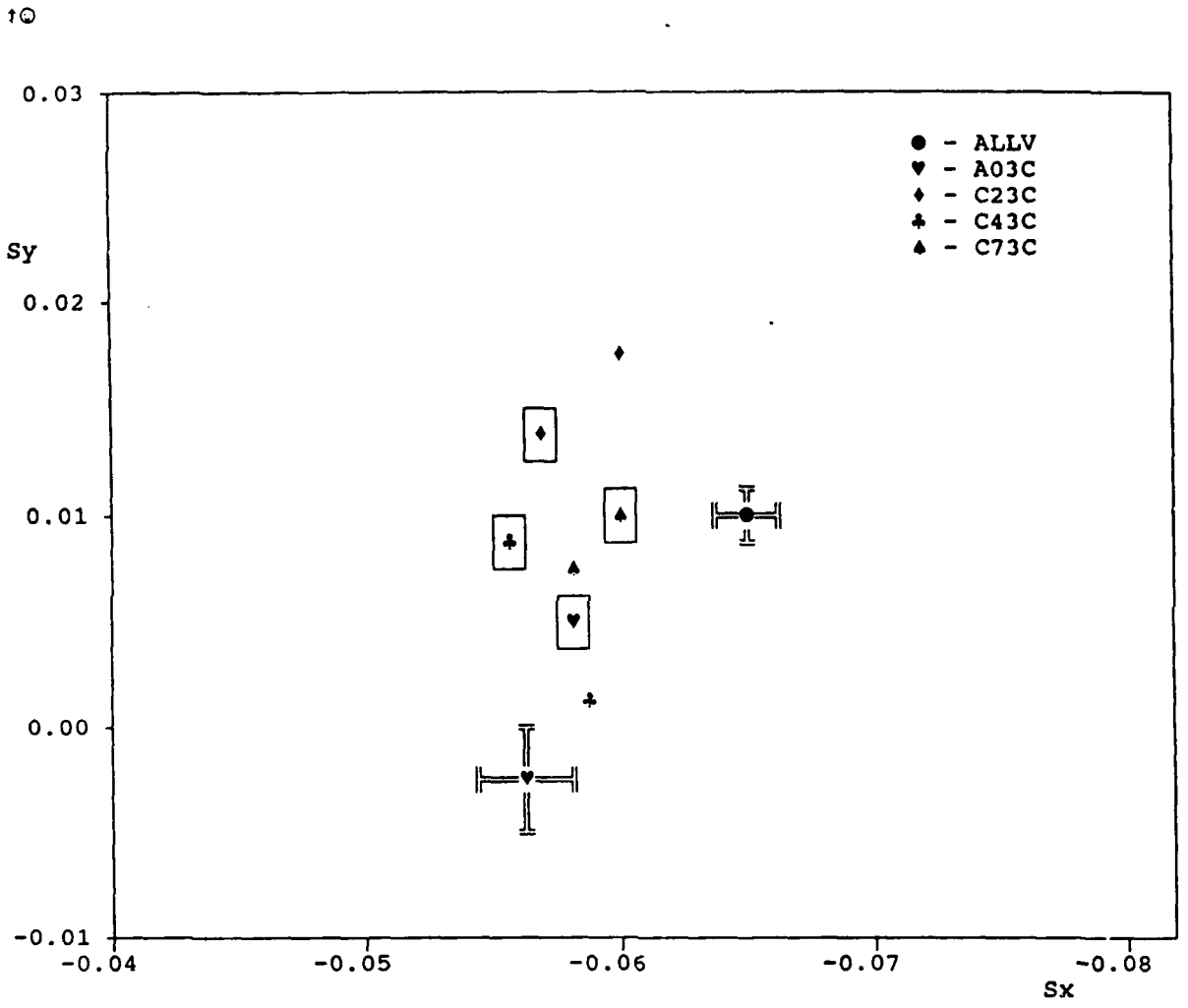

Fig. VII.4.3. Slowness solutions at NORESS. Average over P from 14 events in Eastern Kazakh. Array solution (ALLV) with standard error bars. Three-component solutions at the indicated sites, with standard error bars for site A0. Calculated solutions including response to surface topography are framed.

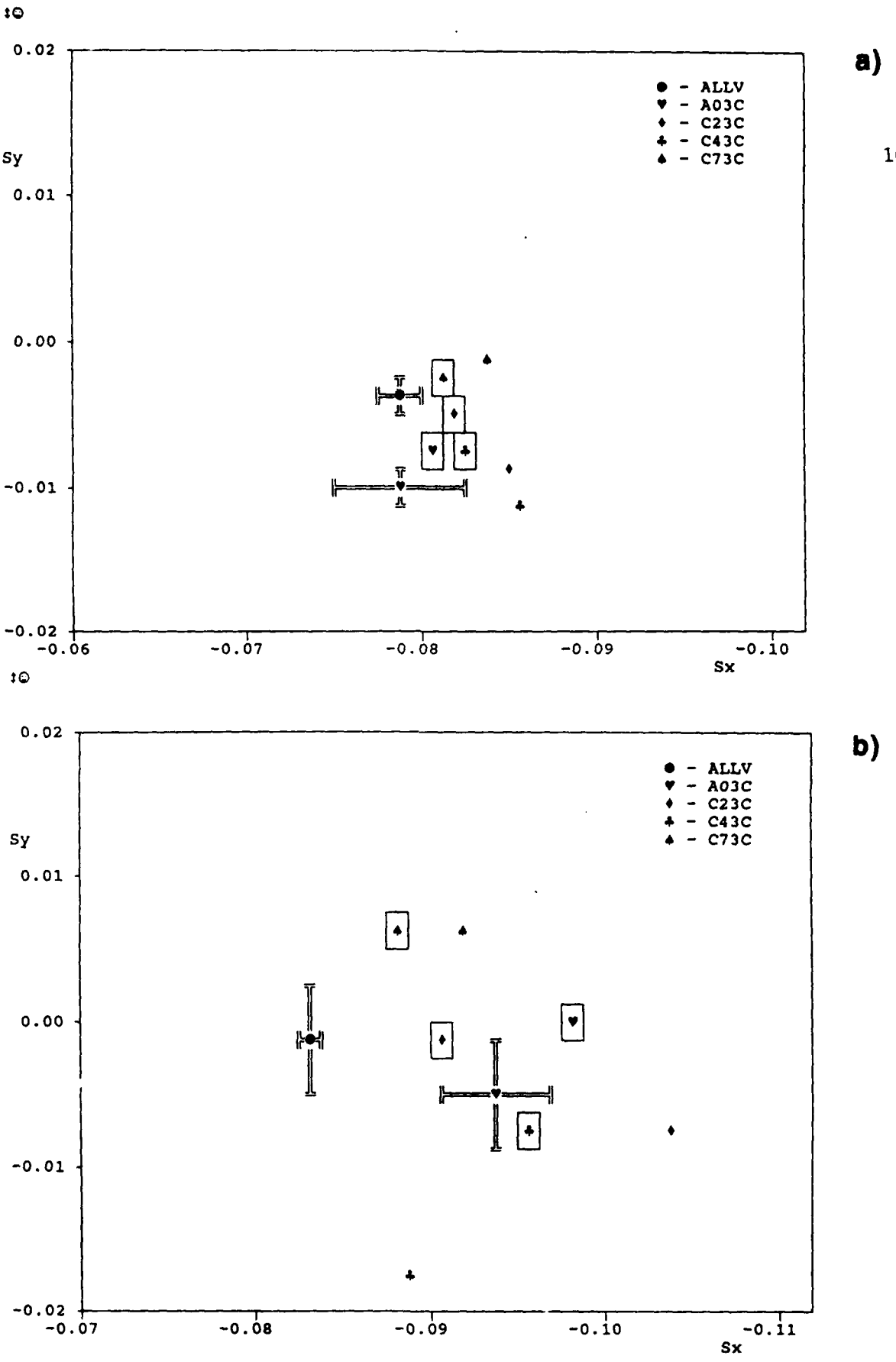

Fig. VII.4.4. Slowness solutions at ARCESS. Details as in Fig. VII.4.3.

a. Average over 4 events from group A.

b. Average over 5 events from group B.

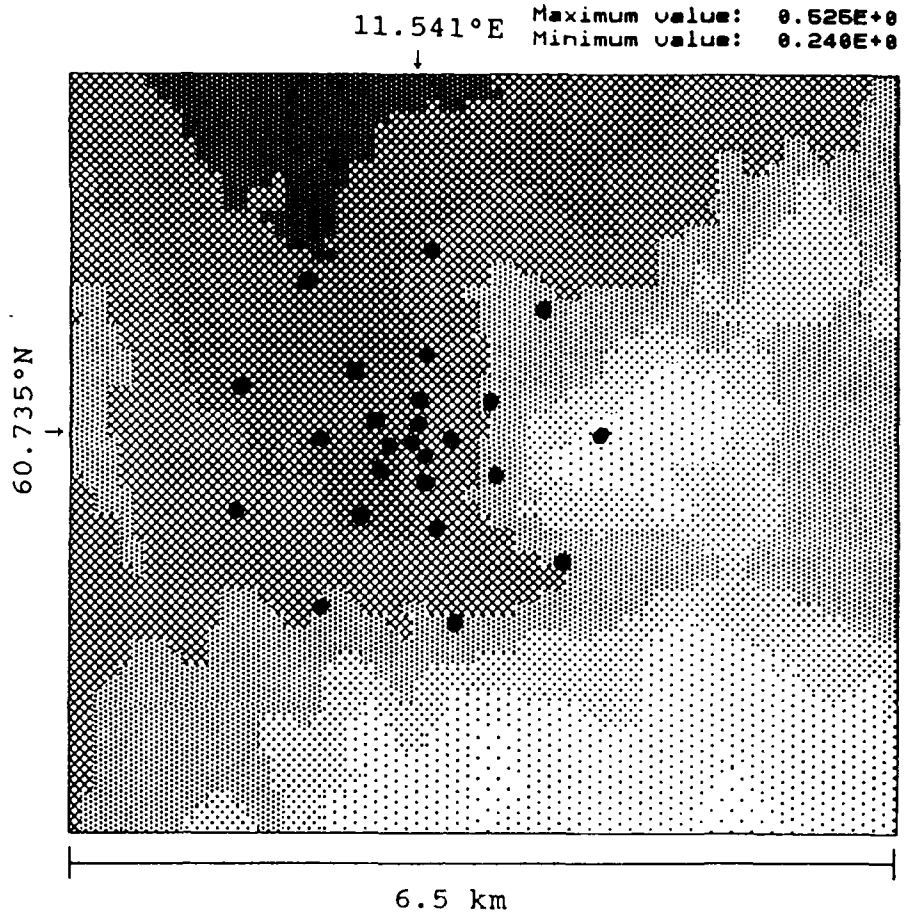

Topographic height in meters

	501	-		311	- 359
	454	- 501		264	- 311
	406	- 454			- 264
	359	- 406			

Fig. VII.4.5. Elevation map for the NORESS array area.

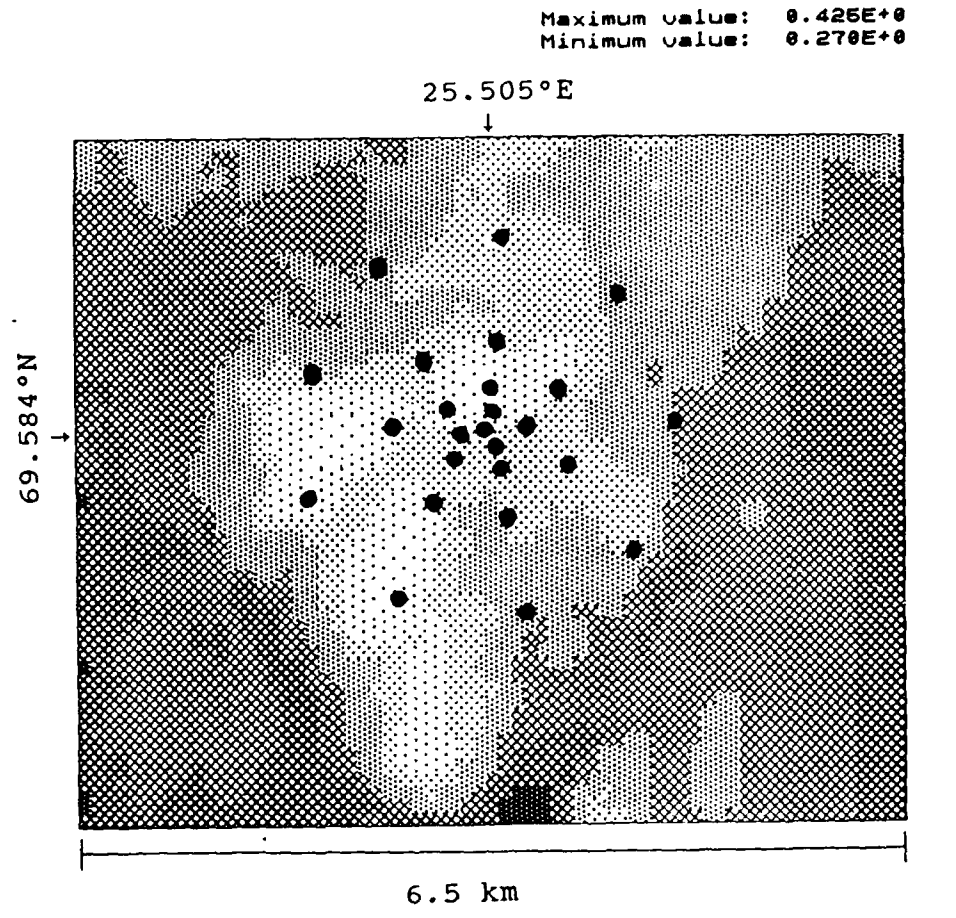

Fig. VII.4.6. Elevation map for the ARCESS array area.

VII.5 Anelastic attenuation from intraplate earthquake recordings

The previous report in this series contained a brief discussion of different models proposed for the anelastic attenuation (Q) in southern Norway, and the effects of these models when used in the calculation of source displacement spectra for earthquakes recorded at distances up to 500 km.

Recently, a different approach to this problem has been taken by Dahle et al (1989), who have collected and analyzed 87 earthquake records from 56 earthquakes occurring in predominantly intraplate areas (North America, Europe, China, Australia). The magnitudes of these events are in the range from M_S 3 to 8, the epicentral distances are from less than 10 to more than 1000 km, and the magnitude/distance correlation is 0.32. Depending on the type of regression analysis used, such correlation may introduce biases in the estimated regression coefficients.

The main purpose of the Dahle et al (1989) analysis was to establish models for strong ground motion (peak ground acceleration and pseudo-relative velocity) as a function of magnitude and distance, as follows:

$$\ln A = c_1 + c_2 M + c_3 \ln R + c_4 R \qquad (1)$$

where A is the ground motion amplitude, M is magnitude, and R is epicentral distance. A step-wise approach to the regression was taken, resulting in 'average intraplate' relations for PGA (peak ground acceleration) and PSV (pseudo-relative velocity), the latter for a number of frequencies from 0.25 to 40 Hz. For more details on the results here, we refer to Dahle et al (1989).

In the present context, the most interesting of the parameters estimated is the anelastic coefficient c_4 in equation (1), when A is Fourier amplitude (of acceleration). Assuming that a frequency dependent anelastic attenuation is causing the decay of these Fourier amplitudes, the c_4 term may then be written as

$$c_4 = -\frac{\pi f}{v \cdot Q(f)} \qquad (2)$$

where f is frequency in Hz, and v is wave velocity (here taken as 3.5 km/s). This relation has been used at times (cf. Nuttli and Herrmann, 1984) to constrain the c_4 parameter using independent information on anelastic attenuation.

In the present case, however, we estimate c_4 (independently of the magnitude regression) and compute Q(f) subsequently using equation (2). In order to avoid the above-mentioned bias effects in the distance coefficients because of the (albeit weak in the present case) magnitude-distance correlation (Fukushima et al, 1989), we perform a two-step multilinear regression analysis (Joyner and Boore, 1981). In that case, the estimation of the distance coefficients is decoupled from the magnitude dependence by introducing dummy variables, and equation (1) is then rewritten as follows:

$$\ln A = \sum_{i=1}^{N} a_i E_i + c_3 \ln R + c_4 R \qquad (3)$$

where

$$E_i = \begin{cases} 1 \text{ for earthquake } j \\ 0 \text{ otherwise} \end{cases}$$

N is the number of dependent variables (spectral points) in the magnitude-distance space, while there are L different earthquakes indexed $j = 1, L$.

The present analysis adopts a geometrical spreading model according to Herrmann and Kijko (1983), where the spreading function is defined as a combination of spherical and cylindrical as follows:

$$G(r,r_o) = \begin{cases} R^{-1} & \text{for } R \le R_o \\ (R_o \cdot R)^{-1/2} & \text{for } R > R_o \end{cases}$$

Herrmann and Kijko (1983) selected R_o = 100 km as a likely value in this model, partly based on a knowledge of at which distance the wave train changes from predominantly S waves (with spherical spreading) to predominantly Lg waves (with cylindrical spreading).

The distance dependent term c_4 is then determined by linear regression in the first step, along with the coefficients a_j, and the second step is performed by linear regression of the equation:

$$a = c_1 + c_2 M \tag{4}$$

In following this method of analysis, a dependence of c_4 with frequency is found as shown in Fig. VII.5.1, resulting in, by using equation (2), Q(f) values as shown in Fig. VII.5.2. The functional appearance of the Q(f) values indicated in this case that a simple polynomial approximation of the following type could be used

$$Q(f) = A + Bf + Cf^2 \ldots. \tag{5}$$

resulting in the following relation:

$$Q(f) = 539 + 152f + 1.43f^2 \tag{6}$$

This relation is shown in Fig. VII.5.2 (lin-log scale) as well as in Fig. VII.5.3 (log-log scale) where also two other relations (for southern Fennoscandia) are shown, namely, Sereno et al 1988):

$$Q(f) = 560 \cdot f^{0.26} \tag{7}$$

and Kvamme and Havskov (1989):

$$Q(f) = 120 \cdot f^{1.1} \tag{8}$$

It is seen from Fig. VII.5.3 that the new relation (Q3) is reasonably close to Kvamme and Havskov (Q2) for high frequencies and reasonably close to Sereno et al (Q1) for low frequencies.

To illustrate the effects in terms of amplitude decay from the anelastic attenuation model derived here, we have plotted the function $e^{C_4 R}$ ($C_4 R$ equals Q^{-1} times number of wavelengths) in a log-linear scale in Fig. VII.5.4, for three different frequencies (0.25, 2.0 and 20 Hz). In addition, the amplitude decay effects of spherical and geometrical spreading are shown together with the Herrmann and Kijko (1983) model for R_o = 50, 100 and 200 km. In the latter case, spreading is spherical up to distance R_o, and cylindrical from there on. The figure clearly shows how the spreading effects dominate the anelastic effects even up to quite large distances, and it is therefore important to consider and to be aware of, in any case when anelastic attenuation is studied, how the results could be affected by the assumption with respect to geometrical spreading.

In the present case, we find that the results obtained for the c_4 coefficient depend on this model in the sense that the choice of a smaller R_o will increase the absolute value of c_4, and decrease Q, while a higher R_o will have the opposite effect. These effects of R_o on Q are, however, stronger for low frequencies than for higher frequencies. This means, in terms of Q models of the more conventional type $Q(f) = Q_o f^{\eta}$, that changes in R_o affect first of all Q_o. In turn, Q_o determines the seismic moment, which means that R_o essentially trades off with moment. For a closer discussion of the source moment for the earthquake discussed in the previous report in this series (8 August 1988), we refer to Hansen et al (1989).

In terms of the other Q relations shown in Fig. VII.5.3 (equations 7 and 8), it should be noted (T.J. Sereno, jr., personal comm.) that the larger epicentral distances (200 - 1400 km) used in the Sereno et al analysis essentially remove the effect of R_o on Q(f), which in that case is primarily determined by the way in which the spectral slopes

change with distance. Kvamme and Havskov, on the other side, and in particular Dahle et al, use data with smaller epicentral distances, leading to a greater dependence of Q(f) on the model used for geometrical spreading.

It would therefore now be valuable to improve our knowledge and understanding of the geometrical spreading and the way in which it depends on wave type, source depth and crustal structure.

H. Bungum
A. Dahle
L.B. Kvamme

References

Dahle, A., H. Bungum and L.B. Kvamme (1989): Attenuation models inferred from intraplate earthquake recordings. Manuscript in preparation.

Fukushima, Y., T. Tanaka and S. Kataoka (1989): A new attenuation relationship for peak ground accelerations derived from strong-motion accelerograms. Proc., Ninth World Conf. on Earthq. Eng., Vol. II, 343-348.

Hansen, R.A., H. Bungum and A. Alsaker (1989): Three recent larger earthquakes offshore Norway. TERRA Nova, in press.

Joyner, W.B. and D.M. Boore (1981): Peak horizontal acceleration and velocity from strong-motion records including records from the 1979 Imperial Valley, California, earthquake. Bull. Seism. Soc. Am., 71, 2011-2038.

Herrmann, R.B. and A. Kijko (1983): Modeling some empirical component Lg relations. Bull. Seism. Soc. Am., 73, 157-171.

Kvamme, L.B. and J. Havskov (1989): Q in southern Norway. Bull. Seism. Soc. Am., in press.

Nuttli, O.W. and R.B. Herrmann (1984): Ground motion of Mississippi Valley earthquakes. J. Tech. Topics in Civ. Eng., 110(1), 54-69.

Sereno, T.S., S.R. Bratt and T. Bache (1988): Simultaneous inversion of regional wave spectra for attenuation and seismic moment in Scandinavia. J. Geophys. Res., 93, 2019-2035.

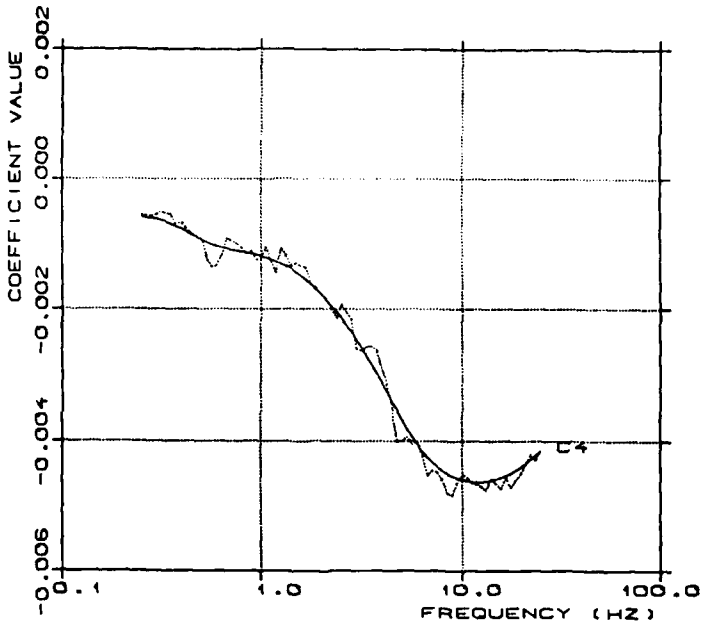

Fig. VII.5.1. Regression coefficient c_4 in equation (1) vs. frequency as derived from Fourier amplitude spectral estimates. The smooth line is a smoothed version of the computed values.

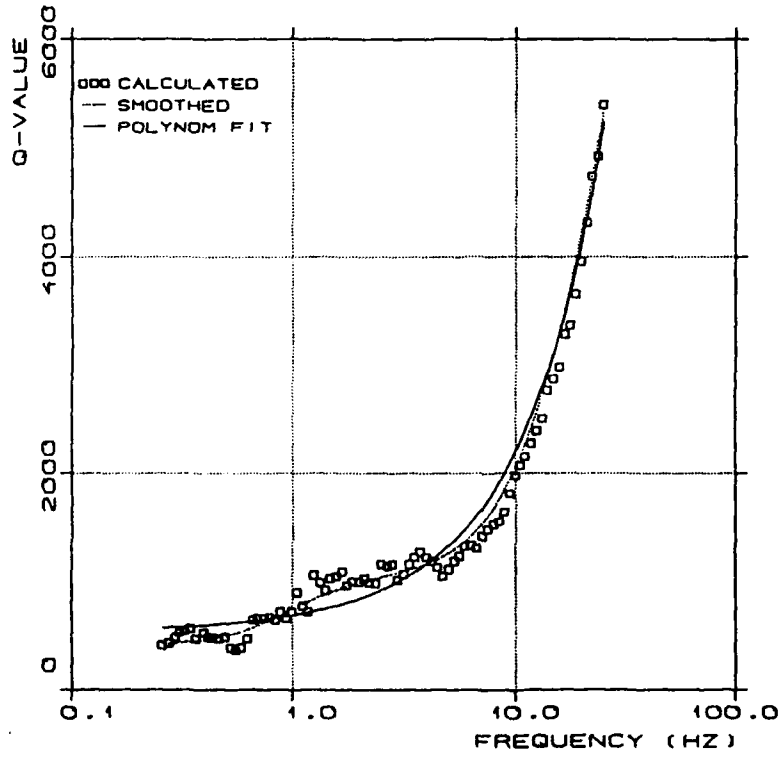

Fig. VII.5.2. Quality factor Q as a function of frequency, as derived from the c_4 coefficients in Fig. VII.5.3 using equation (2). Squares indicate calculated values, the dotted line is a smoothed version, and the fully drawn line is a polynomial fit given by equation (3).

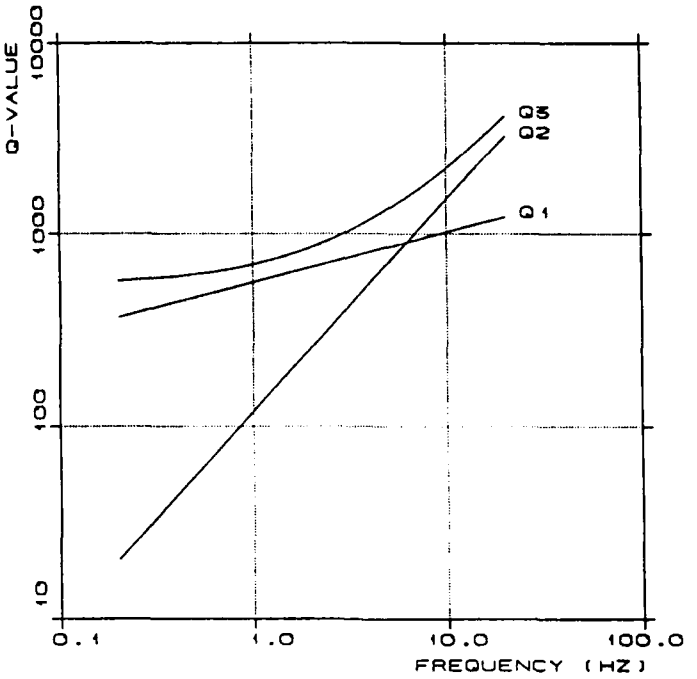

Fig. VII.5.3. Three different relations for anelastic attenuation: (1) $Q = 560f^{0.26}$ (Sereno et al, 1988); (2) $Q = 120\ f^{1.1}$ (Kvamme and Havskov, 1989); (3) $Q = 539 + 152f + 1.43f^2$ (Dahle et al, 1989).

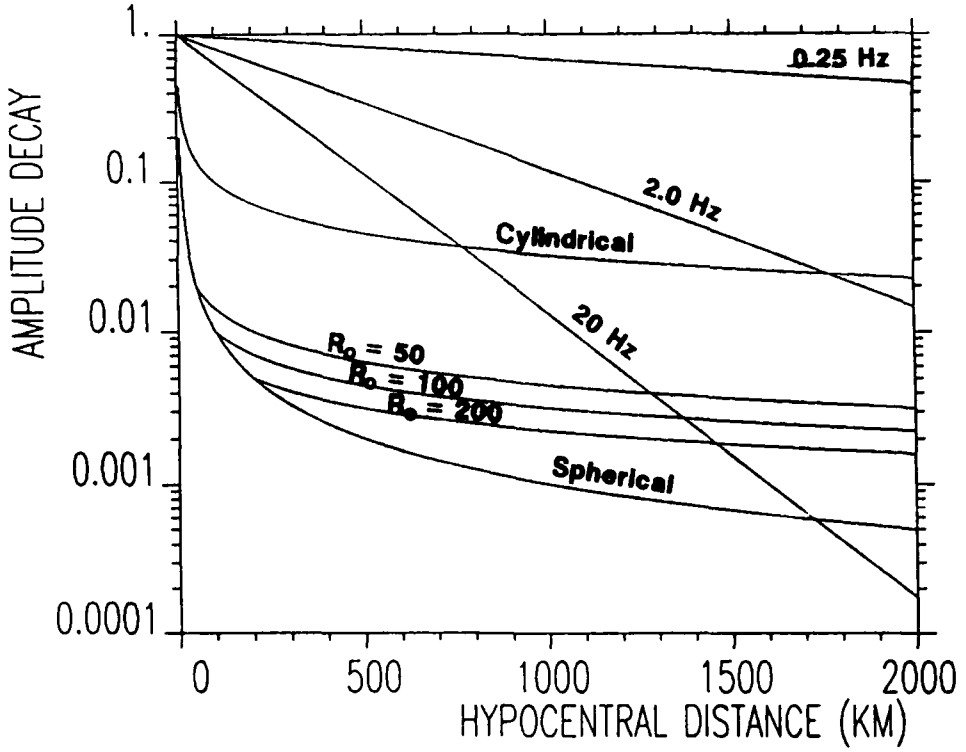

Fig. VII.5.4. Anelasticity and geometrical spreading decay of Fourier spectral acceleration (unit-size at 1 km distance) with increasing hypocentral distance. The anelastic term is shown for 3 frequencies (0.25, 2.0 and 20 Hz) according to the results of this study. Geometrical spreading functions for the limiting cases purely spherical or purely cylindrical are shown, together with the Herrmann and Kijko (1983) model with R_o = 50, 100 and 150 km. A, B and C are the coefficients in the degree 3 polynomial fit to Q(f) as given by equation (3).

VII.6 X.25-based communication link between NORSAR and AFTAC

A new communication link, based on the international Packet Switched Data Network (PSDN) and making use of the X.25 protocol, has been established between NORSAR and AFTAC. This new link enables AFTAC to extract raw data from ARCESS, NORESS and NORSAR in near real time.

The on-line processing of data from the NORSAR array is being conducted at the array data center at Kjeller. Processing results in the form of detection information are transmitted every 8 hours to AFTAC via telex. AFTAC requests raw data by mail and data are transmitted on 1/2" tapes from NORSAR to AFTAC. Both the transmission of processing results and data are delayed compared with what may be achieved with a direct computer access to Norway, and AFTAC has requested NORSAR to assist in implementing a direct computer access and build up necessary programs and routines for accessing NORSAR data. Main goals have been as follows:

- Better connection to NORSAR
- Faster access to detection lists
- Online access to raw data
- Binary file transfer of data

Both NORSAR and AFTAC are users of SUN workstations, and the decision was made to use SUN to set up the new communication link. In this way we can easily make use of efficient transmission protocols, and avoid the difficulties that result from the current lack of standards for communications between computers of different architecture.

In order to implement a reliable link, we considered the following options:

- Modem communication using UUCP or Kermit
- ARPANET connection using the TCP/IP protocol
- X.25 using the TCP/IP protocol on top of X.25.

Fig. VII.6.1 shows the option selected, corresponding to the third alternative above. The X.25 service is a commercially available service and was selected instead of ARPANET. Based on our previous experience with modems using ordinary telephone lines between the US and Europe, we have rejected this option. The GSE group in Geneva has also reached a similar conclusion, and will be using the X.25 service for the upcoming GSETT-2 experiment. X.25 is implemented in more countries than any other high-speed data communication medium.

The X.25 itself offers no more than reliable transport of packets. In addition to X.25, the X.29 protocol must be used for terminal access. Most computers with X.25 implemented have the X.29 protocol available. This protocol is implemented on SUN in a program called PAD (Packet Assembly Disassembly).

There are several ways to implement the file transfer protocol. The likely future solution will be based on OSI and FTAM. SUN offers file transfer by using the well-known TCP/IP protocol on top of the three X.25 layers. A logical link between two computers on X.25 is established and file transfer is done with ftp or rcp commands. Telnet, mail and other TCP/IP-based applications will also work while the link is established.

X.25, PAD and TCP/IP-based services over X.25 are available in SUN's product SUNlink together with a VME MCP board.

Access to information at NORSAR is achieved by using the National Data Center (NDC) program developed at NORSAR. The NDC program has the following functions available:

- Access to detection lists from NORSAR, NORESS and ARCESS
- Access to waveforms from NORSAR, NORESS and ARCESS
- Graphical display of data by using the X window protocol.

The NDC program is easy to use and has a set of well-documented man (manual) pages available online.

AFTAC has its own login account and logs in as a regular user. Thus, all the UNIX features will be available in addition to the NDC program. Fig. VII.6.2 shows how data and detection lists from NORSAR, NORESS and ARCESS are organized at the NORSAR data center. Detection lists from NORSAR, NORESS and ARCESS are accessed by using SUN's NFS (Network File System) protocol. The NDC program sends mail with a request for NORSAR data to a server on the IBM 4381 computer. The server forms a data file with the requested time interval and transfers the data segment to the SUN using ftp. The format of NORSAR data is equal to the original NORSAR tape format.

The first step, terminal access, is already installed and the file transfer functions will be available as soon as AFTAC obtains a direct X.25 connection.

The selected solution will make it possible for AFTAC to access any computer connected to X.25. It may not be possible to achieve file transfer from all installations, but terminal access will normally work. File transfer will be possible when the OSI standard is more commonly available at different computers.

R. Paulsen

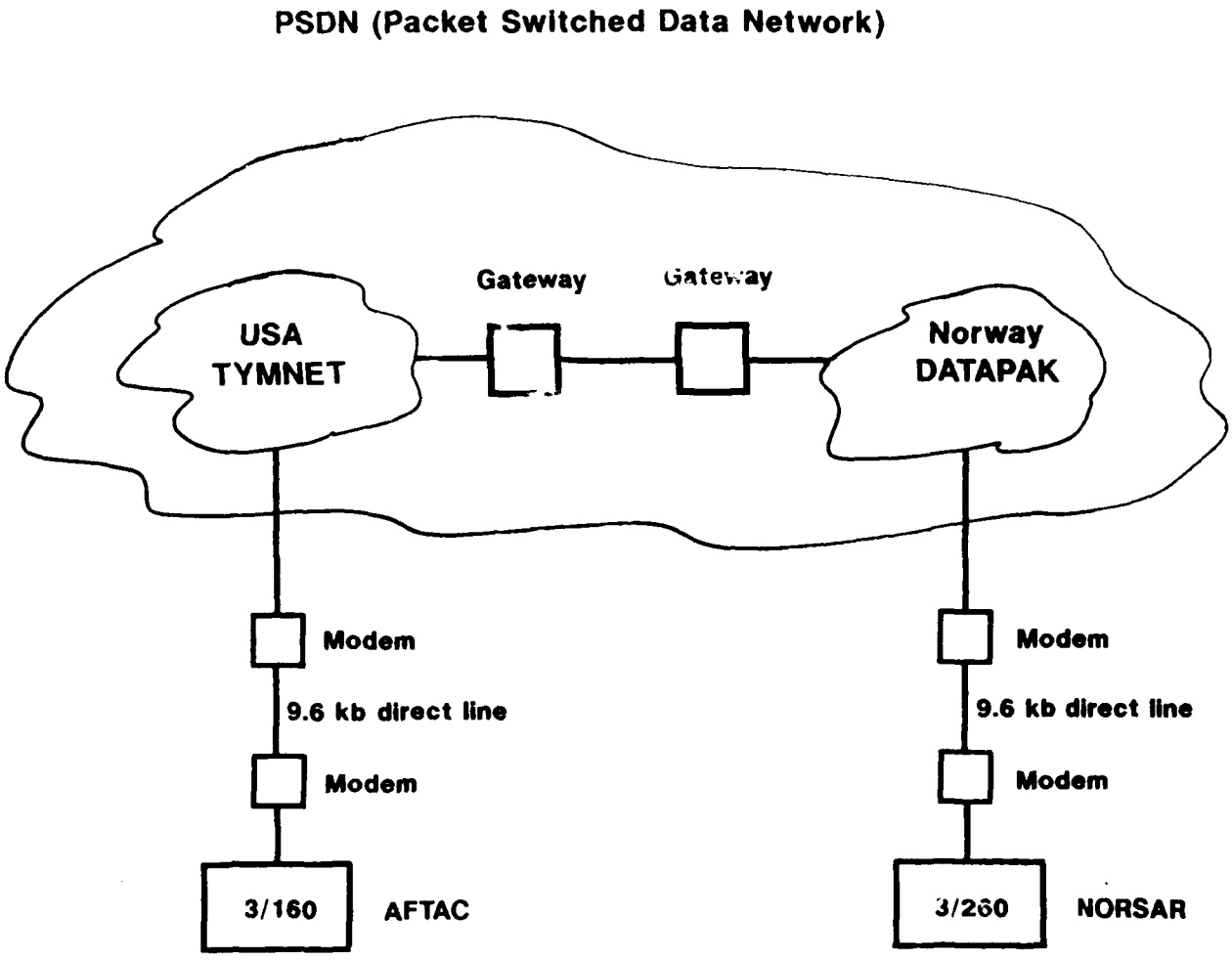

Fig. VII.6.1. Communication implemented for the new link between AFTAC and NORSAR.

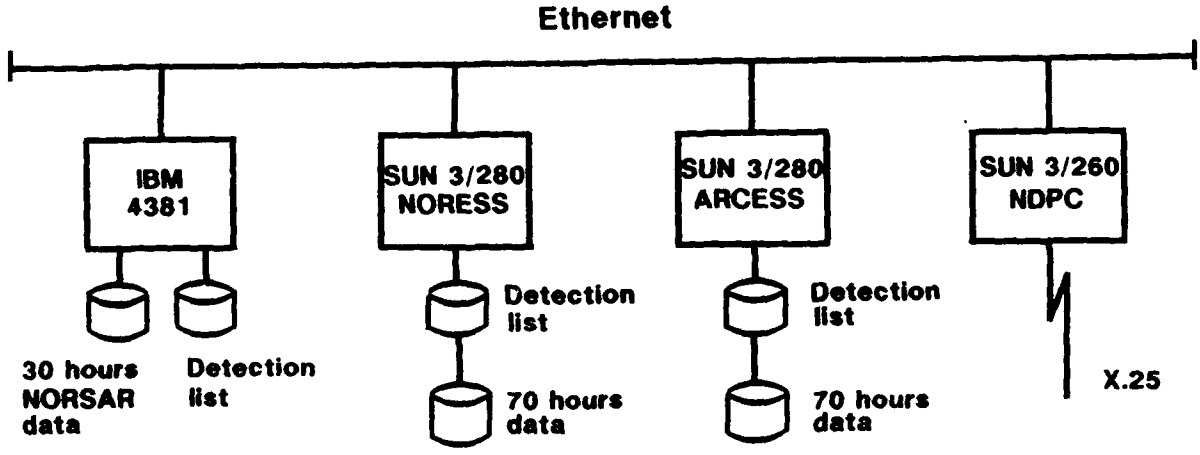

Fig. VII.6.2. Available data and detection lists.

VII.7 Event processor program package

In NORSAR Scientific Report No. 2-86/87, a general detection processing (DP) package for array or single-station data was described (Fyen, 1987). This package was built around an interactive analysis system (SSA - Seismic Signal Analyzer) developed at NORSAR (Harris and Kværna, 1985). Today, the DP package is used in the routine on-line processing of NORSAR, NORESS and ARCESS recordings, and it has also been successfully applied to data from the FINESA, Alice Springs and Gräfenberg arrays, as well as single three-component stations.

Building on the same principles, an Event Processing Package (EP) has recently been developed, and is now in regular use to process ARCESS data (since late 1988) and NORESS data (since early 1989). The EP package represents an extension of the RONAPP system (Mykkeltveit and Bungum, 1984), and is designed primarily for automated processing of single-array or three-component station data, with options to conduct various types of multiarray and multistation analyses in an automatic or interactive mode. In the automatic mode of operation, phase detections will be analyzed, grouped and associated, with automatic location solutions provided together with trace plots as shown in examples later in this section.

Besides the regular (continuous) mode of operation, the EP package also offers the flexibility to provide complete interactive or semi-automatic analysis of seismic recordings, using the SSA macro-language to create, in a simple fashion, sequences of commands that may be built up to execute very complex analysis procedures. This is a feature that has been found extremely useful, both in research projects and for the purpose of evaluating array performance and data quality.

The EP system possesses the same flexibility as the DP and SSA packages as far as diversity of input data is concerned. Thus, it does not rely upon a single data format, but uses instead the general purpose NORSAR package ARRMAN for reading data. ARRMAN supports at present the following data formats: NORSAR, NORESS, ARCESS, FINESA, Gräfenberg, CSS

2.8 and the GSE format. Input medium may be either disk loop (i.e., on-line disk data), disk files or magnetic tapes.

Fig. VII.7.1 gives a flow chart illustrating the general structure of the NORSAR analysis packages (DP,EP,SSA). The systems are modular, with the common interface between the processes consisting of a "data stack" and a "blackboard" resident on disk. A further description of these features may be found in Harris and Kværna (1985).

Figs. VII.7.2 - VII.7.4 give examples of automatically generated output plots from the EP process for a regional event recorded at NORESS. The following three panels are shown: a) six minutes of filtered data, including best P and S beams, b) one minute of P-wave data, including filtered and unfiltered beam traces, c) a corresponding plot for the S (or Lg) phase. Previous experience at NORSAR has shown that this amount of detail is essential in order for the analyst to obtain a proper evaluation of array performance.

In future applications, the EP package will provide a supplement to the IAS system currently under implementation. Whereas the IAS will emphasize the expert system approach to multi-array detection, location and characterization of seismic events, the EP system will comprise extensive automatic and interactive analysis of array data using more traditional methods of analysis. We thus expect that a comparison of the performance between these two systems will give an excellent opportunity to evaluate the improvements offered by IAS. At the same time, we anticipate that this mode of parallel operation and continuous comparison will contribute to identify possibilities for further enhancements of the initial IAS version. Furthermore, the flexibility offered by the EP package will continue to make it useful as a tool in a more general research and evaluation context.

J. Fyen

References

Fyen, J. (1987): Improvements and modifications. Semiann. Tech. Summ., 1 Oct 1986 - 31 Mar 1987, NORSAR Sci. Rep. No. 2-86/87, Kjeller, Norway.

Harris, D.B. and T. Kværna (1985): Interactive analysis program for use with NORESS data, Semiann. Tech. Summ., 1 Oct 1984 - 31 Mar 1985, NORSAR Sci. Rep. No. 2-84/85, Kjeller, Norway.

Mykkeltveit, S. and H. Bungum (1984): Processing of regional events using data from small-aperture arrays, Bull. Seism. Soc. Am., 74, 2313-2333.

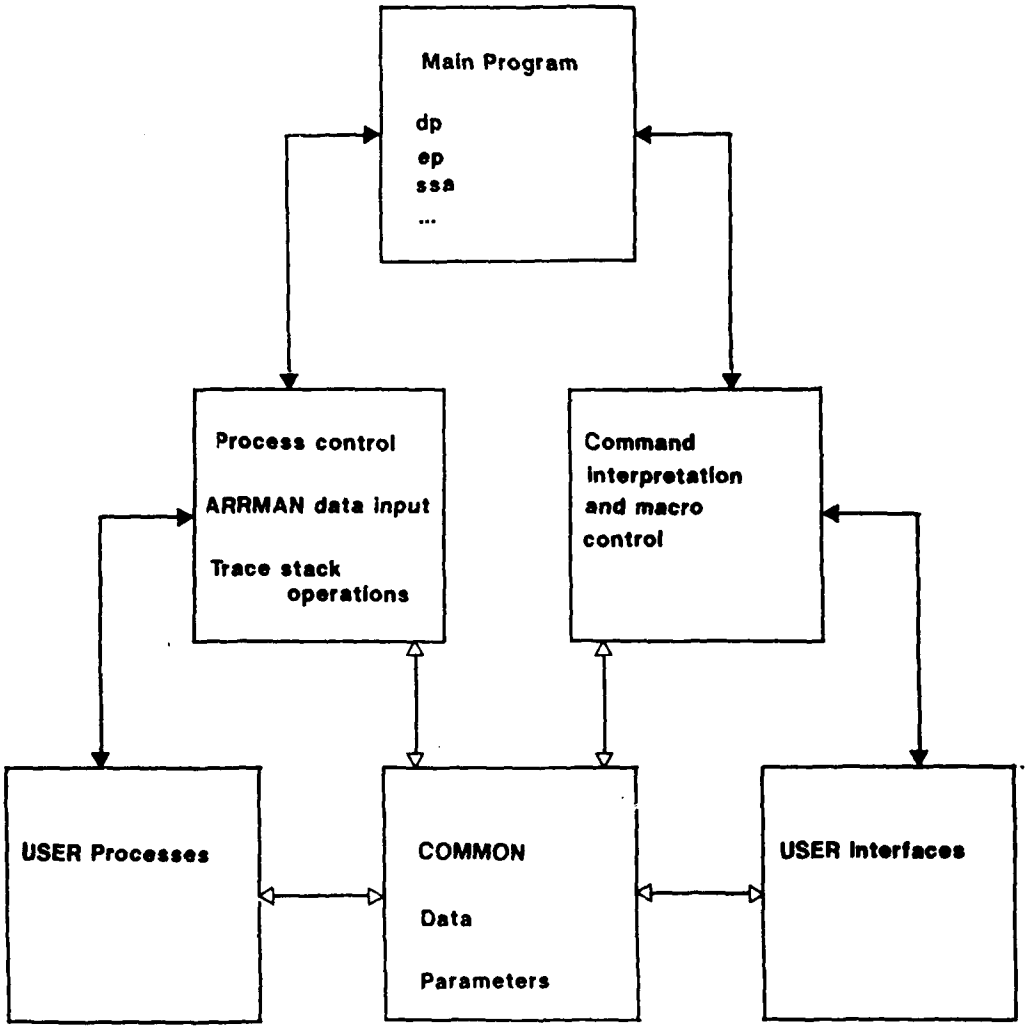

Fig. VII.7.1. Schematic overview of the DP, EP and SSA program structures.

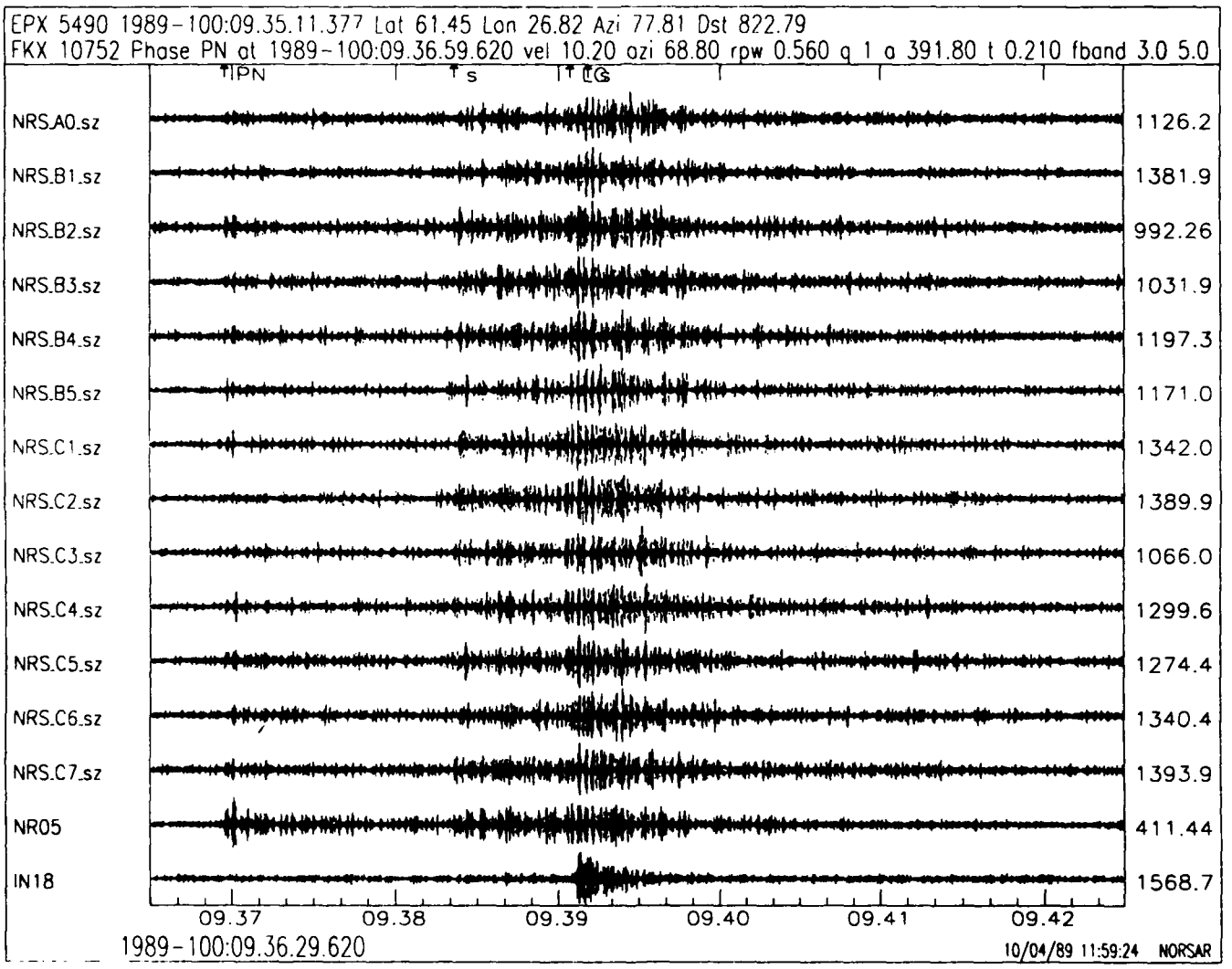

Fig. VII.7.2. Six-minute plot of a regional event located by NORESS. "Best" P and S beams are displayed as the two bottom traces.

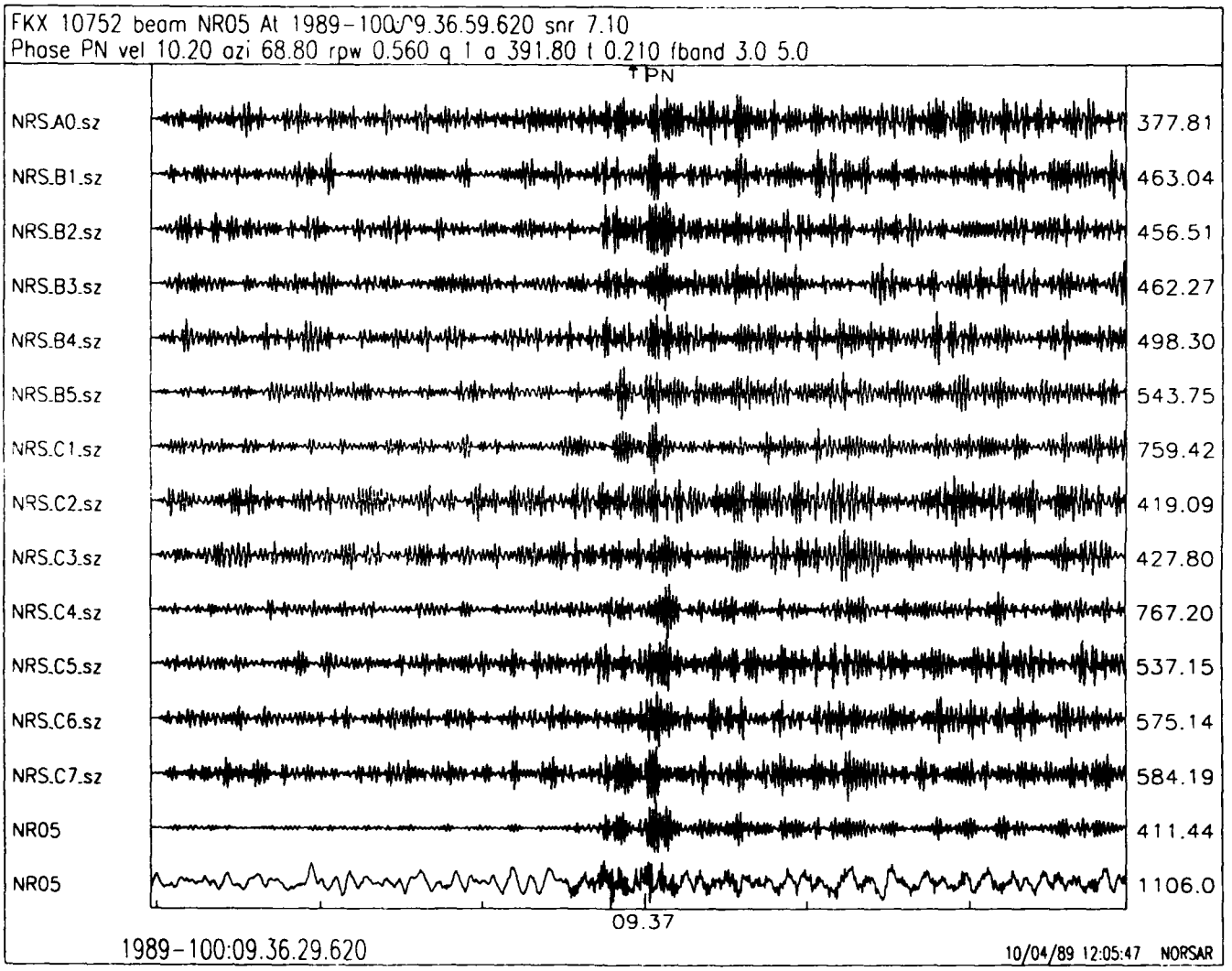

Fig. VII.7.3. Expanded display of the P-phase for the event of Fig. VII.7.2. One minute of data is shown. The best P-beam is shown both filtered and unfiltered.

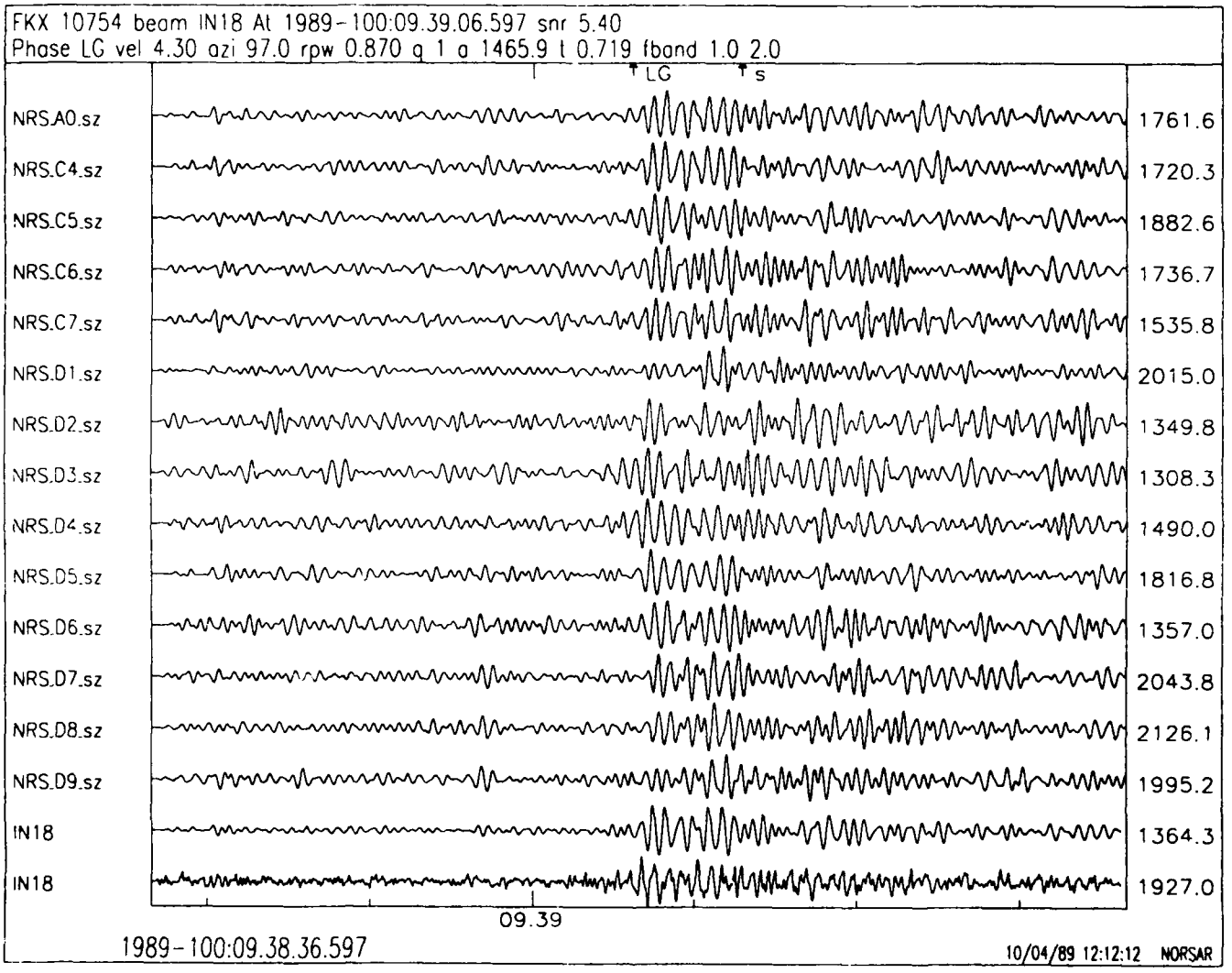

Fig. VII.7.4. Same as Fig. VII.7.3, but corresponding to the Lg phase.

VII.8 Analysis of IRIS data for Soviet nuclear explosions

Introduction

In previous NORSAR Semiannual Technical Summaries, Lg measurements from NORSAR and Grafenberg recordings (at distances greater than 4000 km) have been suggested as a means to provide stable estimates of magnitudes for large underground nuclear explosions. Such estimates are considered stable in that the Lg phase exhibits a much reduced amplitude variability across the arrays compared to the P phase. In this way, the Lg magnitude estimates show promise to provide a valuable supplement to m_b in estimating yield for nuclear explosions. Now data have become available from four modern digital seismic stations installed within the Soviet Union by IRIS (Given and Berger, 1989) for recent explosions in the Semipalatinsk area (see Table VII.8.1, Table VII.8.2 and Fig. VII.8.1). These new data allow the comparison of the stability of the RMS Lg measurement technique (Ringdal and Hokland, 1987) for stations at various distances. As part of our current work, we will compare the detectability and Lg amplitudes of events recorded at the IRIS stations to those of NORSAR, NORESS and ARCESS.

We have found the IRIS recordings to be of excellent quality, providing high resolution digital data with large dynamic range over a wide frequency band. So far, however, the IRIS data comprise only a small number of explosions, and in addition, we did not have complete station coverage for all events (only one station, ARU, had recordings for all explosions in Table VII.8.1, and only vertical components were used for some events in this study). It is therefore too early to state any firm conclusions from this initial study. However, some preliminary results can be summarized as: a) the IRIS stations provide a much improved signal-to-noise ratio for events near Semipalatinsk as compared to NORSAR, b) the scaling of RMS Lg amplitudes between different sized events recorded at the same IRIS site appears to be consistent with that of NORSAR, c) a possibility of reduced scatter in RMS Lg measurements at single sites may be accomplished by averaging the three-component recordings, and d) RMS Lg amplitudes may be made to about 1.5

magnitude units lower than at NORSAR or Grafenberg allowing a much lower threshold for yield determination.

Data analysis

Examples of the IRIS recordings are shown in Figs. VII.8.2 through VII.8.4. Fig. VII.8.2 shows the recordings from all four IRIS sites for the explosion of September 14, 1988. In this figure are the unfiltered 3-component data along with bandpass filtered versions in the frequency range from .6 Hz to 3 Hz. (This frequency range was chosen to obtain consistency with analysis of NORSAR recordings.) On top of each filtered trace is a 120 second window RMS measure of the amplitude. The first striking feature of the three-component seismograms is that the horizontal instruments consistently exhibit a larger value for the Lg phase than the verticals. The closer stations, ARU and GAR, at a distance near 1500 km, show this Lg phase as the largest amplitude, while stations OBN and KIV at a distance nearer to 3000 km have the P phase as the largest amplitude. The station KIV has no discernible Lg phase for this explosion, presumably because Lg does not propagate efficiently in the crustal structure associated with the Caspian Sea.

As a contrast to this well-recorded event, Fig. VII.8.3 illustrates the capabilities of the ARU station to record an m_b 3.8 event from the Shagan River test site on day 270 (September 26) of 1988. (This m_b magnitude is based on the NORSAR m_b of 4.3 with an assumed regional correction of .5 m_b units for comparison to world-wide m_b estimates and therefore must be considered uncertain.) The unfiltered broadband trace essentially shows no signal for this event, however, the bandpass-filtered trace clearly shows energy arriving that can be identified as significant Lg signal with a signal-to-noise ratio of about 2.

In an attempt to enhance the detectability of other phases, the vertical component was filtered in several pass bands as illustrated in Fig. VII.8.4. Even considering frequency bands up to the Nyquist frequency of 10 Hz, we found no additional enhancement of the P phase

or other phases. (It may be noted that ARU and GAR are at distances within a shadow zone for P waves from seismic sources in East Kazakhstan.) The NORESS beam deployment for this event is clearly capable of detecting the P wave arrival as illustrated in Fig. VII.8.5. Therefore, even though the ARU station may not be capable of detecting the event in an automatic fashion, regional arrays such as NORESS and ARCESS can correctly detect the event while the analysis of the Lg phase at a much closer station can provide an estimate of the RMS Lg magnitude suitable for giving independent information on explosion yield.

The seismograms from the IRIS stations were all processed in a manner similar to that used for the NORSAR recordings by first bandpass filtering the seismograms as illustrated above and measuring RMS amplitude for the phase of interest. In this respect, no allowance was made for a particular group velocity window for analysis at this early stage, but rather the same length window of 120 seconds was chosen for all distances and centered at the 3.5 km/sec group velocity arrival time. The RMS measure of Lg was calculated for the particular 120 second window for all recordings stations (and individually for all components of recording). Likewise, an RMS measurement of the noise preceding each event arrival was calculated and applied as a correction term for calculating the Lg amplitude measure as originally defined by Ringdal and Hokland (1987). In contrast to NORSAR, IRIS stations are single-site stations, so no averaging of vertical component measures was possible. However, IRIS stations do provide the possibility to average data from the three components, and we thus computed both individual component RMS data as well as average values to see whether reduced scatter could be achieved in this way.

The first result we wish to illustrate is shown in Fig. VII.8.6. Here we show the variation in the signal-to-noise ratio of the RMS Lg for five events from the Semipalatinsk area as a function of distance. The range in magnitude (m_b) is from 5.2 for the event on day 317 of 1988 to 6.1 for the event on day 258 of 1988. The event on day 317 indicates the minimum for which RMS Lg was measured at NORSAR at a distance of about 4200 km with a signal-to-noise ratio of about 1.1. For this same

event a signal-to-noise ratio of about 30 is still observable at ARU and GAR at a distance of about 1500 km.

In order to verify the stability of the RMS Lg amplitudes within the Soviet Union, the amplitudes were compared with NORSAR amplitudes for common events. Since the instrument response of the different IRIS stations varied as a function of time as well as among themselves (each being different than that of a NORSAR station), we decided for this preliminary study to convert all measurements to the equivalent response of a typical NORSAR short period instrument in the .6 to 3 Hz range. The variation of RMS Lg amplitudes as a function of event size and distance is illustrated in Figs. VII.8.7 and VII.8.8.

First, in Fig. VII.8.7, we compare the difference in log RMS Lg between two events recorded at the same stations. The stations are NORSAR (~4200 km), ARU (~1500 km) and OBN (~3000 km) for the m_b 6.1 event on day 258 of 1988 minus the m_b 5.9 event on day 352 of 1988. We first note that all three stations indicate that the former event has a larger Lg signal by about 0.2 magnitude units, and the observations are thus quite consistent. Furthermore, we see a variation among the three components of ARU and OBN typically on the order of .07 magnitude units. However, the average of the three components is more stable compared to NORSAR, with a variation of only about 0.02 magnitude units. From observing the behavior of similar plots for other events it appears the difference between NORSAR and single station three-component averages may vary by about $\pm$ .05 magnitude units on the average.

For comparison of actual measurements of RMS Lg amplitudes between NORSAR and ARU for all common events, we plot in Fig. VII.8.8 only the vertical component of RMS Lg (Table VII.8.3). This is necessary when comparing ARU to NORSAR, since from Fig. VII.8.2 we see horizontal amplitudes of Lg are consistently larger than vertical and NORSAR measurements were made on only vertical instruments. A line fit to these data with a fixed slope of 1.0 yields a standard deviation of .032 (dotted line on the figure corresponds to 2 standard deviations).

Although the straight-line fit is excellent, it is necessary to interpret this plot with caution, in view of the sparse data. Additional event data will be required before any reliable assessment of the slope and data scatter can be made.

Given this fit with a slope of one, and that Ringdal et al (this volume) have convincingly shown the RMS Lg at NORSAR fits to reported m_b magnitudes also with a slope of one, we plot in Fig. VII.8.9 the RMS Lg amplitude at ARU against m_b magnitudes for all recorded events at Shagan River with an imposed slope of one. The standard deviation of the fit is .154. The Shagan River events with magnitude greater than 5 lie very close to the line with slope of one which strengthens the conclusion that the ARU estimates correlate well with m_b estimates in the same way as the NORSAR data. The exception is the small magnitude 3.8 Shagan River event on day 270 of 1988. If we fit a line to these Shagan River events, we obtain a slope of 1.2 with a standard error of .050. The only objection to this is that the magnitude 3.8 event is contributing too heavily to this fit given the great uncertainties tied to both the m_b estimate (as noted above), and the RMS Lg estimate taken from Fig. VII.8.3. It is for this reason that we display the data with an arbitrary line of slope 1. If, for example, we were to find the m_b estimate was too low, the standard error we obtained of .154 would very much improve.

Discussion

This preliminary study has shown that RMS Lg amplitudes estimated from IRIS stations within the Soviet Union for Semipalatinsk explosions appear to be quite consistent with NORSAR RMS Lg estimates. This has several important implications:

1. RMS Lg appears to be a stable source size estimator when computed at widely distributed stations, and would therefore provide a reliable magnitude estimate once the proper correction term has been estimated for each station.

2. The IRIS stations (notably ARU and GAR) can be used to estimate Lg magnitudes for explosions of much lower yield than is possible using the more distant NORSAR and Grafenberg arrays. Our preliminary analysis indicates that the signal-to-noise ratio improvement allows RMS Lg estimates tc be made down to approximately m_b 4.0 at ARU, compared to a threshold of about m_b 5.5 at NORSAR.
3. Although single stations do not offer the increased stability obtained through array averaging, this is partly compensated by the higher signal-to-noise ratio, which means that modest noise fluctuations will be insignificant for the Lg measurements. Also, a possibility of decreasing scatter of magnitude estimates through averaging the three components of each station exists. Our initial analysis indicates that such an approach could be useful, but it may be necessary to determine correction terms for each component individually.
4. As more data (and possible additional stations) become available, a data base will be developed that will enable us to compute network averages, based on individual station data "calibrated" to NORSAR m_b(Lg). This would allow for both improved uncertainties of future explosions, as well as maintain a comparison to historic data. Potentially, the calibration could be done using direct, independent, yield information.

We have not, in this paper, addressed in detail such topics as the selection of optimum filter band and Lg time window for the IRIS stations. This needs to be done, and it would also be desirable to develop a theoretical basis to allow for correction of attenuation of the Lg phase. Finally, extension of the study to other nuclear explosion sites will be desirable. Of particular interest here is to study the possible differences between the Shagan River and Degelen Mountains regions.

Acknowledgements

We appreciate the help of Dr. Holly Given of the University of California, San Diego, and Dr. Alan Ryall of the Center for Seismic Studies, in providing prompt access to the data from IRIS stations in the USSR, and details of instrument responses.

R.A. Hansen
F. Ringdal
P.G. Richards, Columbia Univ.

References

Given, H.K. and J. Berger (1989): IRIS/IDA stations in the USSR: An update. Am. Geoph. Union meeting, May 1989.

Ringdal, F. and B.Kr. Hokland (1987): Magnitudes of large Semipalatinsk explosions using P coda and Lg measurements at NORSAR. In: Semiannual Tech. Sum., 1 Apr - 30 Sep 1987, NORSAR Sci. Rep. 1-87/88, Kjeller, Norway.

Year	DOY	Month	Day	m_b	IRIS Stations	Test Site
1988	258	9	14	6.1	ARU, KIV, OBN, GAR	Shagan River
1988	270	9	26	3.8	ARU	Shagan River
1988	292	10	18	4.9	ARU, GAR	Degelen Mountain
1988	317	11	12	5.3	ARU, GAR	Shagan River
1988	328	11	23	5.3	ARU, OBN, GAR	Degelen Mountain
1988	352	12	17	5.9	ARU, OBN	Shagan River
1989	022	1	22	6.0	ARU	Shagan River
1989	043	2	12	5.9	ARU, OBN	Shagan River
1989	048	2	17	5.0	ARU	Degelen Mountain

Table VII.8.1. List of events and recording stations used in this study.

Station	Latitude	Longitude	Elevation (m)
OBN	55.10 N	36.60 E	160
ARU	56.40 N	58.60 E	250
KIV	43.95 N	42.68 E	1206
GAR	39.00 N	70.32 E	1300

Table VII.8.2. IRIS station coordinates.

Event Date	NORSAR log RMS Lg	ARU z log RMS Lg
Sept 14, 1988	3.014	4.142
Nov 12, 1988	2.307	3.429
Dec 17, 1988	2.846	3.935
Jan 22, 1989	3.005	4.076
Feb 12, 1989	2.836	3.891

Table VII.8.3. Values of log RMS Lg amplitudes as plotted in Fig. VII.8.8. Note that for comparison the values for ARU have been adjusted to the response of a NORSAR instrument.

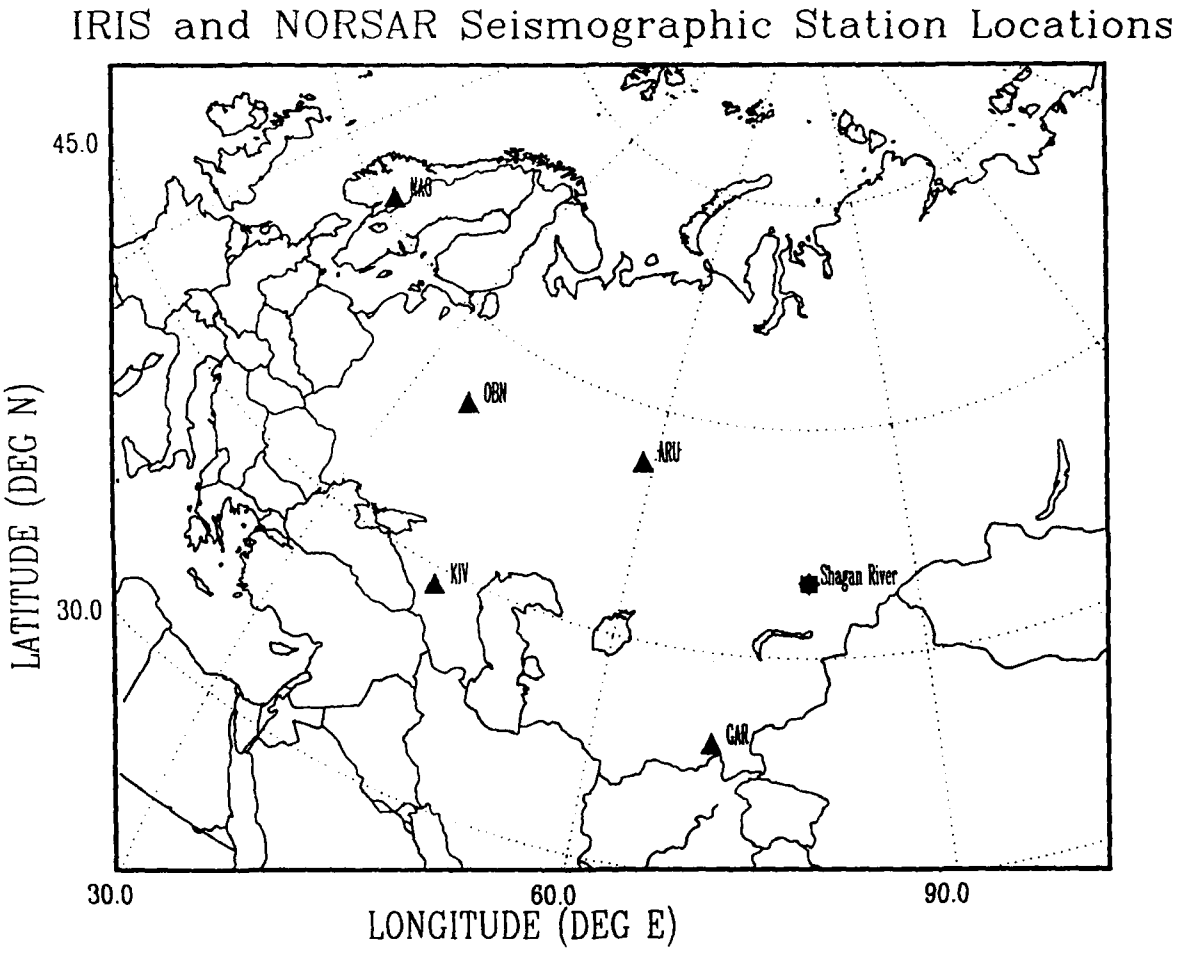

Fig. VII.8.1. Map indicating locations of the Shagan River test site and the IRIS stations in the USSR along with the location of NORSAR array in Norway.

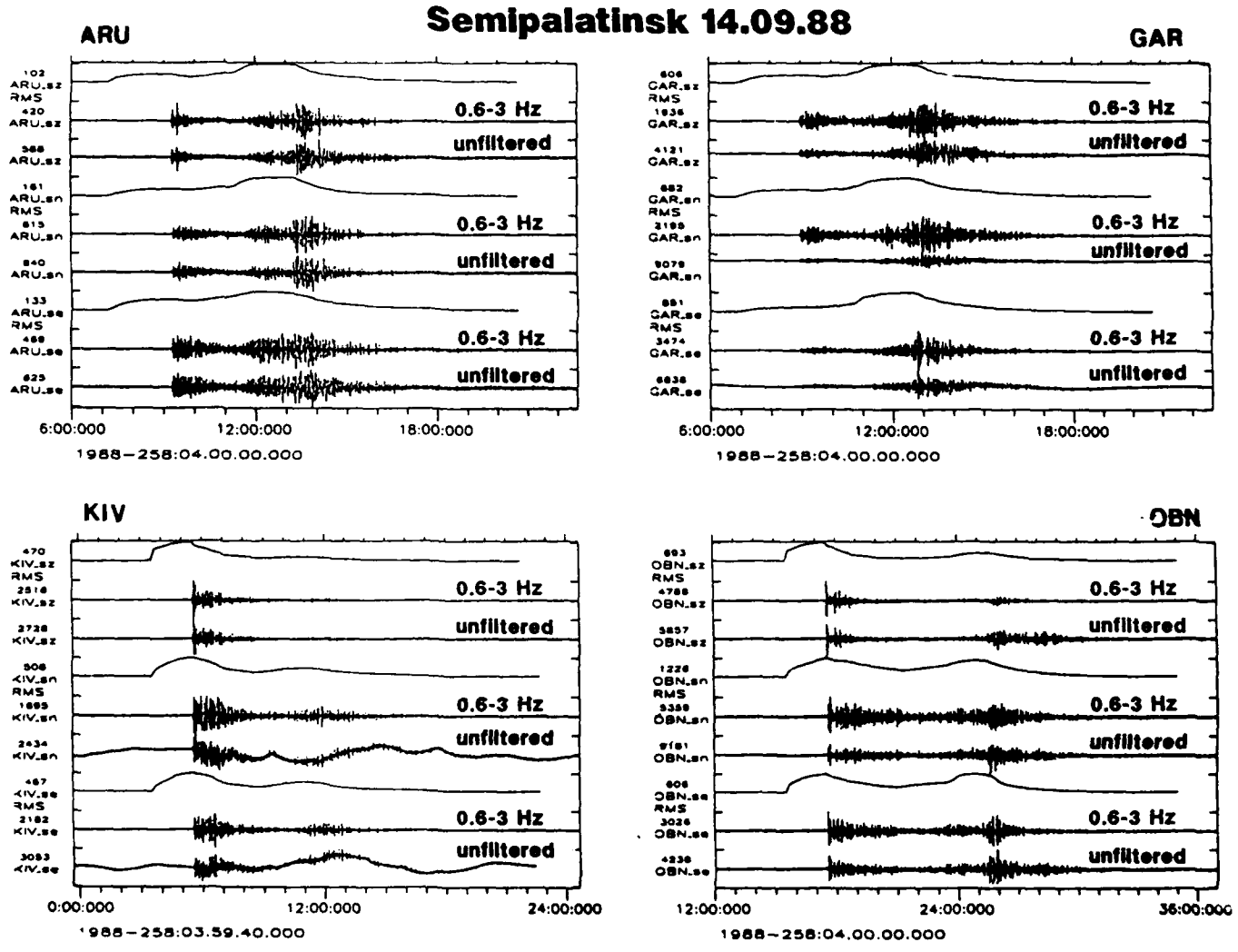

Fig. VII.8.2. Plots of the data recorded on the four IRIS stations located in the USSR for the explosion of September 14, 1988. For each of three components at each site are the unfiltered trace, a filtered version in the band 0.6 to 3 Hz, and the 120 second window RMS amplitude measure as a function of time.

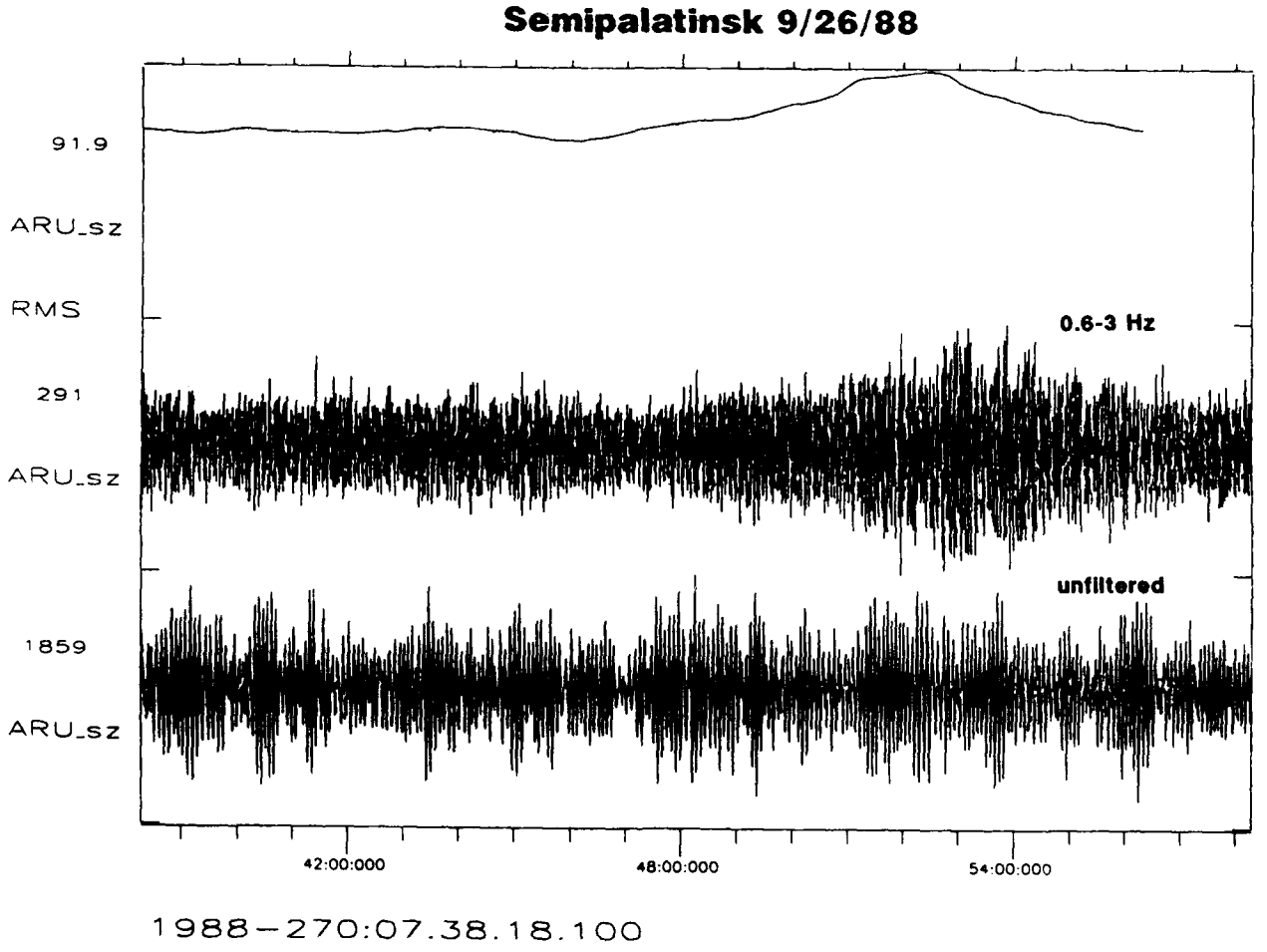

Fig. VII.8.3. The ARU vertical component seismogram from the m_b 3.8 explosion on September 26, 1988. The lower trace is the unfiltered seismogram, the middle trace is the bandpass filtered seismogram between 0.6 and 3 Hz, and the upper trace is the RMS amplitude as a function of time.

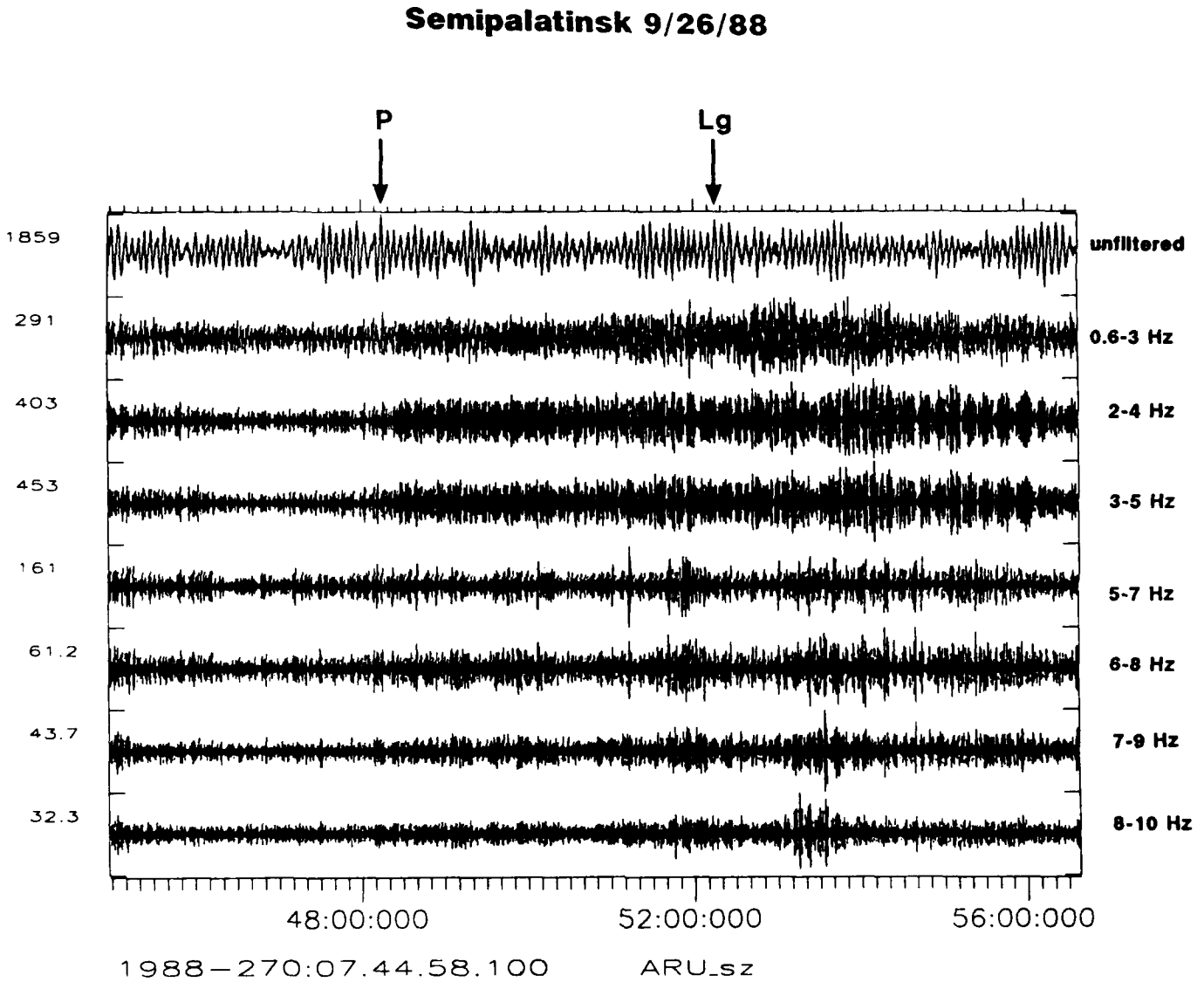

Fig. VII.8.4. The ARU vertical component seismogram from the m_b 3.8 explosion on September 26, 1988. The top trace is the unfiltered seismogram, while subsequent traces show the seismogram resulting from successively higher bandpass frequency intervals. Predicted arrival times of P and Lg (3.5 km/s) are marked as arrows.

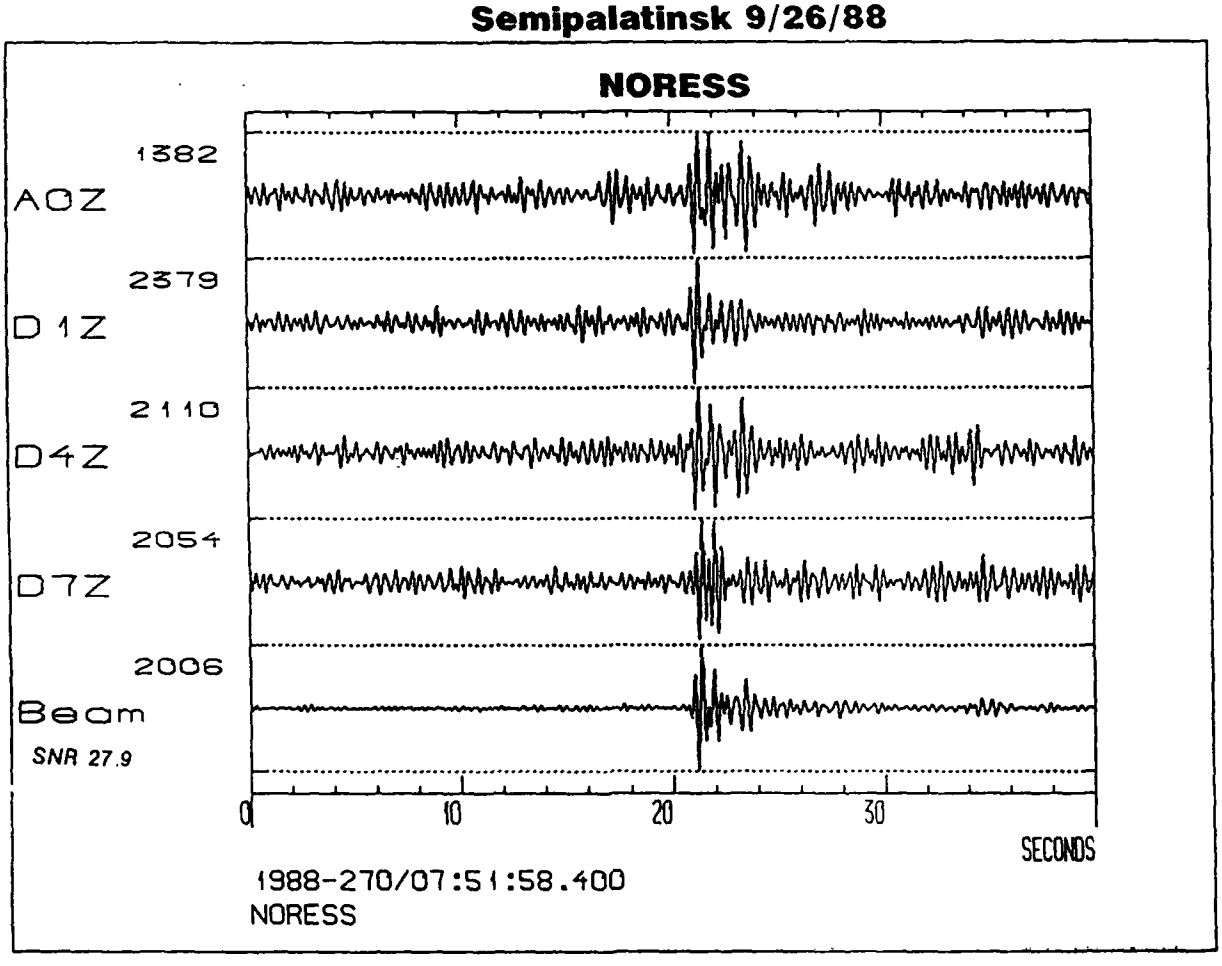

Fig. VII.8.5. Example of three vertical component seismograms from the NORESS array in Norway for the m_b 3.8 explosion on September 26, 1988. Shown on the bottom trace is the beam formed by steering toward the explosion site.

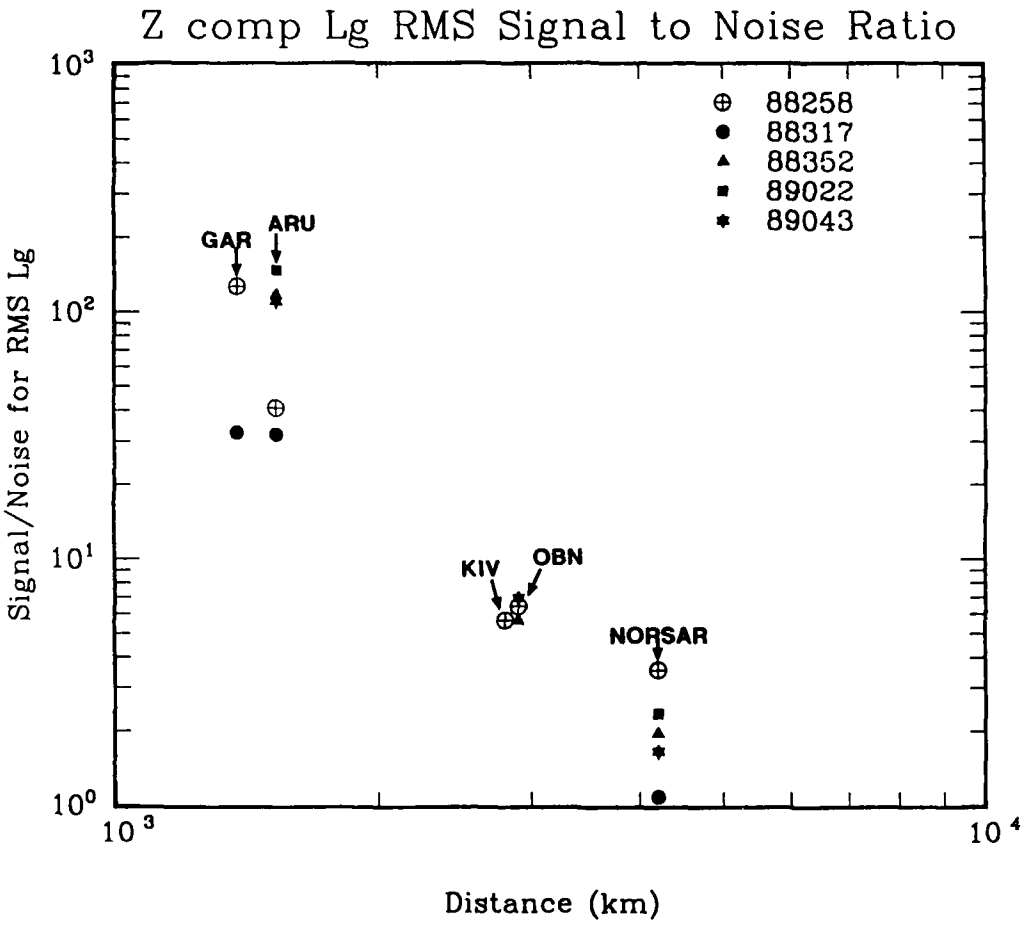

Fig. VII.8.6. Graph showing the variation of the signal-to-noise ratio of the RMS Lg amplitude readings from the four IRIS stations and the NORSAR array on logarithmic scales.

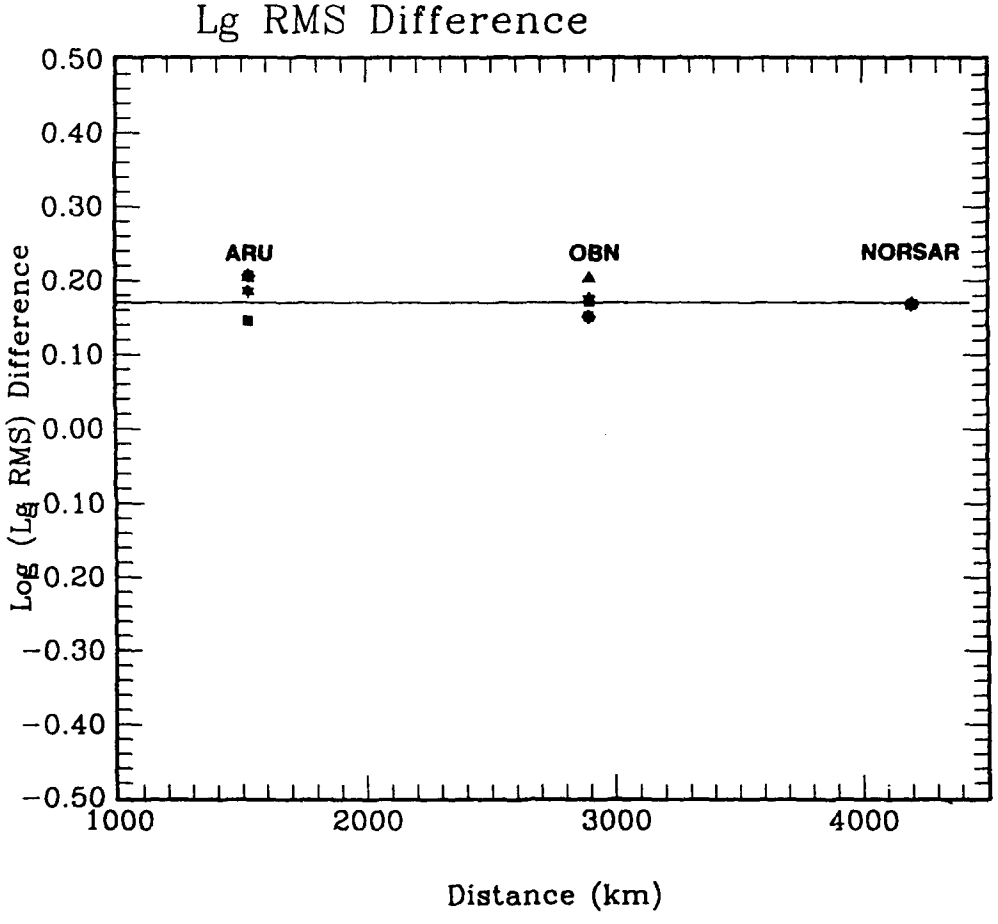

Fig. VII.8.7. The difference in RMS Lg amplitudes (or magnitudes) between the 6.1 m_b explosion on September 14, 1988, and the 5.9 m_b explosion on December 17, 1988 (Day 352) for two IRIS stations and the NORSAR array. The IRIS stations show vertical (8 point star), N-S (triangle) and E-W (box) components and the average (6 point star). The NORSAR point represents the average of readings from vertical instruments.

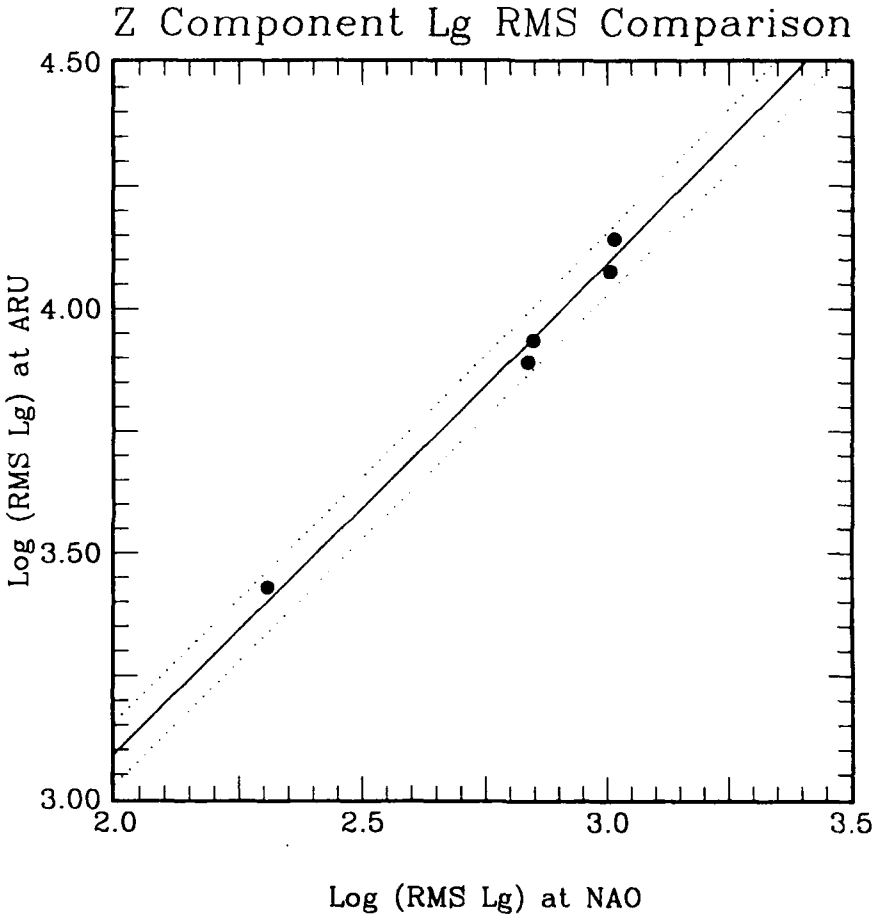

Fig. VII.8.8. Comparison of the RMS Lg amplitudes recorded at ARU and NAO. The solid line represents a slope of one. The standard deviation of the data from the solid line is 0.032. The dotted lines give the plus or minus two standard deviation levels.

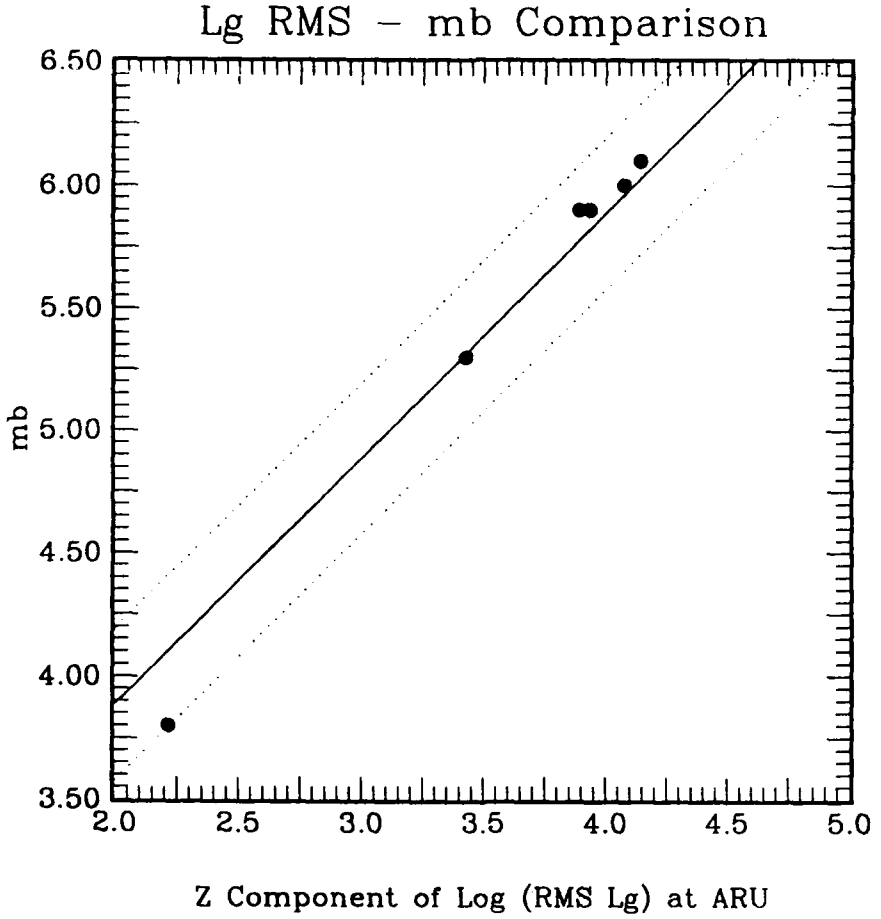

Fig. VII.8.9. Comparison of the vertical component readings of RMS Lg amplitude to world-wide m_b magnitude. The solid line represents a slope of one. The standard deviation of the data from the line is .152. The dotted lines give the plus or minus two standard deviation levels.